Large-scale mutational analysis of Kv11.1 (hERG) proteins reveals molecular insights into type 2 Long QT Syndrome

By

Corey L. Anderson

A dissertation submitted in partial fulfillment of

the requirements for the degree of

Doctor of Philosophy

(Biophysics)

at the

UNIVERSITY OF WISCONSIN-MADISON

2012

Date of final oral examination: 11/26/12

The dissertation is approved by the following members of the Final Oral Committee:

Craig T. January M.D., Ph.D., Professor, Medicine
Baron Chanda Ph.D., Associate Professor, Biophysics
Timothy J. Kamp M.D., Ph.D., Professor, Medicine
Alessardro Senes Ph.D., Assistant Professor, Biophysics
Yongna Xing Ph.D., Assistant Professor, Biophysics

Acknowledgements

This work would not have been possible without the help and support of my family, friends and colleagues. Their support from suggestions to technical assistance has made a big impact on the work described here and my development as a scientist.

Jenni, thank you for being a wonderful mother taking care of our girls on so many occasions when I had to come to the lab at night or on the weekend. I have asked you to do a lot these last four years and I would not have succeeded without your help. Madilyn and Mariana, thank you for helping me identify bacterial colonies and keeping me company on my short visits to the lab. You both have taken a real interest in my work and asked a lot of great questions.

The January lab has been a terrific place to work. Craig, I have really enjoyed working for you for almost ten years now counting my time as a lab tech. Over the course of these ten years, we have had a lot of great scientific discussions. You have also given me the freedom to pursue my own scientific questions, which has allowed me to develop into an independent researcher and scientist. In addition to being a terrific mentor, you are a good friend. I think of the time after I left the lab when we went out for dinner and Irish coffee in San Francisco and you gave me an open invitation to come back to the lab for graduate school. I am glad I did. Thank you.

I also want to thank the other members of the January lab. It has been a pleasure working with all of you. Thank you Evi and Sarah for keeping the lab running smoothly. Thank you to Brian for teaching me electrophysiology and for the numerous discussions about my research. Thank you to Eric for re-teaching me electrophysiology and for your helpful advice. Also, the scope of this project would not have been possible without three undergraduates who did a lot of the experiments. Thank you to Caleb and Ryan for your help on the molecular biology side of things and to Catherine for your help with much of the biochemistry. I'd also like to thank everyone in the CMARP group. There are too many people to mention but the shared resources, joint lab meetings and discussions have been a great help. Finally, thanks to my thesis committee for taking time to participate in my graduate studies.

Funding for this work was provided for by the AHA and NIH through grants to Craig January and direct support from a NIH predoctoral training grant and AHA predoctoral fellowship.

Abstract

Over 300 Kv11.1 missense mutations have been linked to type 2 long QT syndrome (LQT2), a risk factor for sudden cardiac death. The dominant loss-of-function mechanism is likely misfolding of Kv11.1 protein resulting in impaired trafficking to the cell membrane. Interestingly, many can be pharmacologically corrected showing therapeutic potential. However, these observations are based on a small percentage of mostly transmembrane mutations with most mutations uncharacterized, many of which are in intracellular domains. Furthermore, the structural basis for Kv11.1 misfolding and defective trafficking is largely unknown. Understanding differences between and within domains is important for developing targeted therapeutic strategies and may explain why pore mutations are more clinically severe. This thesis addresses these issues by using immunoblot to perform a comprehensive trafficking analysis of 170 LQT2-linked mutations in four of Kv11.1's structural domains combined with bioinformatics and electrophysiology. This largely data-driven approach has yielded new molecular insights into LQT2 including, 1) defective trafficking is the dominant mechanism for all domains except for the distal C-terminus, 2) destabilization of the Per-ARNT-Sim domain (PASD) is one major determinant of LQT2 and correlates with trafficking phenotype, 3) deficient trafficking of PASD and cyclic nucleotide-binding domain (CNBD) mutations can be corrected by second-site suppressor

mutations, 4) dominant-negative interactions explain the increased severity of pore domain mutations, and 5) pharmacological correction of pore mutations is dramatically better for heteromeric channels than it is for homomeric channels.

Table of Contents

Acknowledgements ii
Abstract iv
Table of Contents vi
List of Figures vii
List of Tables viii
List of Abbreviations ix
Methods xi

Chapter I: Literature Review 1
Cardiac Ion Channelopathies 1
Kv11.1 and Kv7.1 Channels 4
Reducing N: Role of Channel Co-assembly 6
Reducing N: Mutations Altering Channel Synthesis 8
Reducing N: Protein (Mis)folding and Quality Control 10
ERADication 13
Vesicular Transport 14
Internalization and recycling 16
Reducing N: Drugs interfering with channel trafficking 17
References 19

Chapter II: PASD LQT2 mutations 28
Introduction 28
Results 30
Discussion 46
References 48

Chapter III: C-terminal LQT2 mutations 52
Introduction 52
Results 54
Discussion 67
References 68

Chapter IV: Pore Domain LQT2 mutations 71
Introduction 71
Results 73
Discussion 84
References 85

Chapter V: Future Directions 87
References 91

List of Figures

Figure Methods-1. Electrophysiology protocols xvii

Figure 1-1. Ion channels of the cardiac AP and their associated diseases **2**

Figure 1-2. Kv11.1, the α-subunit of I_{Kr} **5**

Figure 1-3. Co-assembly vs misassembly of Kv11.1 subunit **6**

Figure 1-4. Kv11.1 channel synthesis and trafficking **9**

Figure 1-5. Kv11.1 channel folding and assembly in the ER **11**

Figure 2-1. The Kv11.1 PASD **28**

Figure 2-2. Trafficking phenotype of PASD mutations **31**

Figure 2-3. Trafficking phenotype of PASD mutations co-expressed with WT **33**

Figure 2-4. Structural context of PASD mutations **34**

Figure 2-5. Biophysical properties of PASD mutation **36**

Figure 2-6. FoldX analysis of PASD mutations **38**

Figure 2-7. Solubility of mutant PASDs **39**

Figure 2-8. Mechanism and correction of PASD mutation **41**

Figure 2-9. Site-saturation mutagenesis of ΔV113. **43**

Figure 3-1. The Kv11.1 C-linker/CNBD **53**

Figure 3-2. Trafficking phenotype of C-linker/CNBD mutation **56**

Figure 3-3. Trafficking phenotype of CNBD mutations co-expressed with WT **57**

Figure 3-4. Structural context of C-linker/CNBD mutations **59**

Figure 3-5. Biophysical properties of C-linker/CNBD mutation **60**

Figure 3-6. FoldX analysis of C-linker/CNBD mutations **62**

Figure 3-7. Structural context of distal C-terminus mutations **64**

Figure 3-8. Biophysical properties of distal C-terminus mutations **65**

Figure 4-1. The Kv11.1 pore domain **72**

Figure 4-2. Trafficking phenotype of pore mutations **74**

Figure 4-3. Trafficking phenotype of pore mutations co-expressed with WT **76**

Figure 4-4. Correction of heteromeric channels **77**

Figure 4-5. Structural context pore mutations **80**

Figure 4-6. Biophysical properties of pore mutations **81**

Figure 5-1. Model of Kv11.1 biogenesis and correction **88**

List of Tables

Table Methods-1. Bioinformatics tools. xiii

Table 2-1. Biophysical properties of Kv11.1 mutation **37**

Table 2-2. Properties of PASD mutations **44**

Table 3-1. Properties of C-linker/CNBD mutations **66**

Table 4-1. S5 and S6 membrane insertion analysis **82**

Table 4-2. Properties of pore domain mutations **83**

Abbreviations

AP	Action potential
CCD	Coiled coil domain
CNBD	Cyclic nucleotide-binding domain
CNG	Cyclic-nucleotide gated channel
DTT	Dithiothreitol
E.coli	*Escherichia coli*
EDTA	(ethylenedinitrilo)tetraacetic acid
ΔG	Gibbs free energy
HEK	Human embryonic kidney cells
HERG	Human ether-a-go-go-related gene
HCN	hyperpolarization-activated cyclic nucleotide-modulated channel
IAD	Inherited Arrhythmias Database
I_{CaL}	L-type calcium current
I_f	pacemaker (funny) current
I_{Kr}	Rapid component of the delayed rectifier potassium current
I_{Ks}	Slow component of the delayed rectifier potassium current
I_{K1}	inward rectifier potassium current
I_{Na}	sodium current
I_{NaCa}	sodium-calcium exchanger current
I_{to}	transient outward current 1
KCNE	Potassium voltage-gated channel subfamily E

LIC	Ligation independent cloning
LQTS	Long QT Syndrome
MinK	Minimal potassium ion channel
MiRP	MinK-related peptide
NMD	Nonsense-mediated mRNA decay
PASD	Per-ARNT-SIM domain
PKA	Protein kinase A
PMSF	phenylmethanesulfonylfluoride
SDS	Sodium dodecyl sulfate
TEV	Tobacco Etch Virus
TMD	Transmembrane domain
VSD	Voltage sensor domain
ΔV113	Valine 113 deletion mutation in Kv11.1
WT	Wild-type
zELK	EAG-like K+ channel from zebrafish

Methods

LQT2 Mutation Database and Mutagenesis

LQT2-associated Kv11.1 mutations were found from the Inherited Arrhythmias Database (IAD) (www.fsm.it/cardmoc), a genotyping study as well as several other literature sources found through PubMed searches[1]. Mutations are listed in **Table 2-2**, **3-1**, and **4-1**. All missense mutations were made using Stratagene's QuikChange II XL kit. Primers were generated using their primer design program and ordered from Integrated DNA Technologies (IDT). A pcDNA3 WT HERG expression vector was used as the template. Restriction analysis was used to test the integrity of all constructs and mutations were verified by sequencing at the UW-Biotechnology Center.

Bioinformatics

The C-linker/CNBD structure was generated with Swiss-Model using the structure of the C-linker/CNBD from zebrafish EAG-like channel (zELK) as a template (PDB 3ukn).[2] The initial model scored in the 80th percentile using MolProbity (100 % being the best) and improved to the 95th percentile after energy minimization using UCSF Chimera's minimization function.[3,4] For comparison, the Kv11.1 PASD structure (PDB 1byw) scored in the 96th percentile. These two models were used for

FoldX stability calculations.[5] FoldX was run in YASARA using a FoldX plugin for YASARA and the FoldXRepair function was performed on both models before stability changes ($\Delta\Delta G$) were calculated.[6] $\Delta\Delta G$ > 1.6 kcal/mol is over the prediction error threshold and considered significant. PASD stability was also determined using the web servers: Polyphen, MUpro, CUPSAT, Eris, and I-Mutant.[7,8,9,10,11] For programs that gave $\Delta\Delta G$ values, mutations were binned into descriptors similar to that used by Polyphen with mutations 'probably destabilizing' having a $\Delta\Delta G$ value greater ≥ 2.0, 'possibly destabilizing' having a $\Delta\Delta G$ 0 ≥ 2 and no effect for mutations with a $\Delta\Delta G \leq 0$. Amino-acid conservation scores were calculated from 150 unique PASD sequences and 125 unique CNBD sequences with ConSurf using default parameters.[12] Solvent accessibilities were calculated using ASAview.[13] Salt bridges and cation-pi interactions were predicted using ESBRI and CaPTURE, respectively.[14,15] ΔG predictor, which is based on a biological hydrophobicity scale, was used to predict the apparent free energy (ΔG_{app}) of insertion for LQT2-S5 and LQT2-S6 TM helices.[16] Amino acids T556-A570 and K638-G669 were used for S5 and S6, respectively based on a report studying a sequence alignment of 360 Kv channels.[17] ClustalW2 was used for the PASD sequence alignment, which was edited in JalView.[18] Pymol was used to generate structural figures.[19] Paircoil2 was used to predict whether LQT2 mutants disrupt the C-terminal coiled coil domain.[20] **Table**

Methods-1 lists the various bioinformatics software and web server addresses used in these experiments.

Table Methods-1. Bioinformatics tools.

Server	Calculation	Website
Swiss-Model	CNBD model	http://swissmodel.expasy.org
Molprobity	CNBD model evaluation	http://molprobity.biochem.duke.edu
Polyphen	PASD stability	http://genetics.bwh.harvard.edu/pph2
MUPro	PASD stability	http://mupro.proteomics.ics.uci.edu
CUPSAT	PASD stability	http://cupsat.tu-bs.de
Eris	PASD stability	http://troll.med.unc.edu/eris
I-Mutant 2.0	PASD stability	http://folding.uib.es/i-mutant/imutant2.0
ConSurf	PASD & CNBD residue conservation score	http://consurf.tau.ac.il
ASAView	PASD & CNBD residue solvent accessibility	http://gibk26.bio.kyutech.ac.jp/jouhou/shandar/neasa/asaview
ESBRI	salt-bridge prediction	http://bioinformatica.isa.cnr.it/ESBRI
CaPTURE	pi-cation prediction	http://capture.caltech.edu
ΔG predictor	membrane insertion efficiency of TMD 5 & 6	http://dgpred.cbr.su.se
Paircoil2	Coiled coil prediction	http://paircoil2.csail.mit.edu

HEK cell culture and stable-cell lines

HEK cells were cultured in complete MEM (Gibco's minimum essential medium supplemented with sodium pyruvate, pens/strep, and non-essential amino acids) at 37^0C unless otherwise noted. Transient transfections were performed with 3μg of cDNA (homomeric channels) or 1.5 μg of WT and 1.5 μg LQT2 cDNA (heteromeric channels) with SuperFect (Qiagen). In some experiments, E4031 (Alamone: 100mmol/L stock dissolved in water) was added to the culture media for 24 hrs before study. Stably transfected cell lines were generated by switching cells to CMEM containing G418 24 hrs after transfection. After 1-2 weeks,

resistant cells were diluted for isolating single colonies, which were subsequently screened for expression by immunoblot.

Kv11.1 trafficking

HEK cells of similar confluence were transiently transfected with SuperFect (Qiagen) and cultured at 37^0C for 24hrs. Cells were then cultured for another 24 hrs at 37^0C, in the presence of 10μM E4031, or at 27^0C without E4031. Whole-cell lysates of similarly confluent cultures were made by solubilizing cells in NP-40 lysis buffer (1% NP-40, 10% glycerol, 150mM NaCl, 5mM EDTA, 50mM Tris-HCl, pH 7.4 and protease inhibitor tablet (Roche)) for 30min on ice. Lysates were spun down for 10min at 16,000xg to remove insoluble debris. The supernatant containing the soluble fraction was mixed with equal volumes of Laemmli sample buffer containing 100mM DTT and subjected to 7.5% SDS-PAGE. Proteins were then electrophoretically transferred onto nitrocellulose membranes and blocked in blocking buffer (PBS containing 0.05% Tween and 5% dry milk). Membranes were incubated with our previously published Kv11.1 antibody directed at the C-terminus and washed 4x for 10min in wash buffer (PBS with 0.05% Tween).[21] Membranes were then incubated with a HRP-conjugated secondary antibody and washed 4X in PBS before detection with the ECL detection kit (Amersham).

Classifying the trafficking phenotype of mutations was based on the glycosylation state of the channel. Mutations that fail to traffic are core-

glycosylated in the ER before proteosomal degradation by quality control. These channels run as a single 135kD band on immunoblot. By contrast, WT channels continue to the Golgi where they are further glycosylated to 155kD before reaching the cell surface membrane. Thus, WT channels show a doublet on immunoblot with both the 135kD and 155kD bands. Mutations that lack or have a diminished 155kD band on immunoblot were classified as trafficking deficient. Mutations that had an increase in intensity of the 155kD band after culture at 27^0C or in 10μM E4031 were classified as correctable.

PASD solubility assay

Amino acids 1-135 containing the PASD (amino acids 26-135) were subcloned into a pET based *E.coli* expression vector containing a TEV cleavable N-terminal 6His tag (gift from Robert Stroud Ph.D. at UCSF) using a ligation-independent-cloning (LIC) strategy.[22] Constructs were transformed into BL21(DE3) cells and single colonies (n≥2) were picked for 2ml overnight growths in auto-induction media. Cells from 1.5ml were harvested, washed 1X (25mM Tris, 150mM NaCl, pH 7.5) and resuspended in 50μL of wash buffer containing 100μM PMSF and benzonase. Cells were lysed using repeated freeze/thaw or Cell-Lytic (Sigma), which gave similar results. Soluble protein was recovered from the supernatant after a 10min, 15,000xg spin and mixed with equal amounts of Laemmli sample buffer containing 100mM DTT and subjected

to 12% SDS-PAGE. PASD protein was detected using a His-HRP antibody (Santa Cruz Biotech). Immunoblots were scanned and band intensities were compared using Image J.

Electrophysiology

Kv11.1 current ($I_{Kv11.1}$) was measured by whole-cell patch-clamp. The extracellular bath solution contained 137mM NaCl, 4mM KCl, 1.8mM $CaCl_2$, 1mM $MgCl_2$, 10mM glucose, and 10mM HEPES (pH 7.4 with NaOH), and the intracellular pipette solution contained 130mM KCl, 1mM $MgCl_2$, 5mM EGTA, 5mM MgATP, and 10mM HEPES (pH 7.2 with KOH). The same solution stocks were used for all recordings. All voltage-clamp experiments were performed at room temperature within 1 to 2 hrs after cells were removed from their culture conditions. Data from cells with less than 10pA leak current at the holding potential -80mV and stable throughout the recording were used for analysis. Patch pipette electrodes were fabricated using a Sutter P-87 micropipette puller and fire polished. All pipettes had a resistance between ~1.5-3 MΩ. Series resistance compensation was ≥70% in all experiments. Data were acquired with an Axopatch-2C amplifier controlled by Clampex 10.0 (Axon Instruments). Data analysis was done with pCLAMP 10.0 and Origin 8.5 (OriginLab). Voltage protocols with representative current traces for studying current

densities (A), activation and deactivation (B) and inactivation (C) are shown in **Figure Methods-1**.

Figure Methods-1. Electrophysiology protocols.

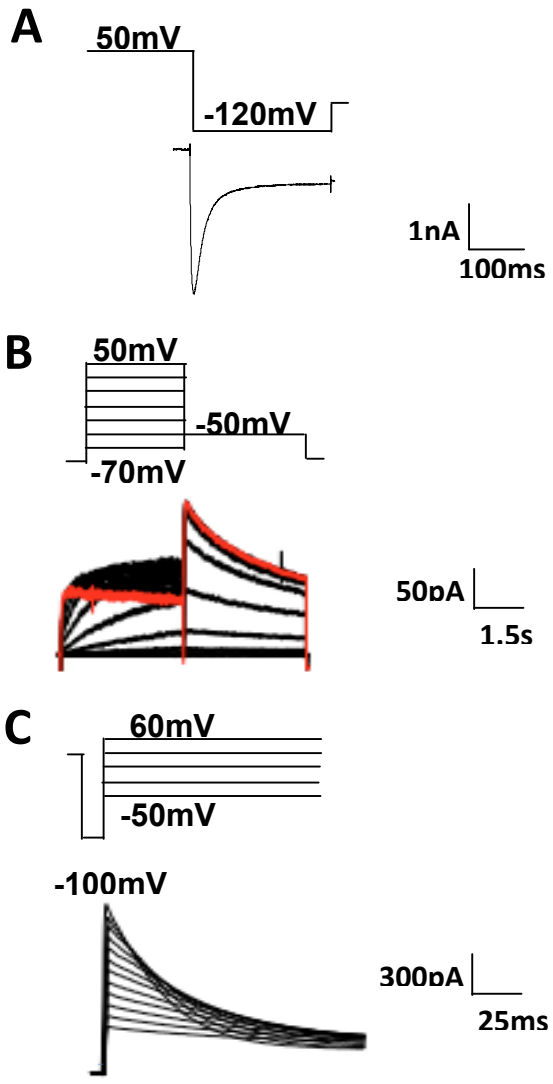

A. Current Density. From a holding potential of -80mV, cells were depolarized to 50mV for 500ms followed by a test pulse to -120mV to generate tail current. Peak $I_{Kv11.1}$ was normalized to cellular capacitance to obtain current density.

B. Activation and deactivation. From a holding potential of -80mV, cells were depolarized to voltages between -70 and 50mV in 10mV increments for 3s followed by a step to -50mV for 3s to quantify tail current. Activation current-voltage (I-V) relations were determined by normalizing peak tail currents (I_{tail}) from each step to the maximal peak I_{tail}. The voltage at which peak current was half-maximal ($V_{1/2}$) and the slope factor (k) were determined by fitting the normalized I-V relationship with the Boltzmann function. The fast (tau_{fast}) and slow (tau_{slow}) time constants of channel deactivation were determined with a double exponential fit of the I_{tail} decay from 50mV to -50mV shown in red.

C. Inactivation. From a holding potential of -80mV, cells were depolarized to 50mV for 1.5s to open and inactivate channels followed by a short 10ms step to -100mV to remove inactivation without allowing enough time for the channels to deactivate. This was followed by test pulses from -50mV to 60mV in 10mV increments. Inactivation time constants for each step were fit as a single exponential.

Statistical Analysis

Data are presented as mean ± SEM. Student's t-test was used for statistical analysis. $P<0.05$ considered significant.

References

1. Kapplinger JD, Tester DJ, Salisbury BA, Carr JL, Harris-Kerr C, Pollevick GD, Wilde AA, Ackerman MJ. Spectrum and prevalence of mutations from the first 2,500 consecutive unrelated patients referred fro the FAMILION long QT syndrome genetic test. *Heart Rhythm*. 2009;9:1297-1303.

2. Arnold K, Bordoli L, Kopp J and Schwede T. The SWISS-MODEL Workspace: A web-based environment for protein structure homology modeling. *Bioinformatics*. 2006;22:195-201.

3. Davis IW, Leaver-Fay A, Chen VB, Block JN, Kapral GJ, Wang X, Murray LW, Arendall III WB, Snoeyink J, Richardson JS, Richardson DC. MolProbity: all-atom contacts and structure validation for proteins and nucleic acids. *Nucleic Acids Res*. 2007;35:375-383.

4. Pettersen EF, Goddard TD, Huang CC, Couch GS, Greenblatt DM, Meng EC, Ferrin TE. *J Comput Chem*. 2004;25(13):1605-1612.

5. Guerois R, Nielsen JE, Serrano L. Predicting changes in the stability of proteins and protein complexes: a study of more than 1000 mutations. *J Mol Bio*. 2002;320:369-387.

6. Van Durme J, Delgado J, Stricher F, Serrano L, Schymkowitz J, Rousseau F. A graphical interface for the FoldX forcefield. *Bioinformatics*. 2011;27(12):1711-1712.

7. Adzhubei IA, Schmidt S, Peshkin L, Ramensky VE, Gerasimova A, Bork P, Kondrashov AS, Sunyaev SR. A method and server for predicting damaging missense mutations. *Nat Methods*. 2010:7(4):248-249.

8. Cheng J, Randall A, Baldi P. Prediction of protein stability changes for single-site mutations using support vector machines. Proteins: Structure, Function, *Bioinformatics*. 2006:62(4):1125-1132.

9. Parhiban V, Gromiha MM, Schomburg D. CUPSAT: a prediction of protein stability upon point mutations. *Nucleic Acids Res*. 2006;34:W239-242.

10. Yin S, Ding F, Dokholyan NV. Eris: an automated estimator of protein stability. *Nat Methods*. 2007;4:466-467.

11. Capriotti E, Fariselli P, Casadio R. I-Mutant2.0: predicting stability changes upon mutation from the protein sequence or structure. *Nucleic Acis Res*. 2005:33:W306-310.

12. Armon A, Graur D, Ben-Tal N. ConSurf: An algorithmic tool for identification of functional regions in proteins by surface-mapping of phylogenetic information. *J Mol Biol*. 2001;307:447-463.

13. Shandar A, Gromiha MM, Fawareh H, Sarai A. ASAView: solvent accessibility graphics for proteins. *BMC Bioinformatics*. 2004;5:51.

14. Costantini S, Colonna G, Facchiano AM. ESBRI: a web server for evaluating salt bridges in proteins. *Bioinformation*. 2008;3(3):137-138.

15. Gallivan JP, Dougherty DA. Cation-pi interactions in structural biology. *Proc Natl Acad Sci*. 1999;96:9459.

16. Hessa T, Meindle-Beinker NM, Bernsel A, Kim H, Sato Y, Lerch-Bader M, Nilsson I, White SH, von Heijne G. Molecular code for transmembrane-helix recognition by the SEC61 translocon. *Nature*. 2007;450(7172):1026-1030.

17. Lee SY, Banerjee A, MacKinnon R. Two separate interfaces between the voltage sensor and pore are required for the function of voltage-dependent K+ channels. *PLoS Biology*. 2009;7(3):676-686.

18. Waterhouse AM, Procter JB, Martin DMA, Clamp M, Barton GJ. Jalview Version 2- a multiple sequence alignment editor and analysis workbench. *Bioinformatics*. 2009;25(9):1189-1191.

19. The PyMOL Molecular Graphics System, Version 1.2r3pre, Schrödinger, LLC.

20. McDonnell AV, Jian T, Keating AE, Berger B. Paircoil2: improved prediction of coiled coils from sequence. *Bioinformatics*. 2006;22(3):356-358.

21. Zhou Z, Gong Q, Ye B, Fan Z, Makielski JC, Robertson GA, January CT. Properties of HERG channels stably expressed in HEK 293 cells studied at physiological temperature. *Biophys J*. 1998:74:230-241.

22. Savage DF, Anderson CL, Yaneth RC, Newby ZE, Stroud RM. Cell-free complements in vivo expression of the E.coli membrane proteome. *Protein Science*. 2007;16(5):966-976.

Chapter I

Literature Review

Cardiac Ion Channelopathies

The concept of cardiac ion channelopathies has steadily evolved from the initial cloning of the first three cardiac ion channel genes linked to Long QT Syndrome (LQTS) types 1-3 (LQT1-3) in the mid-1990's, work founded on the prior identification of the inherited Romano Ward and the Jerville and Lange-Nielsen syndromes, and the Brugagda syndrome. Today, at least 13 genes have been linked to inherited LQTS. Furthermore, at least 12 inherited arrhythmia syndromes (LQTS, Brugada, etc) have been described involving more than 1000 mutations in at least 26 genes, and this grows steadily (for review, see Balijepalli et al, 2010)[1]. Most of the commonly identified genes encode cardiac ion channel proteins (α-subunits, β- or other accessory-subunits, macromolecular complex proteins) although some genes encode signaling pathway and Ca^{2+} regulatory proteins.

Cardiac ion channels, along with electrogenic transporters, are responsible for the electrical activity of heart cells. Ion channels are selectively permeable to Na^{+}, K^{+}, Ca^{2+}, or Cl^{-}. Multiple genes encode a variety of these channels that have unique gating characteristics, densities in the sarcolemma, and varying membrane (caveoli, t-tubules, etc) and regional localization (ventricular, atrial, nodal) to give rise to the finely tuned interplay of membrane currents that shape the cardiac action potential (AP) and govern normal heart rhythm. **Figure 1-1a**

illustrates a ventricular AP with the associated currents below. At rest a myocyte's diastolic potential is near the equilibrium potential for K^+ (around -85mV) due mainly to inward rectifier potassium current (I_{KI}). Currents from adjacent myocytes pass through gap junction channels to depolarize the sarcolemma activating sodium channels and L-type calcium channels. These inward currents (I_{Na} and I_{Ca}) rapidly drive the membrane

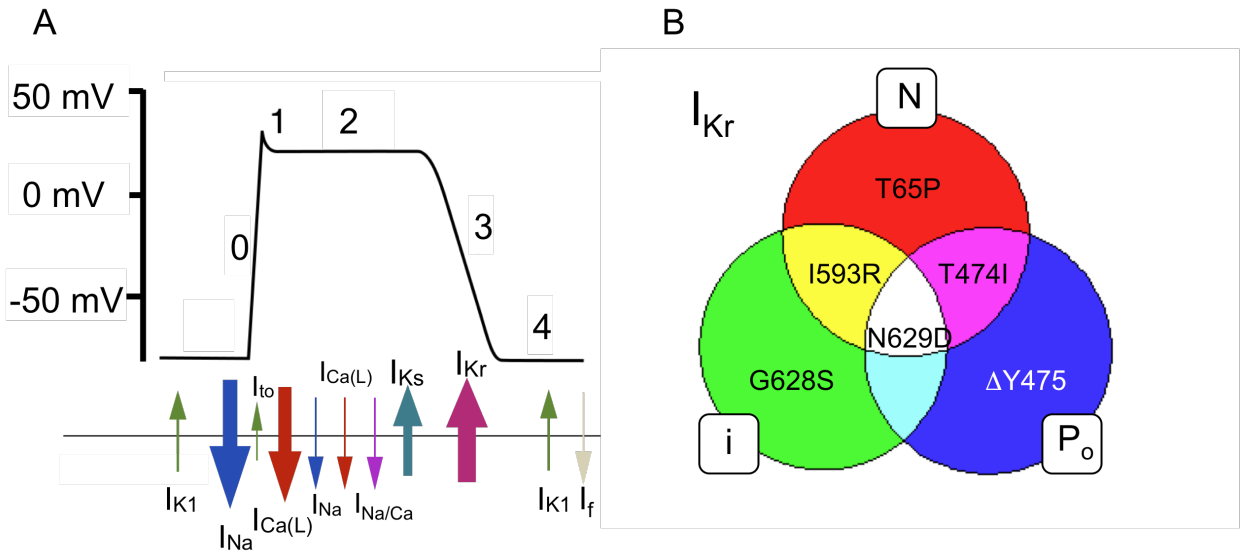

Figure 1-1. Ion channels of the cardiac AP and their associated diseases. A. Phases 0-4 of the cardiac ventricular action potential are illustrated with relative current magnitudes shown below. I_{Na} = sodium current (LQT3, BrS1, SSS, and CCD). I_{CaL} = L-type calcium current (BrS3, BrS4). I_{to} = transient outward current 1. I_{K1} = inward rectifier potassium current (LQT7). I_{Kr} = rapidly activating delayed rectifier potassium current (LQT1 and LQT5, SQT). I_{Ks} = slowly activating delayed rectifier potassium current (LQT1 and LQT5, SQT). I_{NaCa} = sodium-calcium exchanger current. I_f = pacemaker current (SSS). B. Diagram showing mechanism(s) of channel dysfunction modeled using Kv11.1 (N = number of channels, I = unitary conductance, P_0 = probability of channel opening). Mutations that decrease N are Class 2, mutations that alter P_o are Class 3 and mutations that alter or abolish i are Class 4. Not shown is class 1, which alters protein synthesis.

potential to its peak (around +30mV). I_{Na} inactivates quickly whereas L-type I_{Ca} persists longer with both contributing inward current during the plateau. Depolarization activated outward K^+ currents from I_{to}, I_{Kr} and I_{Ks} eventually repolarize the myocyte to its resting potential assisted by recovery of I_{K1}. In some myocytes, I_f adds to depolarization and electrogenic exchangers may contribute current at different times during the AP. Each ion channel's macroscopic current (I) is proportional to three properties: 1) the number of channels at the sarcolemma (N), 2) its unitary conductance (i), and 3) the probability of it being open at a given membrane potential (P_o). The cellular regulation of each of these properties (N, i, P_o), in turn, is complex and incompletely understood. Even modest changes in any of these properties can alter the shape of the cardiac AP waveform, its duration, and potentially contribute to the generation of cardiac arrhythmias. (For reviews, see Nerbonne and Kass, 2005, Delisle et al. 2004, and Amin et al., 2010)[2,3,4].

It is now understood that mutations in ion channels can cause changes in one or more of these three properties. This is illustrated in **Figure 1-1b** for several Kv11.1 mutations linked to LQT2. The three circles represent the properties of N, i, and P_o. Some LQT2 mutations are thought to selectively alter a single property (e.g., T65P, G628S, and ΔY475, respectively), whereas other LQT2 mutations exert combinations of effects illustrated by overlap of the circles. This emphasizes the complex biology underlying mutations to cause abnormalities of channel biogenesis and biophysics. However, decreased expression of ion channels at the cell surface membrane (decreased N) is

increasingly being recognized as an important loss-of-function mechanism with the most known about Kv11.1 and Kv7.1 channels. This trafficking-deficient, or reduced membrane expression phenotype is now known to occur with disease-associated mutations in several cardiac ion channel genes encoding the α-, as well as β- subunits for I_{Kr}, I_{Ks}, I_{K1}, I_{Na}, I_{CaL}, and I_f, (currents described in **Figure 1-1**) and linked to LQTS, Brugada Syndrome, Cardiac Conduction Disease and Idiopathic Sick Sinus Syndrome. [4,5,6,7,8,9] For one disease, LQT2, abnormal protein trafficking is postulated to be the dominant disease causing mechanism.[10] Given the expanding role of protein trafficking defects in cardiac ion channelopathies, understanding the mechanisms underlying trafficking failure is the key to developing potential therapies. The rest of the introduction will focus on Kv11.1 trafficking with some examples from Kv7.1 for comparison.

Kv11.1 and Kv7.1 Channels

Kv11.1 and Kv7.1 are α-subunit proteins for voltage-gated K^+ (Kv) channels. As tetramers they comprise the rapid (I_{Kr}) and slow (I_{Ks}) components of the delayed rectifier K^+ current, respectively. Each Kv11.1 and Kv7.1 α-subunit protein contains six transmembrane (TMD) spanning domains (S1-S6) with a pore region (S5-S6) flanked by N- and C-termini intracellular domains. As shown in **Figure 1-2**, Kv11.1 contains an N-terminal PerArnSim (PASD) domain and a C-terminal nucleotide-binding domain (CNBD), which are important in Kv11.1 deactivation. Both Kv11.1 and Kv7.1 contain C-terminal coiled-coil domains (CCD), which serves as a tetramerization and scaffolding domain in Kv7.1 but its

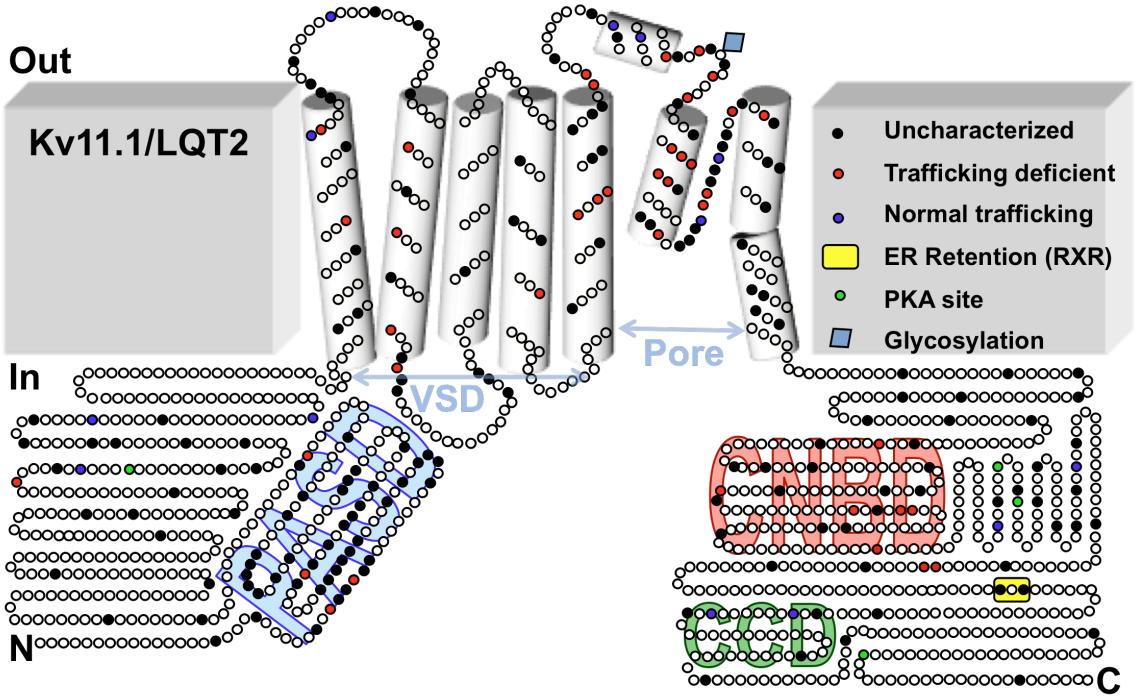

Figure 1-2. Kv11.1, the α-subunit of I_{Kr}. Circles represent amino acids with cylinders representing transmembrane segments S1-S6. Positively charged residues in S4 (not shown) make up the voltage sensor and the pore is located between S5 and S6. The intracellular PerArntSim (PAS), cyclic nucleotide-binding domain (CNBD), and coilied-coil domain (CCD) are shown in light blue. Black circles show the location of all uncharacterized LQT2-linked mutations, red circles indicate trafficking defects, and blue circles indicate normal trafficking. The RXR ER retention signal is highlighted in yellow and the glycosylation site at N598 is shown as a blue diamond.

role in Kv11.1 is unknown.[11,12,13] Both channels play a crucial role in repolarization of the cardiac AP and the majority of LQTS-linked mutations have been identified in these two genes. Most common are missense mutations which account for ~2/3rds of LQTS, followed by mutations that introduced premature termination codons (nonsense, frameshifts) as well as deletion, insertion, and splice site mutations.[14]

Reducing N: Role of Channel Co-assembly

Co-assembly is a complex molecular process where a functional channel is assembled from various subunits. The dynamics of this is thought to contribute to the pathogenicity of ion channelopathies and this is illustrated in **Figure 1-3**.

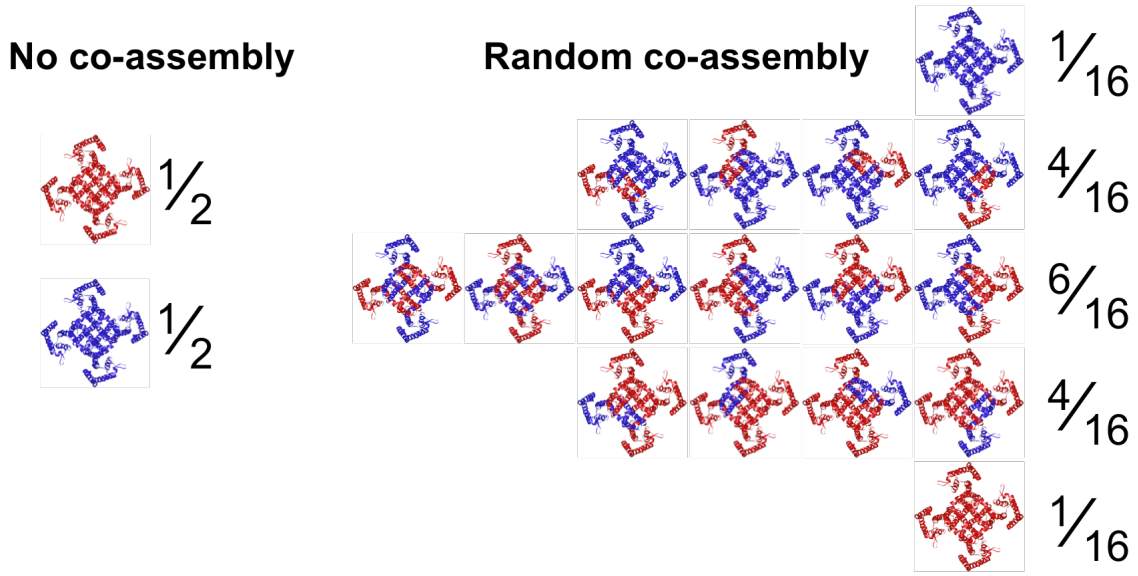

Figure 1-3. Co-assembly vs misassembly of Kv11.1 subunits. Illustration showing WT only on left and mutant subunit co-assembly on right as described in the text.

Happloinsufficiency occurs where WT and mutant α-subunits do not co-assemble with each other and in its simplest form predicts a 50% reduction in current magnitude since only the WT allele contributes to functional channels in the sarcolemma (assuming mutant channels contribute no current). Strategies to selectively increase the abundance of WT might be effective at treating mutations resulting from haploinsufficiency. For example, Kv11.1 channel synthesis can be increased through increased phosphorylation via PKA.[15] Dominant negative

effects, in principle, cause a more severe phenotype because WT and mutant subunits are able to co-assemble and the presence of even a single mutant subunit conveys the negative phenotype. **Figure 1-3** shows the possible combinations and probabilities of having zero, one, two, three, or all four α subunits of a tetrameric channel being mutant. For example, if the presence of a single mutant α-subunit conveys the negative effect, then only 1/16 of the channels would contain four WT α-subunits to function normally, hence causing a 94% reduction of current density.

Kv11.1 and Kv7.1 also co-assemble with β-subunits encoded by the *KCNE* family of genes (see **Figure 1-2**).[16,17,18,19] Although KCNE1 (E1) and KCNE2 (E2) are promiscuous and associate with several different Kv α-subunits, *KCNE1* and *KCNE2* are linked to type 5 and 6 LQTS (LQT5 and LQT6), respectively.[20,21,22] Studies suggest that the I_{Ks} channel minimally consists of Kv7.1 and E1 subunits, because Kv7.1 expressed alone generates small rapidly activating K^+ currents that inactivate, and co-expression of E1 is needed to express large slowly activating K^+ currents that do not inactivate and resemble I_{Ks}. Moreover, E1 traffics more efficiently through the secretory pathway when co-assembled with Kv7.1.[23] One example is a LQT5 mutation (L51H) which can co-assemble with WT-Kv7.1 and prevent its trafficking to the cell surface demonstrating the principle that β-subunit mutations also can convey a trafficking-deficient phenotype.[24] The functional role that E1 and E2 have on the trafficking of Kv11.1 is less clear and may depend on the expression system(s) used.[25]

Reducing N: Mutations Altering Channel Synthesis.

The most common mutation in inherited arrhythmia syndromes is missense; single nucleotide changes leading to single amino acid substitutions. Less common are nonsense mutations, frameshifts, insertions, deletions and splicing errors that can alter markedly gene transcription and RNA stability leading to attenuated protein synthesis (class 1) and this is illustrated in **Figure 1-4**, Step 1. To highlight just a few examples of each, Gong and co-workers reported a LQT2 splice site mutation that creates an in frame 18 amino acid insertion in the C-terminal of Kv11.1, which causes dominant-negative suppression of WT-Kv11.1. This insertion disrupts the CNBD shown to be required for trafficking.[26,27] Similarly, two frameshift mutations, LQT1-linked A78fs/105-Kv7.1 and LQT2-linked Y420fs/12-Kv11.1 generate severely truncated proteins that co-assemble with WT and cause a dominant-negative trafficking defect.[28,29] However, not all trafficking-deficient mutations cause dominant-negative suppression such as the LQT1 mutation P631fs/19-Kv7.1 and two deletion mutations (ΔS276 and ΔV595).[30,31,32] Interestingly, P631 fs/19-Kv7.1 was retained in the ER due to the newly added 19-amino acid sequence containing two ER retention (R-X-R) signals. Until recently, nonsense mutations, which create premature stop codons, were thought to act predominantly through dominant-negative or haploinsufficient effects.[33] However, Gong and co-workers have shown that nonsense mediated mRNA decay (NMD) is likely responsible for reducing N.[34] Interestingly, drugs such as aminoglycoside antibiotics can cause read-through of premature stop codons resulting from nonsense and fs

mutations to produce full-length, functional proteins in the Cystic Fibrosis Transmembrane Conductance Regulator Cl^- (CFTR), Nav1.5, and Kv11.1 channels.[35,36,37]

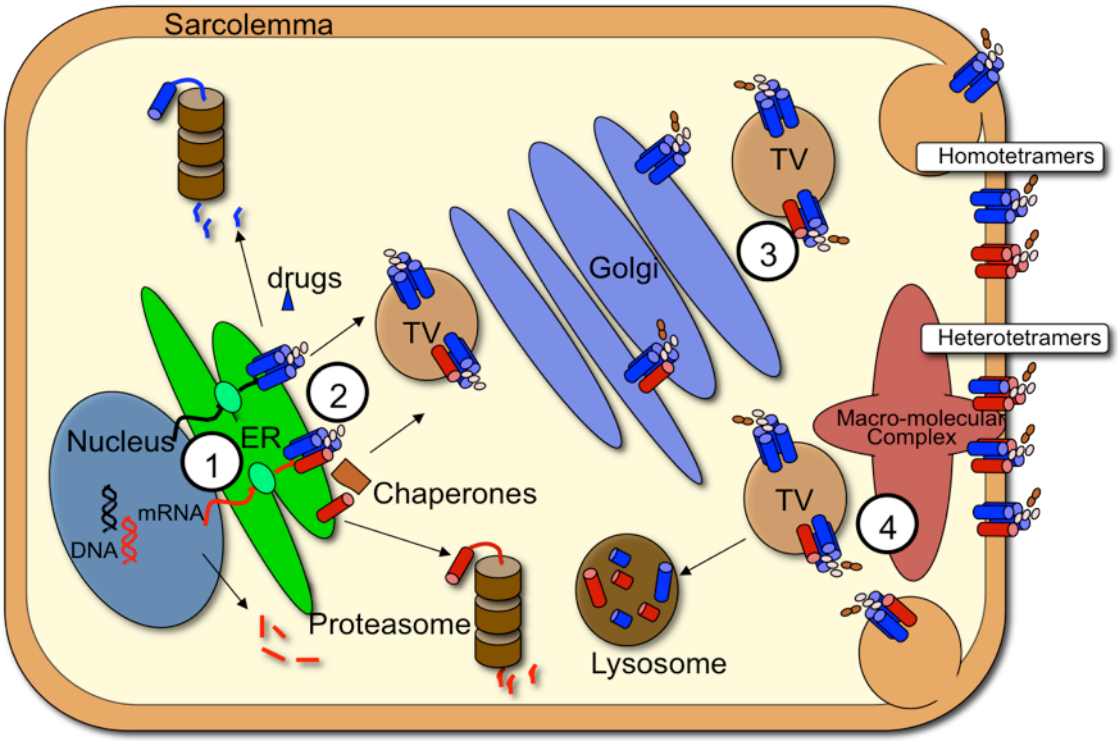

Figure 1-4. Kv11.1 channel synthesis and trafficking. The major compartments involved Kv11.1 biosynthesis are shown including the nucleus, ER, transport vesicles (TV) Golgi, and the sacrolemma. Degradation is mediated by proteasomes and lysosomes. WT and mutant DNA, mRNA, and protein are shown in blue and red, respectively. A decrease in N can be due to haploinsufficiency whereby mutations 1) create premature stop codons, which are degraded by NMD or 2) produce mutant channels that fail to co-assemble with WT channels. Alternatively, mutations can act dominant-negatively by producing mutant channels that co-assemble with WT and inhibit further trafficking. These mutant proteins are thought to misfold and be targeted for ER-associated degradation (ERAD) by the proteasome. All channels are core-glycosylated in the ER (pink circles) and for those that are not degraded, are packaged, and trafficked in transport vesicles (TV) to the Golgi for complex glycosylation (red circles) and ultimately to the sarcolemma. Besides decreasing N, some mutations make it to the sarcolemma, but with altered function. The tetrameric channels at the surface can be comprised of only WT homotetramers due to haploinsufficiency or any combination of heterotetramers (or mutant homotetramers) depending on dominant-negative effects. The tetrameric

channels are eventually internalized and degraded by the lysosome. Numerous Kv11.1 channel interacting proteins have been identified and Kv11.1 is likely part of a macromolecular complex.

These examples highlight the complex ways that the less frequent types of mutations in LQTS can reduce surface expression, some of which might be correctable with drugs.

Reducing N: Protein (Mis)Folding and Quality Control

Membrane proteins like Kv11.1 are very complex with hydrophillic intracellular domains and hydrophobic TM spanning domains, where folding is driven by different mechanisms (For review, see Mackenzie 2006).[38] Further complexity comes from cooperativity between domains that may be necessary for proper folding, as well as chaperone molecule interactions (discussed below). **Figure 1-5** is a schematic cartoon of Kv11.1 trafficking illustrating the various steps and interactions that may be important for obtaining a native, trafficking competent channel structure. Over 50 mostly TMD-LQT2 mutations have been characterized to some degree and about 80% of these are thought to be misfolded, trafficking deficient channels targeted for ER associated degradation (ERAD), a well documented cellular mechanism for 'cleaning up' misfolded proteins.[10,39,40] While the molecular mechanisms for Kv11.1 protein misfolding are mostly undefined, studies from other disease-associated membrane proteins like cystic fibrosis (CFTR), retinitis pigmentosa (ADRP) and many others may lend insight into cardiac ion channel misfolding.[41,42]

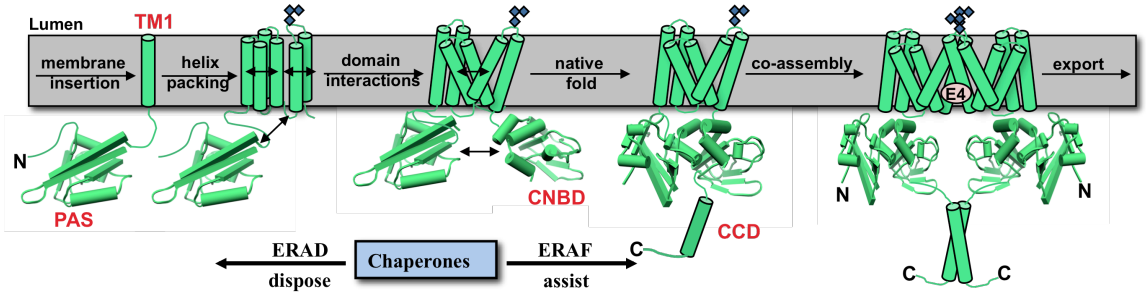

Figure 1-5. Kv11.1 channel folding and assembly in the ER. Ribosomal synthesis begins with the N-terminus. The intracellular PAS domain folds first, followed by insertion and packing of the TM spanning helices making up the voltage sensor and pore domains. The intracellular C-terminal CNBD folds next, followed by oligomerization and then formation of the CCD (only two of four α-subunits are shown). Intra-domain interactions (i.e. hydrogen-bonding, salt bridges and van der Waals interactions) as well as possible cooperative interactions between domains are indicated with double-ended arrows. Some of these steps may occur co-translationally, including oligomerization, which may be facilitated with biological (ERAD or ERAF proteins) or chemical (E4) chaperones. Channels are then exported from the ER.

80% of disease-associated mutations in hydrophillic proteins are destabilizing.[43] As shown in **Figure 1-2**, LQT2 mutations are overrepresented in the PAS domain, which has been shown to interact with the PAS domain of other subunits, the CNBD, and the S4-S5 linker.[29,44,45,46] It is therefore probable, that loss of stability of the PAS domain causes multiple intra and inter-domain disruptions, which are recognized by quality control and targeted for ERAD. In fact, this has been shown for several PASD mutations.[47] Similar mechanisms may apply to the CNBD as evidenced by the fact that all CNBD LQT2 mutations characterized to date are trafficking deficient.[27]

TMDs also cause misfolding through destabilization and are more susceptible to disease-causing mutations.[48,48,50] Formation of the

transmembrane domain is a dynamic process of translocon mediated helix insertion and helix-helix interactions.[51] Only about 15% of TM residues have polar side-chains, yet mutations that cause a gain or loss of a polar residue have the highest propensity for disease.[52] In CFTR, gain of polar residues have been shown to alter the TM alignment through non-native H-bonds or in the case of the $GABA_A$ receptor mutation A322D linked to epilepsy, disrupt membrane insertion through loss of TM hydrophobicity.[53,54] Similar mechanisms may exist with similar Kv11.1 mutations.[14] Ionic interactions are important for helix-helix interactions, folding, and assembly in the homologous Shaker Kv channel.[55,56,57] Kv11.1 contains many LQT2 mutations of charged residues in the TMD including the voltage sensor and several of these have been characterized as trafficking deficient.[10]

Finally, formation of the pore seems to be a critical determinant of Kv11.1 maturation as evidenced by 1) the numerous trafficking deficient mutations located there (see **Fig 1-2**), 2) the second-site suppressor mutation Y652C in the pore can reverse trafficking defects, and 3) pore blocking drugs like E4031 not only rescue pore mutations, but also those in the PASD and voltage sensor domains (VSD).[10,58,59] Clearly there is a mechanistic link between the pore, PASD, and VSD folding, but the cooperativity between these domains to achieve the final fold is not understood. Interestingly, some Kv11.1 mutations can also be corrected through reduced temperature, glycerol, and thapsigargin with different correction phenotypes.[10,59,60] One interpretation is that mutations cause Kv11.1 channels to reach different misfolded states, some which can still fold

correctly if stabilized, and this is supported by studies of differentially targeted VSD mutations in Shaker Kv channels.[61]

It is less clear whether LQT1 is a misfolding disease to the extent of LQT2. Only about a dozen trafficking deficient LQT1 missense mutations have been described, strategies used to correct protein misfolding do not enhance trafficking deficient LQT1 mutations, and little is known about cellular quality control mechanisms that regulate Kv7.1. In summary, (mis)folding of multidomain membrane proteins like Kv11.1 is very complex with numerous helix-helix, protein-lipid, as well as chaperone-mediated interactions, which is illustrated in **Figure 1-5**.

ERADication.

Much of what is known about the cellular quality control mechanisms that regulate ion channels comes from studies of CFTR. Approximately 70-80% of cystic fibrosis patients have a phenylalanine deletion at residue 508 (ΔF508-CFTR), which prevents its ER export and cell surface expression. The chaperones calnexin, Hsp40, Hscp70, and Hsp90 all associate with CFTR and ΔF508-CFTR. Several studies suggest that modulation of calnexin, Hsp40, Hscp70, and Hsp90 activities can affect the folding and stability of WT and ΔF508-CFTR (Amaral 2004). Proteomic analyses demonstrate that the 'chaperome' for ΔF508-CFTR actually consists of at least 31 different chaperones and co-chaperones. Small interfering (siRNA) strategies directed against specific co-chaperones were found to 1) facilitate the degradation of

ΔF508-CFTR, 2) increase the stability (but not functional expression) of ΔF508-CFTR, or 3) increase functional expression of ΔF508-CFTR.[63] The data suggest that selectively modifying different co-chaperones can facilitate ER Associated Folding (ERAF) and ERAD or inhibit ERAD. Several studies have identified similar components for the Kv11.1 chaperome including calnexin, the heat-shock proteins Hsp40, Hscp70, Hsp90, FKBP38 (38 kDa FK506-binding protein), Sigma 1-receptor, and Caveolin 3.[64,65,66,67,68,69] Pharmacological inhibition of Hsp90, siRNA knockdown of FKBP38, or overexpression of Hsp40 inhibit the trafficking WT-Kv11.1, suggesting that the chaperones and co-chaperones are important for ERAF of WT-Kv11.1. Perhaps modulation of the Kv11.1 chaperome is one strategy for correcting trafficking deficient Kv11.1 mutants.

Vesicular Transport.

In addition to ERAF and ERAD, the trafficking of proteins exiting the ER depends on their packaging into transport vesicles. Vesicular transport between the ER and Golgi compartments is mainly regulated by coat-associated protein I and II (COPI and COPII) vesicles. In addition to COPI and COPII vesicles, the cells also contain other coat associated complexes, such as clathrin or caveolins, that regulate the recycling pathway of ion channel proteins between the cell surface, endosomes, lysosomes, and Golgi (see **Figure 1-4**).

The recruitment of proteins into COPII vesicles is facilitated by ER export sequences (i.e. D-X-E, where X is any amino acid) that are recognized by adaptor proteins, which assist the packaging of proteins into COPII vesicles[70].

The formation of COPI vesicles is a GTP-dependent process that is very similar to COPII vesicles. COPI vesicles are thought to primarily mediate retrograde transport of proteins that have ER retention signals (i.e. K-K-X-X or R-X-R) back to the ER, but they may also regulate the antegrade transport of proteins to the Golgi. Many studies demonstrate that ion channels contain functional ER export and retention signals. The trafficking of some ion channels appears to rely on the "masking" of ER retention signals during channel folding and assembly. For example, models for the trafficking of K_{ATP} and K_{IR} channels suggest that 14-3-3 proteins recognize correctly oligomerized K^+ channels and mask ER retention signals to prevent retrograde transport back to the ER in COPI vesicles.[71,72,73] Other models suggest that once a channel has achieved a native-like conformation, ER export signals are exposed, which enables adaptor proteins to facilitate packaging into COPII vesicles.[70] Moreover, an ER to Golgi adaptor protein, GM130, was shown to associate with the carboxy terminus of WT-Kv11.1 (encompassing amino acid residues 667-1159)[74,75]. Interestingly two trafficking deficient LQT2 mutations (V822M and R823W) do not associate with GM130, suggesting that the recruitment of these mutations to COPII vesicles may be compromised (**Figure 1-4** Step 3).[75] Although the ER retention/export models appear to be mutually exclusive, the trafficking of K^+ channels is likely regulated by multiple signals within the same subunit or co-assembled subunits.[76]

Several ion channels have "non-conventional" vesicular transport properties because they rely only on COPI or COP II vesicular transport. For example,

Hasdemir and colleagues have proposed that the A-type Kv subunits, Kv4.2 and K^+ channel Interacting Protein 1 (KChIP1) traffic in a vesicular pathway that is dependent on COPI but not COPII vesicular transport, whereas Yoo and colleagues show that the trafficking of CFTR is sensitive to inhibition of COPII but not COPI vesicular transport.[77,78] Delisle and co-workers recently showed that the trafficking of WT-Kv11 is more sensitive to inhibition of COP II vesicular transport.[79] These data show that various trafficking pathways exist among different ion channels.

Internalization & Recycling

A study of Kv7.1 suggests that serum- and glucocorticoid-inducible kinase (SGK1), together facilitates the recycling of Kv7.1 to the cell surface membrane. Thus far three LQT1 (P117L, Y111C, and L114P) and one LQT5 mutation (D76N) disrupt SGK1-stimulated plasma membrane insertion of Kv7.1 and E1.[80,91] These mutations are located in an intracellular juxtamembranous region raising the possibility that these regions of Kv7.1 and E1 interact to promote trafficking of the heteromeric channel complex.

Less is known about the role of internalization as a mechanism for LQT2 mutations. However, expression of Kv11.1 in the cell surface is tightly linked to extracellular K^+ concentration.[80,82,83,84] In conditions of low external K^+, Kv11.1 is rapidly internalized via a caveolin-dependent pathway. These series of studies raise the intriguing possibility that QT prolongation associated with hypokalemia may be caused by a reduction in I_{Kr} due to enhanced internalization of Kv11.1 to

reduce N, as illustrated in **Figure 1-4**.

Reducing N: Drugs Interfering with Channel Trafficking.

In addition to mutations, numerous pharmacological inhibitors of trafficking have also been discovered, some seemingly specific to Kv11.1.[1,85] These potentially may cause drug-induced LQTS by disrupting channel trafficking rather than direct block of the channel. For example, Ficker and co-workers discovered that high concentrations of cardiac glycosides such as digoxin, which inhibit the sarcolemmal Na^+/K^+ ATPase pump, also block Kv11.1 channel trafficking.[86] In general, the cellular mechanisms and molecular targets for drugs that disrupt tracking are not known, and it is possible that multiple drug binding sites representing different steps in protein processing can mediate trafficking disruption.

Summary

Inherited arrhythmia syndromes, and more broadly genetically based diseases, have expanded our understanding of the underlying biology of disease mechanisms for the regulation of membrane, as well as non-membrane proteins. In this literature review, we have shown examples of inherited mutations that can cause failure of Kv11.1 channels to reach the surface by several mechanisms. Promisingly, several proof-of-principle experiments show that pharmacological strategies might be beneficial to loss of function mutations such as 1) drugs that readthrough premature stop codons to correct nonsense and frameshift

mutations, 2) drugs that upregulate channels synthesis to compensate for haploinsufficiency, and 3) drugs that correct misfolding directly through binding the channel or indirectly through chaperone modulation. In addition, drugs may alter directly channel activity (P_o, "activators") or modify internalization and recycling. While there are several caveats to each of these approaches; these are nevertheless exciting areas for potential therapeutic exploration and development.

Finally, new experimental models are becoming available. To date, most of our mechanistic insights have come from studies done in heterologous expression systems and how well this translates to humans is uncertain. Advances in inducible pluripotent stem cell (iPS) technology promise the ability to generate cardiomyocytes carrying the genetics of the donor[87]. For example, Moretti and co-workers created cardiomyocytes from induced pluripotent stem cells (iPSCMs) derived LQT1 patients carrying the R190Q mutation in the Kv7.1 channel that was originally characterized as trafficking deficient.[88,89] Interestingly, they found a 75% reduction in I_{Ks}, supporting reduced surface expression, but when they looked at I_{Kr}, they did not see any concomitant reduction; a mechanism found in over-expression models.[90,91] This study highlights the potential importance iPS-CMs will have in understanding mechanisms of trafficking defects of cardiac channelopathies. Also, recent advances in genome editing should make it possible to study any LQTS iPSCM for comparison with cells of the same genetic background.[92]

While a lot of work has been done in understanding the pathogenic

mechanisms of LQT2, most of it is based on a small percentage of mostly TMD mutations and many unknowns remain. For example, is deficient trafficking the dominant mechanism for all domains? Is pharmacological correction mostly limited to pore mutations? Why are pore mutations more clinically severe? What is the structural basis of misfolding? To address these questions, a largely data-driven approach was used. Overall, 170 LQT2-linked missense mutations and dozens of engineered mutations covering the PASD, pore, C-linker/CNBD and distal C-terminus were characterized. As a result, several new molecular insights into LQT2 were revealed, which are discussed in the following chapters.

References

1. Balijepalli SY, Anderson CL, Lin EC, January CT. Rescue of Mutated Cardiac Ion Channels in Inherited Arrhythmia Syndromes. *J Cardiovasc Pharmacol*. 2010;56(2):113-122.

2. Nerbonne JM, Kass RS. Molecular physiology of cardiac repolarization. *Physiol Rev*. 2005;85:1205-1253.

3. Delisle BP, Anson BD, Rajamani S, January CT. Biology of cardiac arrhythmias: Ion channel protein trafficking. *Circ Res*. 2004;94:1418-1428.

4. Amin AS, Tan HL, Wilde AAM. Cardiac ion channels in health and disease. *Heart Rhythm*. 2010;7(1):117-126.

5. Bendahhou S, Donaldson MR, Plaster NM, Tristani-Firouzi M, Fu, Y-H, Ptacek LJ. Defective potassium channel Kir2.1 trafficking underlies Andersen-Tawil syndrome. *J Biol Chem*. 2003;278(51):51779-51785.

6. Baroudi G, Pouliot V, Denjoy I, et al. Novel mechanism for Brugada syndrome: Defective surface localization of an SCN5A mutant (R1432G). *Circ Res*. 2001;88:78-83.

7. Antzelevitch C, Pollevick GD, Cordeiro JM, Casis O, Sanguinetti MC, Aizawa Y, Guerchicoff A, Pfeiffer R, Oliva A, Wollnik B, Gelber P, Bonaros EP, Burashnikov E, Wu Y, Sargent JD, Schickel S, Oberheiden R, Bhatia A, Hsu L-F, Haissaguerre M, Schimpf R, Borggrefe M, Wolpert C. Loss-of-function mutations

in the cardiac calcium channel underlie a new clinical entity characterized by ST-segment elevation, short QT intervals, and sudden cardiac death. *Circulation*. 2007;115:442-449.

8. Wilson AJ, Quinn KV, Graves FM, Bitner-Glindzicz M Tinker A. Abnormal KCNQ1 trafficking influences disease pathogenesis in hereditatry long QT syndromes (LQT1). *Cardiovasc Res*. 2005;67:476-486.

9. Ueda K, Nakamura K, Hayashi T, Inagaki N, Takahashi M, Arimura T, Morita H, Higashiuesato Y, Hirano Y, Yasunami M, Takishita S, Yamashina A, Ohe T, Sunamori M, Hiraoka M, Kimura A. Functional Characterization of a Trafficking-defective HCN4 Mutation, D553N, Associated with Cardiac Arrhythmia. *J Biol Chem*. 2004; 279(26) 27194-27198.

10. Anderson CL, Delisle BP, Anson BD, Kilby JA, Will ML, Tester DJ, Gong Q, Zhou Z, Ackerman MJ, January CT. Most LQT2 mutations reduce Kv11.1 (hERG) current by a class 2 (trafficking-deficient) mechanism. *Circulation*. 2006;113:365-373.

11. Jenke M, Sanchez A, Monje F, Stuhmer W, Weseloh RM, Pardo LA. C-terminal domains implicated in the functional surface expression of potassium channels. *EMBO J*. 2003;22(3):395-403.

12. Kanki H, Kupershmidt S, Yang T, Wells S, Roden DM. A structural requirement for processing the cardiac K+ channel KCNQ1. *J Biol Chem*. 2004;279(32):33976-33983.

13. Wiener R, Haitin Y, Shamgar L, Fernandez-Alonso MC, Martos S, Chomsky-Hecht O, Rivas G, Attali B, Hirsch JA. The KCNQ1 (Kv7.1) COOH terminus, a multitiered scaffold for subunit assembly and protein interaction. *J Biol Chem*. 2008;283(9):5815-5830.

14. Inhertited Arrhythmias Database (www.fsm.it/carmoc)

15. Chen J, Sroubek J, Krishnan Y, Li Y, Bian J, McDonald TV. PKA phosphorylation of HERG protein regulates the rate of channel synthesis. *Am J Physiol Heart Circ Physiol*. 2009;296:1244-1254.

16. Barhanin J, Lesage F, Guillemare E, Fink M, Lazdunski M, Romey G. K(V)LQT1 and IsK (minK) proteins associate to form the I(Ks) cardiac potassium current. *Nature*. 1996;384:78–80.

17. Sanguinetti MC, Curran ME, Zou A, Shen J, Spector PS, Atkinson DL, et al. Coassembly of K(V)LQT1 and minK (IsK) proteins to form cardiac I(Ks) potassium channel. *Nature*. 1996;384:80-83.

18. McDonald TV, Yu Z, Ming Z, Palma E, Meyers MB, Wang KW, Goldstein SA, Fishman GI. A minK-HERG complex regulates the cardiac potassium current I(Kr). *Nature*. 1997 Jul 17;388(6639):289-292.

19. Tinel N, Diochot S, Borsotto M, Lazdunski M, Barhanin J. KCNE2 confers background current characteristics to the cardiac KCNQ1 potassium channel. *EMBO J*. 2000;19(23):6326-6330.

20. Splawski I, Timothy KW, Vincent GM, Atkinson DL, Keating MT. Molecular basis of the long-QT syndrome associated with deafness. *N Engl J Med*. 1997; 336:1562–1567.

21. Abbott GW, Sesti F, Splawski I, Buck ME, Lehmann MH, Timothy KW, Keating MT, Goldstein SA. MiRP1 forms IKr potassium channels with HERG and is associated with cardiac arrhythmia. *Cell*. 1999;97:175–187.

22. Abbott G.W., Goldstein S.A. Disease-associated mutations in KCNE potassium channel subunits (MiRPs) reveal promiscuous disruption of multiple currents and conservation of mechanism. *FASEB J*. 2002;16:390-400.

23. Chandrasekhar KD, Bas T, Kobertz WR. KCNE1 subunits require co-assembly with K+ channels for efficient trafficking and cell surface expression. *J Biol Chem*. 2006 ;281(52):40015-40023.

24. Krumerman, A., Gao, A., Bian, J., Melman, Y.F., Kagan, A. and McDonald, T.V. *Am J Physiol Cell Physiol*. 2004;286:1453-1463.

25. Anantharam A, Lewis A, Panaghie G, Gordon E, McCrossan ZA, Lerner DJ, Abbott GW.RNA interference reveals that endogenous Xenopus MinK-related peptides govern mammalian K+ channel function in oocyte expression studies. *J Biol Chem*. 2003;278(14):11739-45

26. Gong Q, Zhang Li, Moss AJ, Vincent MG, Ackerman MJ, Robinson JC, Jones MA, Tester DJ, Zhou Z. A splice site mutation in hERG leads to cryptic splicing in human long QT syndrome. *J Mol Cell Cardiol*. 2008;44(3);502-509.

27. Akhavan A, Atanasiu R, Noguchi T, Han W, Holder N, Shrier A. Identification of the cyclic-nucleotide-binding domain as a conserved determinant of ion-channel cell-surface localization. *J Cell Sci*. 2005;118:2803-2812.

28. Aizawa Y, Ueda K, Wu LM, Inagaki N, Hayashi T, Takahashi M, Ohta M, Kawano S, Hirano Y, Yasunami M, Aizawa Y, Kimura A, Hiraoka M. Truncated KCNQ1 mutant, A178fs/105, forms hetero-multimer channel with wild-type causing a dominant-negative suppression due to trafficking defect. *FEBS Lett*. 2004;574(1-3):145-150.

29. Li X, Xu J, Li M. The human 1261 mutation of the HERG potassium channel results in a truncated protein that contains a subunit interaction domain and decreases the channel expression. *J Biol Chem*. 1997;272(2):705-708.

30. Sato A, Arimura T, Makita N, Ishikawa T, Aizawa Y, Ushinohama H, Aizawa Y, Kimura A. Novel mechanisms of trafficking defect caused by KCNQ1 mutations found in long QT syndrome. *J Biol Chem*. 2009;284(50):35122-35133.

31. Gouas L, Bellocq C, Berthet M, Potet F, Demolombe S, Forhan A, Lescasse R, Simon F, Balkau B, Denjoy I, Hainque B, Baró I, Guicheney P; D.E.S.I.R. Study Group. New KCNQ1 mutations leading to haploinsufficiency in a general population; Defective trafficking of a KvLQT1 mutant. *Cardiovasc Res*. 2004;63(1):60-68.

32. Wilson AJ, Quinn KV, Graves FM, Bitner-Glindzicz M, Tinker A. Abnormal KCNQ1 trafficking influences disease pathogenesis in hereditary long QT syndromes (LQT1). *Cardiovasc Res*. 2005;67(3):476-86.

33. Gong Q, Keeney DR, Robinson JC, Zhou Z. Defective assembly and trafficking of mutant HERG channels with C-terminal truncations in long QT syndrome. *J Mol Cell Cardiol*. 2004;37(6):1225-1233.

34. Gong Q, Zhang L, Vincent M, Horne BD, Zhou Z. Nonsense mutations in hERG cause a decrease in mutant mRNA transcripts by nonsense-mediated mRNA decay in human long-QT syndrome. *Circulation*. 2007;116(1):17-24.

35. Howard M, Frizzell RA, Bedwell DM. Aminoglycoside antibiotics restore CFTR function by overcoming premature stop mutations. *Nat Med*. 1996;2(4):467-469

36. Teng S, Gao L, Paajanen V, Pu J, Fan Z. Readthrough of nonsense mutation W822X in the SCN5A gene can effectively restore expression of cardiac Na+ channels. *Cardiovascular Research*. 2009;83:473-480.

37. Yao Y, Teng S, Li N, Zhang Y, Boyden PA, Pu J Aminoglycoside antibiotics restore functional expression of truncated HERG channels produced by nonsense mutations. *Heart Rhythm*. 2009;6:553-560.

38. Mackenzie KR. Folding and stability of alpha-helical integral membrane proteins. *Chem Rev*. 2006;106(5):1931-1977.

39. Gong Q, Keeney DR, Molinari M, Zhou Z. Degradation of trafficking-defective long QT syndrome type II mutant channels by the ubiquitin-proteasome pathway. *J Biol Chem*. 2005;280: 19419-19425

40. Brodsky JL. The protective and destructive roles played by molecular

chaperones during ERAD (endoplasmic-reticulum-associated degradation). *Biochem J*. 2007;404(3):353-363.

41. Cheung JC, Deber CM. Misfolding of the cystic fibrosis transmembrane conductance regulator and disease. Biochem. 2008;47(6):1465-1473.

42. Rajan RS, Kopito RR. Suppression of wild-type rhodopsin maturation by mutants linked to autosomal dominant retinitis pigmentosa. *J Biol Chem*. 2005;280(2);1284-1291.

43. Yue P, Li Zhaolong, Moult J. Loss of protein structure stability as a major causative factor in mongenic disease. *J Mol Biol*. 2005;353:459-473.

44. Cabral JHM, Lee A, Cohen SL, Chait BT, Li M, Mackinnon R. Crystal structure and functional analysis of the HERG potassium channel N terminus: a eukaryotic PAS domain. *Cell*. 1998;95:649-655.

45. Gustina AS, Trudeau MC. A recombinant N-terminal domain fully restores deactivation gating in N-truncated and long QT syndrome mutant hERG potassium channels. *Proc Natl Acad Sci*. 2009;106(31):13082-13087.

46. Al-Owais M, Bracey K, Wray D. Role of intracellular domains in the function of the herg potassium channel. *Eur Biophys J*. 2009;38:569-576.

47. Harley CA, Jesus CS, Carvalho R, Brito RM, Morais-Cabral JH. Changes in channel trafficking and protein stability by LQT2 mutations in the PAS domain of the EHRG channel. *PLoS One*. 2012;7(3):e32654.

48. Nagy JK, Sanders CR. Destabilizing mutations promote membrane protein misfolding. *Biochemistry*. 2004;43:19-25.

49. Choi MY, Partridge AW, Daniels C, Du K, Lukacs G, Deber CM. Destabilization of the transmembrane domain induces misfolding in a phenotypic mutant of cystic fibrosis transmembrane conductance regulator. *J Biol Chem*. 2005;280(6):4968-4974.

50. Oberai A, Joh NH, Pettit FK, Bowie JU. Structural imperatives impose diverse evolutionary constraints on helical membrane proteins. *Proc Nat Acad Sci*. 2009;106(42):17747-17750.

51. Kauko A, Hedin LE, Thebausd E, Cristobal S, Elofsson A, von Heijne G. Repositioning of transmembrane alpha-helices during membrane protein folding. *J Mol Biol*. 2010;397(1):190-201.

52. Partridge AW, Therien AG, Deber CM. Missense mutations in transmembrane domains of proteins: phenotypic propensity of polar residues for

human disease. *Proteins*. 2004;54(4):648-656.

53. Therien AG, Grant FE, Deber CM. Interhelical hydrogen bonds in the CFTR membrane domain. *Nat Struct Biol*. 2001;8(7):597-601.

54. Gallagher MJ, Ding L, Maheshwari A, Macdonald RL. The GABAA receptor alpha1 subunit epilepsy mutation A322D inhibits transmembrane helix formation and causes proteasomal degradation. *Proc Natl Acad Sci*. 2007;104(32):12999-13004.

55. Meindl-Beinker NM, Lundrin C, Nilsson I, White SH, von Heijne G. *EMBO*. 2006;7(11):1111-1116.

56. Tiwari-Woodruff SK, Schulteis CT, Mock AF, Papazian DM. Electrostatic interactions between transmembrane segments mediate folding of Shaker K+ channel subunits. *Biophys J*. 1997;72:1489-1500.

57. Zhang L, Sato Y, Hessa T, von Heijne G, Lee JK, Kodama I, Sakaguchi M, Uozumi N. Contribution of hydrophobic and electrostatic interactions to the membrane integration of the Shaker K+ channel voltage sensor domain. *Proc Natl Acad Sci*. 2007;104(20):8263-8268.

58. Delisle BP, Slind JK, Kilby JA, Anderson CL, Anson BD, Balijepalli RC, Tester DJ, Ackerman MJ, Kamp TJ, January CT. Intragenic suppression of trafficking-defective KCNH2 channels associated with long QT syndrome. *Mol Pharmacol*. 2005;68:233-40.

59. Zhou Z, Gong Q, January CT. Correction of defective protein trafficking of a mutant HERG potassium channel in human long QT syndrome. Pharmacological and temperature effects. *J Biol Chem*. 1999; 274: 31123–31126.

60. Delisle BP, Anderson CL, Balijepalli RC, Anson BD, Kamp TJ, January CT. Thapsigargin selectively rescues the trafficking deficient LQT2 channels G601S and F805C. *J Biol Chem*. 2003; 278: 35749–35754.

61. Myers MP, Khanna R, Lee EJ, Papazian DM. Voltage sensor mutations differentially target misfolded K+ channel subunits to proteasomal and non-proteasomal disposal pathways. *FEBS Letters*. 2004;568:110-116.

62. Amaral MD. CFTR and chaperones: processing and degradation. *J Mol Neurosci*. 2004; 23: 41-48.

63. Wang X, Venable J, LaPointe P, Hutt DM, Koulov AV, Coppinger J, Gurkan C, Kellner W, Matteson J, Plutner H, Riordan JR, Kelly JW, Yates JR, 3rd, Balch WE. Hsp90 cochaperone Aha1 downregulation rescues misfolding of CFTR in cystic fibrosis. *Cell*. 2006; 127: 803-815.

64. Ficker E, Dennis AT, Wang L, Brown AM. Role of the cytosolic chaperones Hsp70 and Hsp90 in maturation of the cardiac potassium channel HERG. *Circ Res*. 2003; 92:87-100.

65. Gong Q, Keeney DR, Molinari M, Zhou Z. Degradation of trafficking-defective long QT syndrome type II mutant channels by the ubiquitin-proteasome pathway. *J Biol Chem*. 2005;280:19419-19425.

66. Walker VE, AR, Lam H, Shrier A. Co-chaperone FKBP38 promotes HERG trafficking. *J Biol Chem*. 2007;282:23509-23516.

67. Walker VE, WM, Atanasiu R, Hantouche C, Young JC, Shrier A. Hsp40 chaperones promote degradation of the HERG potassium channel. *J Biol Chem*. 2010;285:3319-3329.

68. Crottes D, Martial S, Rapetti-Mauss R, Pisani DF, Loriol C, Pellissier B, Martin P, Chevet E, Borgese F, Soriani O. Sig 1R protein regulates HERG channel expression through a post-translational mechanism in leukemic cells. *J Biol Chem*. 2011;286(32):27947-27958.

69. Guo J, Wang T, Li X, Shallow H, Yang T, Li W, Xu J, Fridman MD, Yang X, Zhang S. Cell surface expression of human ether-a-go-go-related gene (hERG) channels is regulated by Caveolin-3 via the ubiquitin ligase Nedd4-2. *J Biol Chem*. 2012;287(40):33132-33141.

70. Wang X, Matteson J, An Y, Moyer B, Yoo JS, Bannykh S, Wilson IA, Riordan JR, Balch WE. COPII-dependent export of cystic fibrosis transmembrane conductance regulator from the ER uses a di-acidic exit code. *J Cell Biol*. 2004;167:65-74.

71. Heusser K, Yuan H, Neagoe I, Tarasov AI, Ashcroft FM, Schwappach B. Scavenging of 14-3-3 proteins reveals their involvement in the cell-surface transport of ATP-sensitive K+ channels. *J Cell Sci*. 2006;119:4353-4363.

72. Shikano S, Coblitz B, Sun H, Li M. Genetic isolation of transport signals directing cell surface expression. *Nat Cell Biol*. 2005;7:985-992.

73. Nufer O, Hauri HP. ER export: call 14-3-3. *Curr Biol*. 2003;13:391-393.

74. Seemann J, Jokitalo EJ, Warren G. The role of the tethering proteins p115 and GM130 in transport through the Golgi apparatus in vivo. *Mol Biol Cell*. 2000;11:635-645.

75. Roti EC, Myers CD, Ayers R, Boatman DE, Delfosse SA, Chan EK, Ackerman MJ, January CT, Roberston GA. Interaction with GM130 during

HERG ion channel trafficking. Disruption by type 2 congenital long QT syndrome mutations. Human Ether-a-go-go-Related Gene. *J Biol Chem*. 2002;277:47779-47785.

76. Ma D, Jan LY. ER transport signals and trafficking of potassium channels and receptors. *Curr Opin Neurobiol*. 2002;12:287-292.

77. Hasdemir B, Fitzgerald DJ, Prior IA, Tepikin AV, Burgoyne RD. Traffic of Kv4 K+ channel mediated by KChIP1 is via a novel post-ER vesicular pathway. *J Cell Biol*. 2005;171:459-469.

79. Yoo JS, Moyer BD, Bannykh S, Yoo HM, Riordan JR, Balch W.E. Non-conventional trafficking of the cystic fibrosis transmembrane conductance regulator through the early secretory pathway. *J Biol Chem*. 2002; 277:11401-11409.

79. Delisle BP, Underkofler HA, Moungey BM, Slind JK, Kilby JA, Best JM, Foell JD, Balijepalli RC, Kamp TJ, January CT. Small GTPase determinants for the golgi processing and plasmalemmal expression of human ether-a-go-go related (hERG) K+ channels. *J Biol Chem*. 2009;284(5):2844-2853.

80. Seebohm G, Strutz-Seebohm N, Birkin R, Dell G, Bucci C, Spinosa MR, Baltaev R, Mack AF, Korniychuk G, Choudhury A, Marks D, Pagano RE, Attali B, Pfeufer A, Kass RS, Sanguinetti MC, Tavare JM, Lang F. Regulation of endocytic recycling of KCNQ1/KCNE1 potassium channels. *Circ Res*. 2007;100(5):686-692.

81. Seebohm G, Strutz-Seebohm N, Ureche ON, Henrion U, Baltaev R, Mack AF, Korniychuk G, Steinke K, Tapken D, Pfeufer A, Kääb S, Bucci C, Attali B, Merot J, Tavare JM, Hoppe UC, Sanguinetti MC, Lang F. Long QT syndrome-associated mutations in KCNQ1 and KCNE1 subunits disrupt normal endosomal recycling of IKs channels. *Circ Res*. 2008 ;103(12):1451-1457.

82. Guo J, Massaeli H, Xu J, Jia Z, Wigle JT, Mesaeli N, Zhang S. Extracellular K+ concentration controls cell surface density of IKr in rabbit hearts and of the HERG channel in human cell lines. *J Clin Invest*. 2009;119(9):2745-57.

83. Massaeli H, Guo J, Xu J, Zhang S. Extracellular K+ is a prerequisite for the function and plasma membrane stability of HERG channels. *Circ Res*. 2010;106(6):1072-1082.

84. Massaeli H, Sun T, Li X, Shallow H, Wu J, Xu J, Li W, Hanson C, Guo J, Zhang S. Involvement of caveolin in low K+-induced endocytic degradation of cell-surface human ether-a-go-go-related gene (hERG) channels. *J Biol Chem*. 2010;285(35):27259-27264.

85. van der Heyden MA, Smits ME, Vos MA. Drugs and trafficking of ion channels: a new pro-arrhythmic threat on the horizon? *Br J Pharmacol*. 2008;153(3):439-447.

86. Wang L, Dennis AT, Trieu P, Charron F, Ethier N, Hebert TE, Wan X, Ficker E. Intracellular potassium stabilizes human ether-a-go-go-related gene channels for export from endoplasmic reticulum. *Mol Pharmacol*. 2009;75(4):927-937.

87. Zhang J, Wilson GF, Soerens AG, Koonce CH, Yu J, Palecek SP, Thomson JA, Kamp TJ. Functional cardiomyocytes derived from human induced pluripotent stem cells. *Circ Res*. 2009;104(4):30-41.

88. Chouabe C, Neyroud N, Richard P, Denjoy I, Hainque B, Romey G, Drici MD, Guicheney P, Barhanin J. Novel mutations in KvLQT1 that affect Iks activation through interactions with Isk. *Cardiovasc Res*. 2000;45(4):971-980.

89. Moretti A, Bellin M, Welling A, Jung CB, Lam JT, Bott-Flugel L, Dorn T, Goedel A, Hohnke C, Hofmann F, Seyfarth M, Sinnecker D, Schomig A, Laugwitz KL. Patient-specific induced pluripotent stem-cell models for Long-QT syndrome. *N Engl J Med*. 2010;363(15):1397-1409.

90. Biliczki P, Girmatsion Z, Brandes RP, Harenkamp S, Pitard B, Charpentier F, Hebert TE, Hohnloser SH, Baro I, Nattel S, Ehrlich JR. Trafficking-deficient long QT syndrome mutation KCNQ1-T587M confers severe clinical phenotype by impairment of KCNH2 membrane localization: evidence for clinically significant IKr-IKs alpha-subunit interaction. *Heart Rhythm*. 2009;6(12):1792-1801.

91. Ren XQ, Liu GX, Organ-Darling LE, Zhen R, Roder K, Jindal HK, Centracchio J, McDonald TV, Koren G. Pore mutants of HERG and KvLQT1 downregulate the reciprocal currents in stable cell lines. *Am J Physiol Heart Circ Physiol*. 2010;299(5):1525-1534.

92. Soldner F, Laganiere Josee, Cheng AW, Hockemeyer D, Gao Q, Alagappan R, Khurana V, Golbe LI, Myers RH, Lidquist S, Zhang L, Guschin D, Fong LK, Vu BJ, Meng X, Urnov FD, Rebar EJ, Gregory PD, Zhang HS, Jaenisch R. Generation of isogenic pluripotent stem cells differing exclusively at two early onset Parkinson point mutations. *Cell*. 2011;146;318-331.

Chapter II

PASD LQT2 mutations

Introduction

The 354 amino acid N-terminus of Kv11.1 contains a conserved 'EAG' domain (amino acids 1-135) present in the EAG family of K_v channels. The first 25 amino acids contain an amphipathic helix followed by a PASD; a protein module found in signaling proteins throughout prokaryotes and eukaryotes.

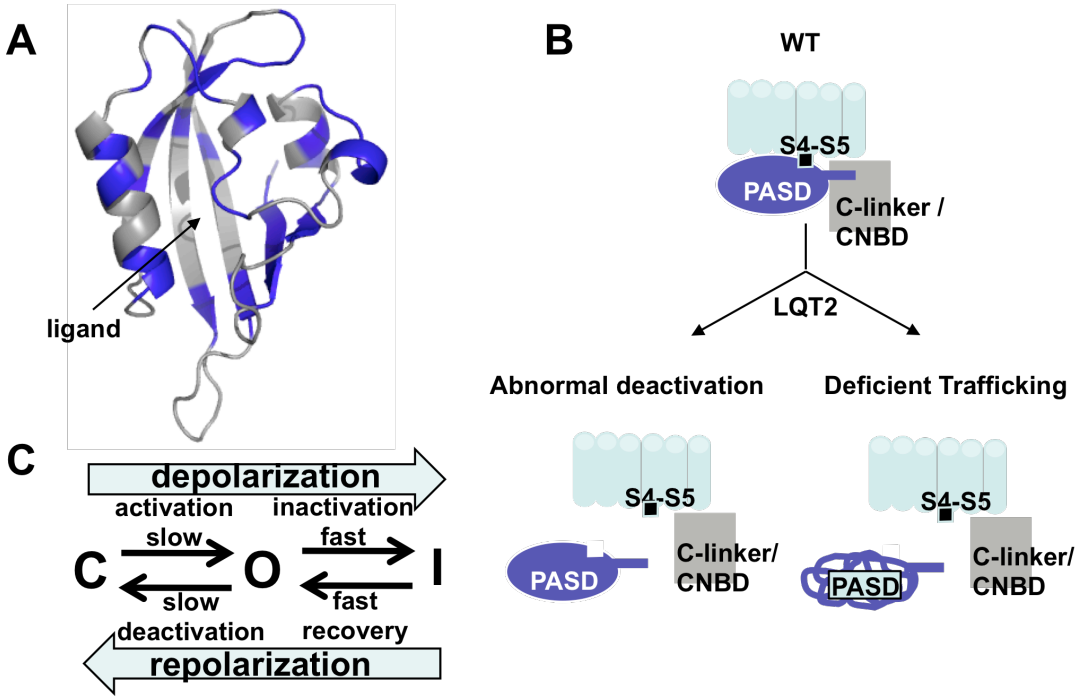

Figure 2-1. The Kv11.1 PASD. A. Structure of the Kv11.1 PASD with LQT2-linked residues in blue. Arrow indicates ligand-binding pocket for most other PASDs. B. Mechanistic model of how PASD mutations cause LQT2. Conformational changes can disrupt interactions between the PASD and CNBD resulting in abnormal deactivation or can misfold resulting in deficient trafficking. C. Gating scheme of Kv11.1. Starting from the closed state (C) channels slowly activate upon depolarization to the open state (0) and then quickly inactivate (I). Upon repolarization, channels quickly recover from inactivation and slowly close.

The crystal structure of the Kv11.1 PASD (PDB 1byw) is available and shown in **Figure 2-1A**.[1] PASDs generally consist of about 100 amino acids that form a structural motif containing a central antiparallel β-sheet flanked by several α-helices. In most proteins, they act as a sensor detecting a variety of inputs from light to chemicals that are transduced to effector domains but no modulatory ligand has been found for the Kv11.1 PASD.[2] However, it is important for Kv11.1 gating. Specifically, interactions between the PASD, CNBD, and S4-S5 linker are thought to give Kv11.1 its slow deactivation property important for its role in the cardiac action potential where the probability of a channel being open (Po) is greater during repolarization than depolarization (**Figure 2-1C)**.[1,3,4,5,6,7,8] From this gating scheme it can be seen that mutations that slow or speed deactivation can cause gain of function or loss of function, respectively. For example, one mutation, E50D, has recently been identified to slow deactivation and cause short QT Syndrome (SQTS) while many others have been identified to speed deactivation and cause LQT2 by disrupting interactions between the PASD and "core" of the channel including the S4-S5 linker and CNBD (**Figure 2-1B**)[1,7,9] However, many of these studies were done using a Xenopus Oocyte expression model where cells are cultured at non-physiological temperature and many LQT2 mutations have been found to be temperature sensitive in mammalian cells.[10,11,12] In fact, many mutations studied in oocytes fail to traffic when expressed in HEK cells.

As shown in **Figure 2-1B**, there seems to be two mechanisms (i.e. gating or defective trafficking) underlying PASD mutations, each of which likely requires

different therapeutic strategies (i.e correcting gating or restoring trafficking). As proof-of-principle, correction of the deactivation mutants R56Q and an EAG deletion was achieved by co-expressing the isolated WT PASD or just the EAG amphipathic helix in Xenopus Oocytes.[13,14] Likewise, trafficking can be restored in HEK cells by targeting mutant mRNA for degradation by RNAi or by culturing cells in high affinity Kv11.1 pore blockers like E4031.[12,15] Developing these therapeutic approaches however requires an understanding of the molecular basis of these mutations. A recent study of ten PASD mutations suggests that PASD mutations behave differently than TMD mutations. Most were not trafficking deficient or correctable with E4031.[16] However, the PASD is a mutational "hotspot" with at least 61 LQT2 mutations at 47 unique sites (**Table 2-2)**. Given the number of mutations and different mechanisms reported within this domain, classifying each mutation is needed to further our molecular understanding of LQT2 and develop mutant-specific therapies.

Results

Trafficking phenotype of homomeric LQT2 PASD mutations

Over 60 PASD missense mutations and a few deletion mutations have been linked to LQT2, yet most have not been studied. To determine the trafficking phenotype of these LQT2 mutations, immunoblot was performed on HEK cells expressing homomeric Kv11.1 cultured at physiological temperature

(37^{0}C), reduced temperature, (27^{0}C) or in the presence of 10μM E4031 (see methods).

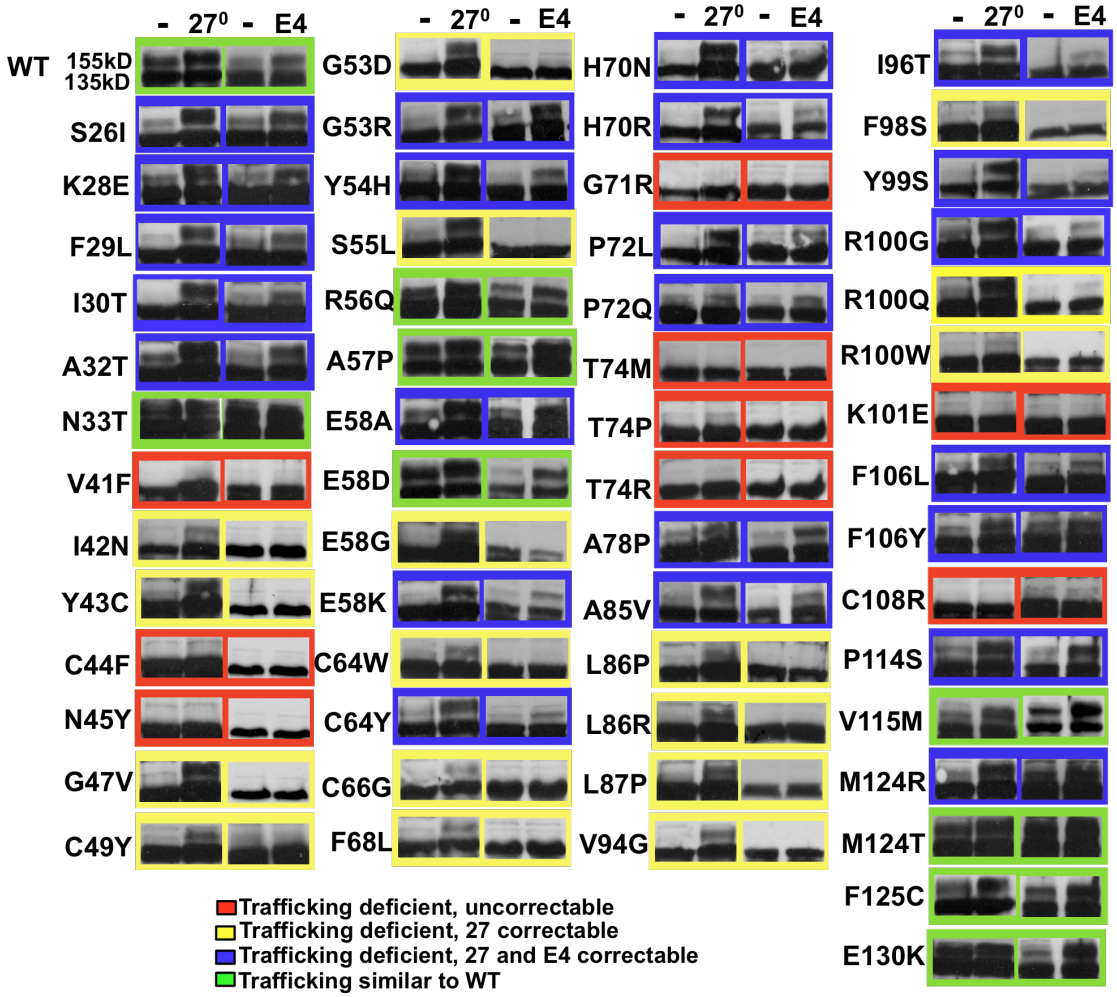

Figure 2-2. Trafficking phenotype of PASD mutations. Immunoblots of transiently transfected HEK cells comparing trafficking under control conditions at 37^{0}C (-), with reduced temperature (27^{0}C) or 24 hrs of culture in E4031 (E4). Mutations are color-coded as follows: trafficking deficient and uncorrectable in red, trafficking deficient but correctable at 27^{0}C in yellow, trafficking deficient but correctable at 27^{0}C and with E4031 in blue and those that traffic similar to WT in green.

Figure 2-2 shows representative immunoblots (n≥2) for 57 mutations studied and color-coded as follows: trafficking deficient and uncorrectable in red, trafficking

deficient but correctable at 27^0C in yellow, trafficking deficient but correctable at 27^0C and with E4031 in blue, and those that traffic similar to WT in green. (Summary in **Table 2-2**) Most mutations were trafficking deficient with 49/57 (86%) having a diminished 155kD band on immunoblot when cultured at 37^0C. 40 of those 49 (82%) could be corrected by culturing cells at reduced temperature and 22 (45%) could be corrected by culturing cells in E4031. While 18 mutations were only temperature correctable, none were only E4031 correctable.

Trafficking phenotype of PASD mutations co-expressed with WT

Since LQT2 is autosomal dominant where only one abnormal allele is present, immunoblots were also performed on HEK cells co-transfected with equal amounts of WT and mutant DNA. Immunoblot analysis showed that nearly all mutants exhibited a decrease in the 155kD band intensity compared to WT alone (**Figure 2-3A**) This decrease was comparable to cells transfected with WT and empty vector. Most of the mutations with a 155kD band similar to WT showed a weak 155kD band when expressed alone (**Figure 2-2**).

To determine if co-expression changes the trafficking phenotype of E4031 treated cells, ten mutations were tested and no differences were found. Eight mutations remained uncorrectable with E4031 while two positive controls (F106L and E58K) were still correctable (**Figure 2-3B**).

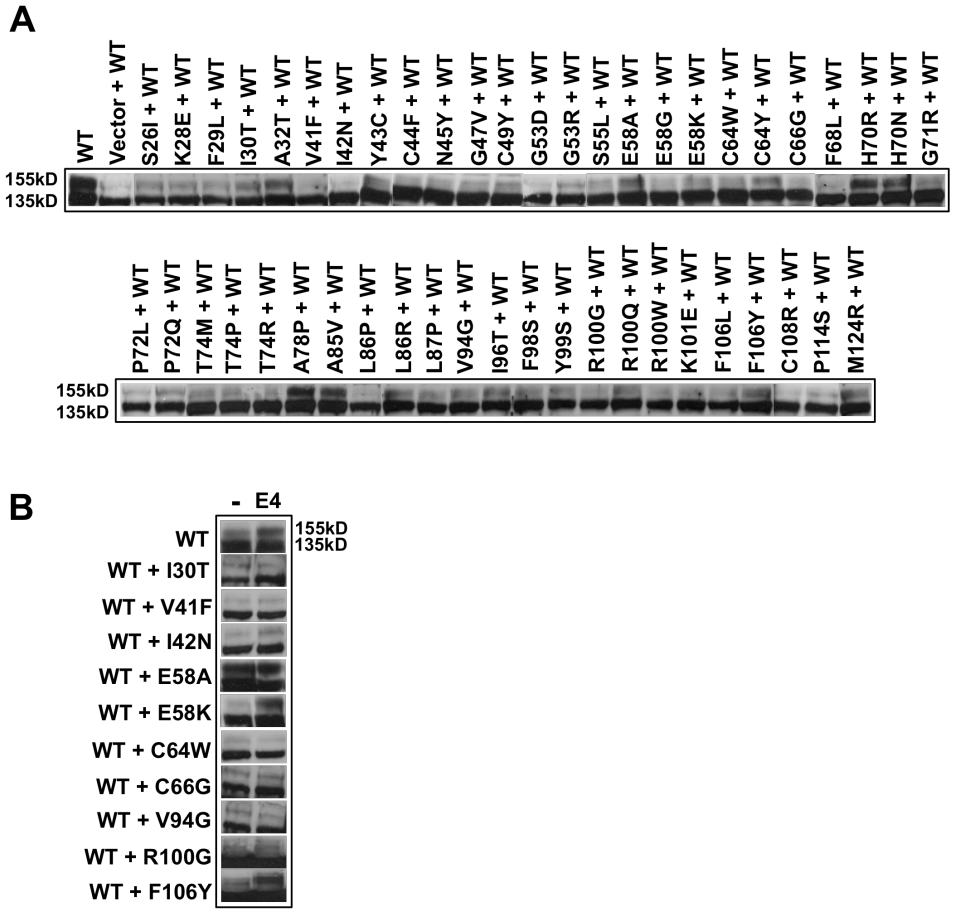

Figure 2-3. Trafficking phenotype of PASD mutations co-expressed with WT. A. Immunoblot analysis of co-expressed channels under control conditions of culture at 37^0C. B. Immunblot analysis of heteromeric channels under control conditions (-) at 37^0C compared to culture for 24hrs in E4031 (E4).

Structural context of LQT2 PASD mutations

PASD mutations are located throughout the structure (see **Figure 1A**). To determine if any relationships exist between trafficking phenotype and location, mutations were mapped onto the structure (PDB 1byw) (**Figure 2-3)**. While no phenotype/location relationship exists for E4031 or 27^0C, mutations that traffic

normally all lie near a hydrophobic surface important for deactivation (**Figure 2-3B**).

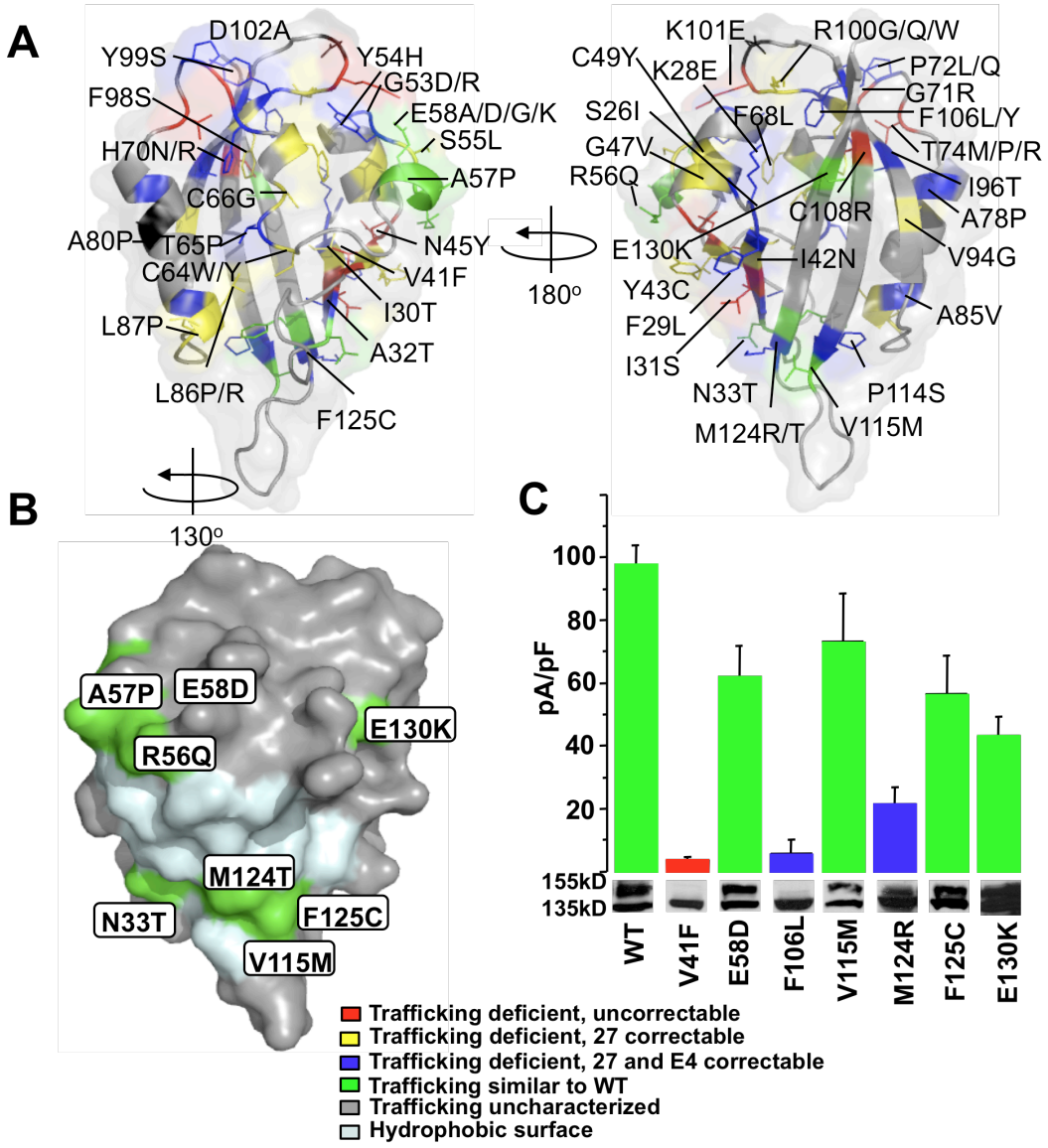

Figure 2-4. Structural context of PASD mutations. A. Location of all LQT2 mutations. Mutations are color-coded as follows: trafficking deficient and uncorrectable in red, trafficking deficient but correctable at 27^{0}C in yellow, trafficking deficient but correctable at 27^{0}C and with E4031 in blue and those that traffic similar to WT in green. B. Surface representation showing the location of mutations that traffic normally. Hydrophobic surface colored cyan. C. Current densities and immunoblots of stably transfected cells and color-coded the same as in panel A.

For example, N33T and R56Q were reported to have faster deactivation and E58D, A57P, V115M, M124T and F125C are located nearby. E130K also traffics normally but is not located in the hydrophobic patch. To determine if these trafficking-competent mutations express currents, current densities were measured using stably transfected cells for each mutation (except A57P) as well as trafficking-deficient V41F and F106L for comparison. V41F (3.7±1.1 pA/pF, n=5) and F106L (5.6±4.6 pA/pF, n=5) showed no current while mutations that trafficked similar to WT (97.7 ±6.2, n=9) showed large currents (**Figure 2-4C**). See **Table 2-1** for values. M124R, which showed a weak 155kD band on most immunoblots expressed some current (21.5 ±5.3 pA/pF, n=7). Since there is variability between different stable cell lines of the same mutation, statistical comparisons to WT were not done. To determine if these mutations exhibit abnormal gating, activation, deactivation, and inactivation properties were studied using stably transfected cells. Values are reported in **Table 2-1.** Statistically significant differences from WT were found for E130K, M124R and F125C **(Figure 2-5)**. The $V_{1/2}$ of E130K was shifted -10mV (**Figure 2-5A**). Deactivation measured at -50mV was faster for M124R and F125C (**Figure 2-5B**). E58D had slower inactivation (**Figure 2-5C**). The gating properties of V115M were similar to WT.

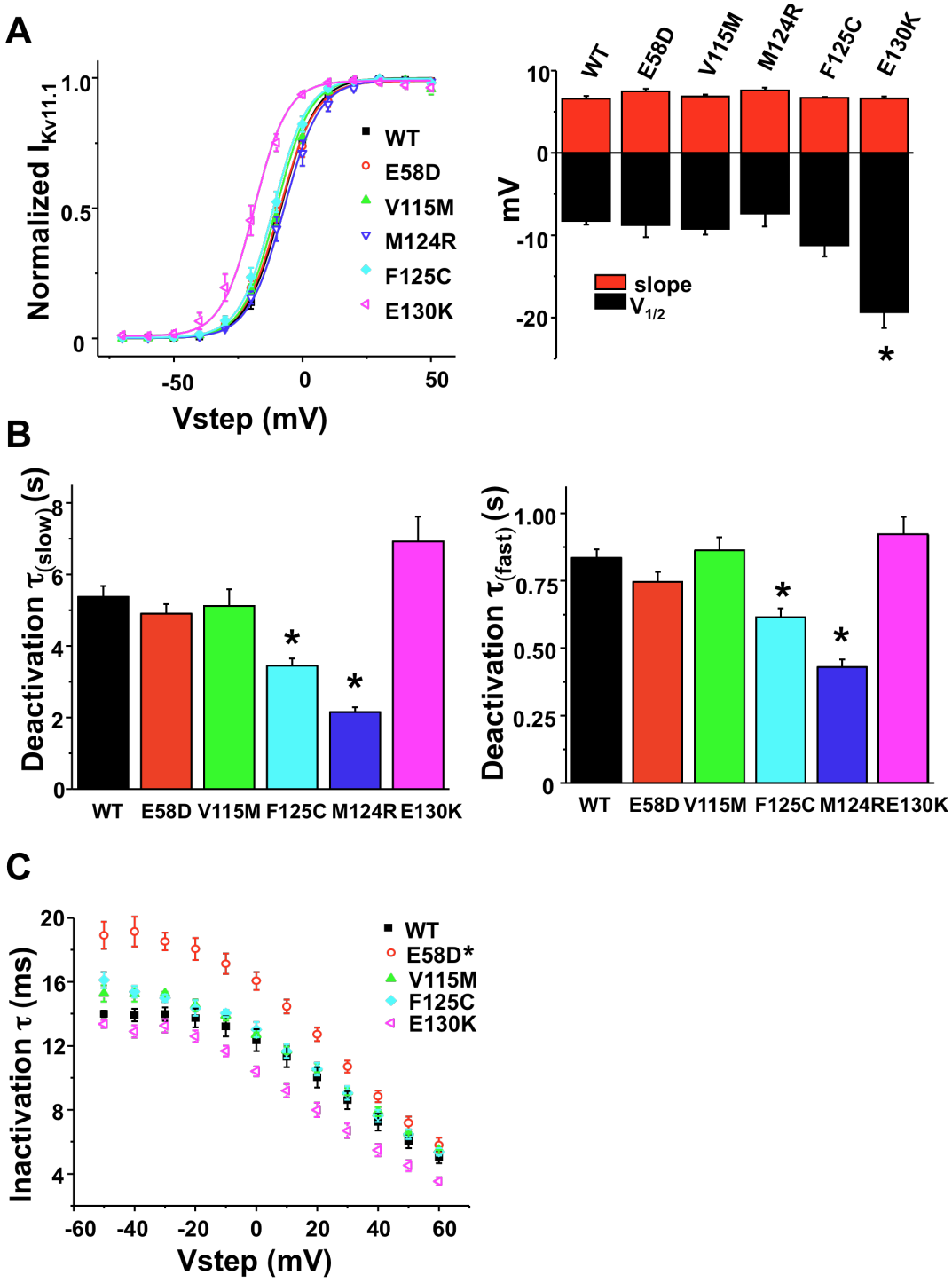

Figure 2-5. Biophysical properties of PASD mutations. A. I-V relationships and slope factors. B. Deactivation time constants determined at Vstep to -50mV. C. Inactivation time constants determined at 0mV. Asterisks indicate statistical significance ($p<0.05$).

Table 2-1. Biophysical properties of Kv11.1 mutations

LQT2	Current Density	Activation		Deactivation at -50mV		Inactivation at 0mV
	pA/pF	$V_{1/2}$ (mv)	slope (mv/e-fold)	tau slow (s)	tau fast (ms)	tau (ms)
WT	97.7±6.2 (9)	-8.3±0.4 (5)	6.5 ±0.4 (5)	5.3±0.3 (5)	835±32 (5)	12.4±0.7 (3)
E58D	62.2±9.7 (8)	-8.8±1.5 (7)	7.5±0.3 (7)	4.9±0.3 (8)	746±37 (8)	**16.1±0.6*** (4)
V115M	73.1±15.3 (9)	-9.2±0.7 (8)	6.8±0.2 (8)	5.1±0.5 (4)	863±48 (4)	12.7±0.1 (3)
M124R	21.6±5.3 (7)	-7.3±1.6 (4)	7.6±0.3 (4)	**2.2±0.1*** (5)	**430±28*** (5)	n/a
F125C	54.1±13.7 (9)	-11.2±1.4 (9)	6.7±0.1 (9)	**3.4±0.2*** (9)	**615±33*** (9)	13.0±0.5 (4)
E130K	43.2±6.1 (7)	**-19.4±1.9*** (9)	6.6±0.3 (9)	6.9±0.7 (7)	922±65 (7)	10.4±0.3 (6)
S706C	97.7±6.2 (6)	-14.4±2.3 (5)	6.6±0.4 (5)	5.6±0.7 (5)	914±65 (5)	13.4±1.6 (3)
I711V	45.5±4.0 (4)	-5.9±1.8 (4)	7.6±0.6 (4)	**3.2±0.2*** (4)	**512±16*** (4)	n/a
D767Y	73.1±9.7 (5)	**-21.0±1.2*** (5)	6.1±0.2 (5)	**3.8±0.3*** (4)	741±82 (4)	11.4±0.4 (4)
R791W	105±11 (4)	**-20.5±1.4*** (4)	6.1±0.2 (4)	**3.1±0.6*** (4)	620±104 (4)	16.0±2.6 (4)
R835W	17.2±1.8 (5)	**7.8±1.6*** (5)	**9.0±0.6*** (5)	**1.9±0.2*** (4)	**416±31*** (4)	12.6±0.2 (3)
R1005Q	97.7±6.2 (7)	**-14.6±0.5*** (7)	6.4±0.3 (7)	4.7±0.3 (6)	823±43 (6)	**15.1±0.6*** (5)
L1049P	34.6±4.5 (7)	**-17.0±2.5*** (5)	7.7±0.6 (5)	**11.3±1.0*** (5)	**1440±24*** (5)	10.6+0.5 (5)
L1066V	74.3±8.7 (6)	**-0.5±0.8*** (5)	7.1±0.4 (5)	4.0±0.2 (4)	719±29 (4)	**18.9±1.1*** (4)
V644L	62.0±6.4 (12)	-10.6±1.7 (7)	6.6±0.4 (7)	4.8±0.3 (4)	790±87 (4)	**8.9±0.3*** (5)
I662T	73.1±10.0 (8)	-8.4±1.0 (6)	7.3±0.1 (6)	7.5±0.6 (5)	822±57 (5)	10.6±0.6 (4)

Bold asterisks indicate statistical significance from WT ($p<0.05$)

PASD mutations are destabilizing

Several LQT2 mutations have been reported to destabilize the PASD. To test destabilization as a possible cause for the 49 mutations identified in **Figure 2-2**, several bioinformatics tools were used. First, evolutionary conserved and buried residues have been shown to be important for protein stabilization and occur more frequently in disease.[17] Using ASAView and ConSurf, the average solvent accessibility of LQT2 residues was 26 % compared to 32% for all residues and the average conservation score for LQT2 residues was 6.8 (9 being the highest) compared to 4.7 for all residues. Values for all LQT2 residues are listed in **Table 2-2**. Next, the stability prediction web servers: PolyPhen, MUpro, CUPSAT, Eris, and I-Mutant 2.0 in addition to FoldX found that overall, about 75% or more of

LQT2 mutations are “possibly to probably destabilizing” (inset **Figure 2-6)** (see methods). Since FoldX was reported to be successful in correlating FoldX energy changes with the phenotype of disease-linked rhodopsin mutations, values for each mutation were plotted and color-coded based on trafficking phenotype (**Figure 2-6**).[18]

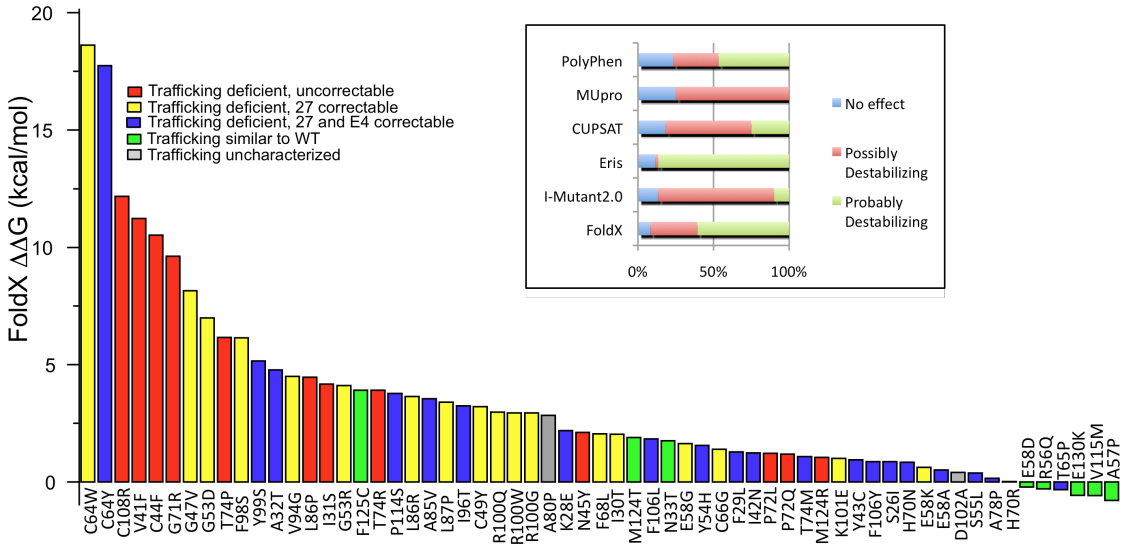

Figure 2-6. FoldX analysis of PASD mutations. The more positive DDG is, the more destabilizing the mutation is. Mutations are color-coded as follows: trafficking deficient and uncorrectable in red, trafficking deficient but correctable at 27^{0}C in yellow, trafficking deficient but correctable at 27^{0}C and with E4031 in blue and those that traffic similar to WT in green. Uncharacterized mutations are shown in gray.

Overall, there is a broad range of stabilities with some correlations. Most of the uncorrectable mutations shown in red group near the left (most destabilizing) whereas many that traffic normally (green) group near the right (no effect).

To complement the bioinformatics analysis, the solubility of each mutant domain expressed in *E.coli* was used as a qualitative measure of stability (see methods). **Figure 2-7** shows the total soluble protein for 52 LQT2 mutations normalized to WT and color-coded according to their trafficking phenotype. Example immunoblots are shown in the inset. In general, solubility correlated with trafficking phenotype where the least soluble mutations having the most severe trafficking phenotype and vice versa. In addition, E4031 correctable mutations are generally more soluble than uncorrectable ones. To rule out loss of protein expression as the reason for less protein on immunoblots, total cell lysates were also run and all mutations expressed similarly to WT (inset **Figure 2-7**).

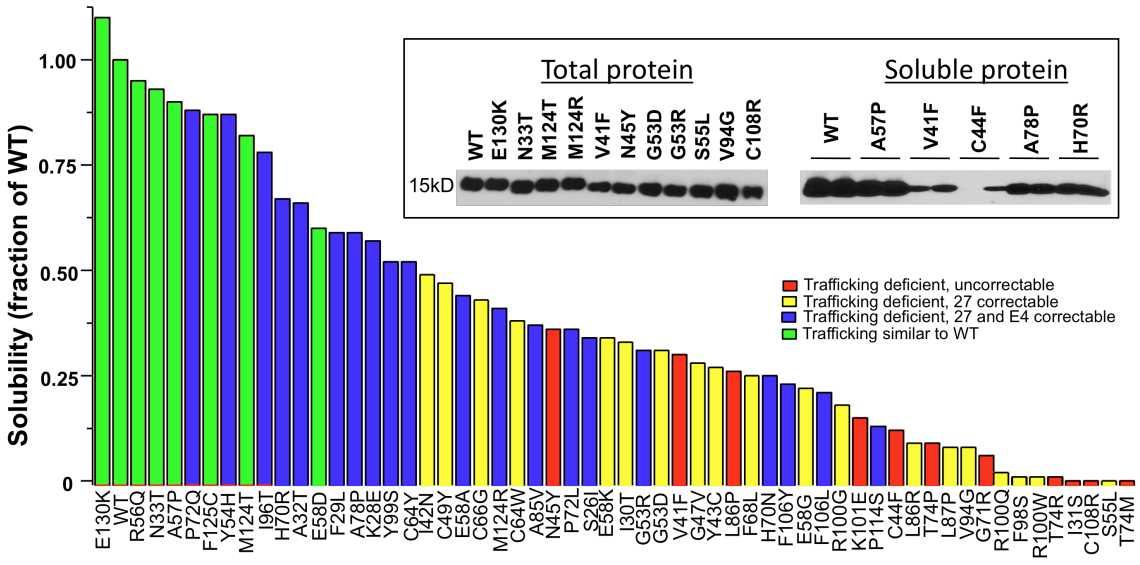

Figure 2-7. Solubility of mutant PASDs. Inset shows representative immunoblots of total protein and soluble protein (in duplicate). Mutations are color-coded as follows: trafficking deficient and uncorrectable in red, trafficking deficient but correctable at 27^0C in yellow, trafficking deficient but correctable at 27^0C and with E4031 in blue and those that traffic similar to WT in green.

PASD second-site suppressor mutations

While PASD misfolding seems to be one major determinant of LQT2, the structural basis of misfolding is largely unknown. Misfolding can be due to many factors including over-packing, cavity formation, loss of ionic interactions, etc. For example, V41 and C64 are buried buried in the core of the PASD. Since the LQT2 mutations V41F and C64Y/W introduce larger hydrophobic side-chains, overpacking was tested as a cause for misfolding and deficient trafficking (**Figure 2-8A**). Hydrophobic mutations of different sizes were generated at V41 and C64 to test their trafficking phenotype at 37^0C and 27^0C. The trend shows a more severe trafficking phenotype as the hydrophobic side-chain size increases (**Figure 2-8C**). In addition, the solubility of the mutant domains expressed in *E.coli* decreases as the side-chain size increases (**Figure 2-8E**).

To further support over-packing as the cause of misfolding, nearby side-chains that likely clash with LQT2-V41F or LQT2-C64W were mutated to smaller residues. Immunoblots in **Figure 2-8C** show that trafficking of LQT2-V41F was improved with C64A, C64G or Q61G at 27^0C but not 37^0C. Immunoblots and current densities of stably transfected cells showed that trafficking of LQT2-C64W (3.8±0.8 pA/pF, n=4) can be improved at 37^0C with C39G (37.8±3.5 pA/pF, n=3) or Q61G (69.6±12.7 pA/pF, n=3) (**Figure 2-8D**). Immunoblot also shows that LQT2-C64Y can also be improved with C39G. Q61G was not tested. A sequence alignment with other distantly related PASDs reveals that nearly all other PASDs contain a glycine at position 61 in contrast to a glutamine for the EAG family of channels (**Figure 2-8B**).

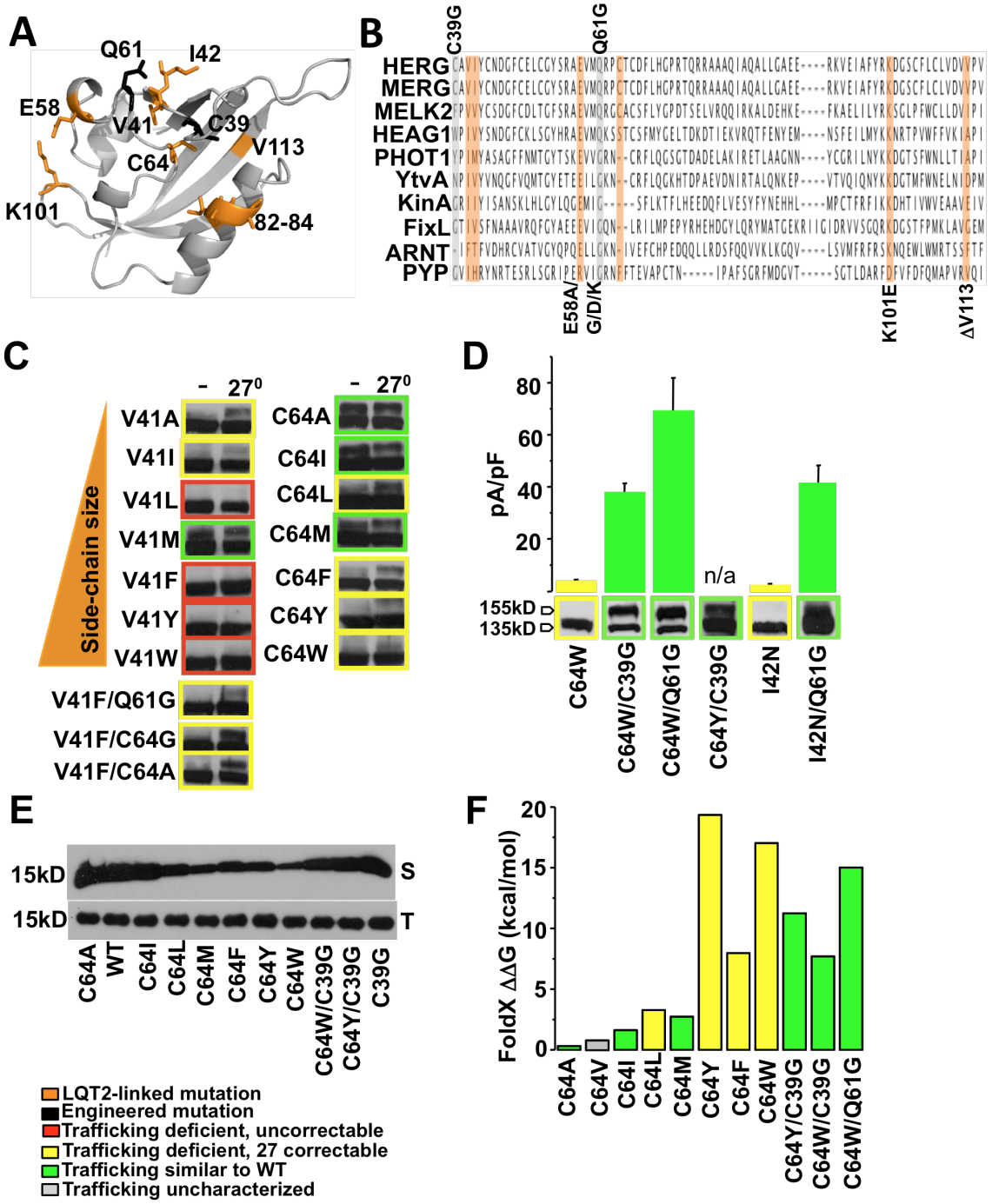

Figure 2-8. Mechanism and correction of PASD mutations. A. Location of LQT2 (orange) and suppressor (black) mutations. B. Sequence alignment of PASDs. LQT2 mutations highlighted in orange and suppressor mutations highlighted in gray. C. Immunblots of V41 and C64 mutations color-coded as follows: trafficking deficient and uncorrectable in red, trafficking deficient but correctable at 27^{0}C in yellow and those that traffic similar to WT in green. D.

Current densities of LQT2 mutations with and without suppressor mutations and color-coded the same as in panel C. E. Immunoblots of recombinant PASDs (T=total protein, S=soluble fraction). F. FoldX analysis of C64 mutations color-coded the same as in C. Gray indicates uncharacterized.

Q61G was then tested on other nearby LQT2 mutations. Immunoblots and current densities of stably transfected cells show that trafficking of LQT2-I42N (2.2±0.7 pA/pF, n=3) can be improved at 37^0C with Q61G (41.9±6.3 pA/pF, n=6) (**Figure 2-8D).** These second-site suppressor mutations also increase the solubility and FoldX predicted stability compared to WT (**Figure 2-8E and F**).

Using ESBRI, a program that predicts potential ionic interactions within a protein, two highly conserved residues E58 and K101 were identified. Five LQT2-mutations locate to these two residues (E58A,D,G and K and K101E) and all but the conserved E58D mutation are trafficking deficient. Neither K101E nor K101D corrected E58K (data not shown). Using CaPTURE, a program that predicts potential cation-pi interactions within a protein, the highly conserved residues R100 and F106 were identified. Five mutations locate to these two residues (F106L,Y and R100G,Q, and W) and all are trafficking deficient but with different phenotypes. R100G,Q and W are correctable by culturing at 27^0C only whereas R100G, F106L and Y are also E4031 correctable. (**Figure 2-2**).

Trafficking analysis of PASD deletion mutations

The Kv11.1 PASD also contains two uncharacterized LQT2 deletion mutations ΔV113 and Δ82-84 (**Figure 2-8A**). Immunoblot analysis of transiently

transfected cells shows that both are trafficking deficient (**Figure 2-9**). Neither can be corrected at 27^0C or with E4031 (data not shown).

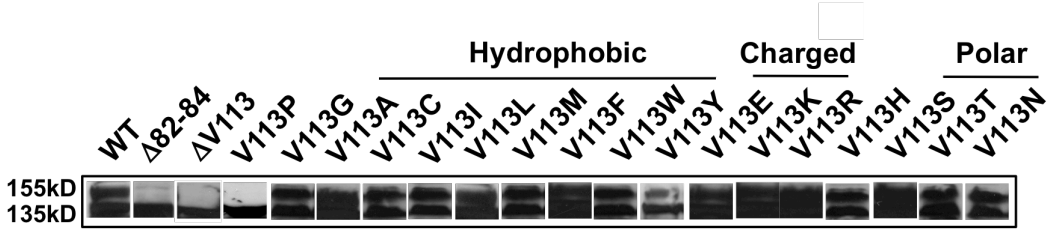

Figure 2-9. Site-saturation mutagenesis of ΔV113. Immunoblot analysis under control conditions.

Unlike missense mutations, which disrupt side-chains (and backbone for proline substitutions), deletion mutations might disrupt trafficking from loss of backbone interactions, side chain interactions, or both. Inspired by a similar rationale and study of the Δ508 CFTR mutation, site-saturation mutagenesis of ΔV113 (except aspartate) revealed that all mutations traffic normally except for proline indicating that loss of backbone interactions solely contribute to the trafficking-deficient phenotype.[19]

Table 2-2. Properties of PASD mutations

LQT2 PAS	Class 2	27	E4	WT	Gen Ref	Phen Ref	Con Surf	ASA View	FoldX	Solubility
S26I	Y	+	+	+	1	a	6	83.6	0.87	0.34
K28E	Y	+	+	+	1	a	7	27.2	2.19	0.57
F29L	Y	+	+	+	1	a	7	25.4	1.29	0.59
I30T	Y	+	+	+	2	a	4	0	2.03	0.33
I31S	Y	-	-	+	1	b	8	17.8	4.17	0
A32T	Y	+	+	+	2	a	6	0	4.78	0.66
N33T	N				1	a	9	36.2	1.76	0.93
V41F	Y	-	-	+	2	a	7	0	11.24	0.3
I42N	Y	+	-	+	3	a	6	35.7	1.24	0.49
Y43C	Y	+	-	+	1	a	7	45.4	0.95	0.27
C44F	Y	-	-	+	1	a	7	0	10.53	0.12
N45Y	Y	-	-	+	2	a	9	11.6	2.12	0.36
G47V	Y	+	-	+	1	a	7	14	8.15	0.28
C49Y	Y	+	-	+	1	a	4	11.1	3.21	0.47
G53D	Y	+	-	+	2	a	9	50.8	6.99	0.31
G53R	Y	+	+	+	1	a	9	50.8	4.11	0.31
Y54H	Y	+	+	+	2	a	9	17.3	1.56	0.87
S55L	Y	+	-	+	1	a	3	46.1	0.38	0
R56Q	N				1	a	1	40.6	-0.29	0.95
A57P	N				2	a	1	78	-0.78	0.9
E58A	Y	+	+	+	1	a	8	28.6	0.62	0.44
E58D	N			+	1	a	8	28.6	0.51	0.6
E58G	Y	+	-	+	1	a	8	28.6	1.64	0.22
E58K	Y	+	-	+	1	a	8	28.6	-0.22	0.34
C64W	Y	+	-	+	2	a	6	0.7	18.62	0.38
C64Y	Y	+	+	+	1	a	6	0.7	17.74	0.52
T65P	Y	+	+	+	1	c	9	21.6	-0.33	n/a
C66G	Y	+	-	+	1	a	7	0	1.39	0.43
F68L	Y	+	-	+	1	a	7	18.9	2.05	0.25
H70N	Y	+	+	+	2	a	9	33	0.84	0.25
H70R	Y	+	+	+	1	a	9	33	0.02	0.67
G71R	Y	-	-	+	1	a	7	36.8	9.62	0.06
P72L	Y	+	+	+	2	a	1	85.3	1.23	0.36
P72Q	Y	+	+	+	1	a	1	85.3	1.19	0
T74M	Y	-	-	+	2	a	7	16.6	6.16	0
T74P	Y	-	-	+	2	a	7	16.6	3.91	0.09
T74R	Y	-	-	+	2	a	7	16.6	1.08	0.09
A78P	Y	+	+	+	1	a	2	5.4	0.15	0.59
A80P	n/a				3	n/a	1	50.8	2.84	n/a
A85V	Y	+	+	+	1	a	8	0	3.55	0.37
L86P	Y	-	-	+	2	a	4	8.2	4.46	0.26
L86R	Y	+	-	+	1	a	4	8.2	3.64	0.09

L87P	Y	+	-	+	1	a	1	8.2	3.4	0.08
V94G	Y	+	-	+	2	a	6	3.9	4.5	0.08
I96T	Y	+	+	+	1	a	6	0.5	3.25	0.78
F98S	Y	+	-	+	?	a	9	1	6.14	0.01
Y99S	Y	+	+	+	1	a	8	18.2	5.16	0.52
R100G	Y	+	+	+	1	a	9	19.6	2.95	0.18
R100Q	Y	+	-	+	1	a	9	19.6	2.95	0.02
R100W	Y	+	-	+	2	a	9	19.6	2.98	0.01
K101E	Y	-	-	+	1	a	8	53	1.01	0.15
D102A	n/a				2	n/a	8	82.4	0.41	n/a
F106L	Y	+	+	+	3	a	9	0.5	0.87	0.21
F106Y	Y	+	+	+	2	a	9	0.5	1.84	0.23
C108R	Y	-	-	+	2	a	9	0	12.17	0
P114S	Y	+	+	+	1	a	9	12	3.77	0.13
V115M	N				2	a	7	26.7	-0.58	n/a
M124R	Y	+	+	+	1	a	7	29.5	1.04	0.41
M124T	N				1	a	7	29.5	1.9	0.82
F125C	N				2	a	5	2.5	3.91	0.87
E130K	N				3	a	4	25.8	-0.57	1.1

The column labeled class 2 indicates which mutations are trafficking deficient in control (37^{0}C) conditions (Y=yes, N=no). The columns labeled 27 (27^{0}C) and E4 (E4031) indicate the trafficking phenotype of the class 2 (trafficking deficient) LQT2-Kv11.1 channels in these conditions. The plus (+) indicates an increase in the density of the 155kDa Kv11.1 protein band and a minus (-) indicates no change from the control immunoblot pattern. The column labeled WT indicates whether a 155kDa band was present or not upon co-expression of WT and LQT2-Kv11.1 channels. The ConSurf column indicates the ConSurf computed conservation score for each residue ranging from 1 (highly variable) to 9 (highly conserved). The ASAView column indicates the ASAView computed % solvent accessibility of each residue. The FoldX column indicates the FoldX computed change in stability of each mutation where $\Delta\Delta G \geq 0$ is destabilizing and $\Delta\Delta G \leq 0$ is stabilizing. The solubility column indicates what % of the recombinant mutant domain was soluble when expressed in *E.coli* compared to WT (N≥2). The GenRef and PhenRef columns indicate the resources for the genotyping and trafficking phenotype classifications. Refereneces are: (1) IAD[20], (2), Kapplinger[21], (3) other, (a) this study, (b) Anderson[12], (c) other.

Discussion

In contrast to a recent report of 10 PASD mutations by Harley and co-workers, the 57 mutations characterized in this study show that most PASD mutations are indeed trafficking deficient and that many can be corrected by E4031.[16] This underscores the importance of this comprehensive analysis in understanding the molecular properties of PASD mutations. Also, they found that H70R and A78P trafficked normally in contrast to the results shown in **Figure 2-1**. These differences are not surprising, which may reflect the different techniques used for characterization. Immunoblots of H70R and A78P showed a weak to strong 155kD band but were less than WT. Another example is M124T, which is trafficking-competent based on immunoblot but shows a 30% current reduction using *Xenopus oocytes* in another study.[22] Another example is the TMD T421M mutation, which is trafficking-competent in HEK cells but slightly trafficking-deficient in a rat cardiomyocyte over-expression model (**Figure 2-1**).[23] Similarly, E4031 correction is not as reproducible for some mutations. K28E was correctable in this study and in another report but was not reproducible in the Harley study.[10,16] These examples illustrate that not all mutations show a clear phenotype which may reflect the expression model used and/or technique used for characterization.

Electrophysiological characterization of the trafficking-competent mutations revealed that most mutations had a small, if any, effect on Kv11.1 gating. The trafficking-deficient M124R and trafficking-competent F125C both have faster deactivation similar to other mutations located in the same region.

This is consistent with loss-of-function. Interestingly, the E130K channels open sooner and E58D channels have slower inactivation, which predict gain of function characteristic of SQTS and V115M had no effect. [24] Possible explanations for these confounding results are 1) they are trafficking deficient, which is not recapitulated in the HEK model, 2) an unknown mechanism accounts for their loss of function, or 3) they are simply benign variants, which has been suggested for other LQT2-linked mutations.[12,25]

Despite these few exceptions, a clear loss-of-function mechanism (i.e. defective trafficking) was reported for nearly all other mutations. A few trafficking deficient mutations did show a robust 155kD when co-expressed with WT and these mutations need to be tested further. In a study of R56Q, which traffics normally and deactivates faster, currents from co-expression of WT Kv11.1 and R56Q Kv11.1 subunits had properties intermediate to that form either subunit alone.[26]

One interesting and important correlation was that E4031 only corrects mutations that are less severe. That is, most E4031 correctable mutations 1) already show a slight 155kD band like H70R and A78P, 2) are all correctable at 27^0C, and 3) are more soluble than uncorrectable mutations. Supporting this is a quantitative analysis done by Harley and co-workers of ten mutations showing that trafficking deficient mutations in general are more destabilizing, some with decreased folding efficiency. Interestingly they found that F29L and G53R are not destabilizing but still fail to traffic normally. Since they lie near a hydrophobic surface thought to interact with other parts of the channel, they suggest that

these mutations may affect other parts of the channel that lead to misfolding. This mechanism has been reported for the TMD mutation N470D.[27] Given that at least 86% of the mutations are trafficking deficient and most are likely destabilizing, one correction strategy might be to identify drugs that target and improve PASD stability. Since many PASD mutations are temperature and E4031 correctable, their affect on Kv11.1 misfolding does not seem to be too severe and small increases in stabilization might be enough to improve trafficking. This strategy has been successful in correcting the misfolding ΔF508 CFTR mutation, the p53 tumor suppressor protein and others.[28,29,30] Strategies like these are needed that can improve trafficking without also blocking the channel as E4031 does.

References

1. Morais-Cabral JH, Lee A, Cohen SL, Chait BT, Li M, Mackinnon R. Crystal structure and functional analysis of the HERG potassium channel N terminus: a eukaryotic PAS domain. *Cell.* 1998;95(5):649-55.

2. Moglich A, Ayers RA, Moffat K. Structure and Signaling Mechanism of Per-ARNT-Sim Domains. *Structure*. 2009;17(10):1282-94.

3. Li Q, Gayen S, Chen AS, Huang Q, Raida M, Kang C. NMR solution structure of the N-terminal domain of hERG and its interaction with the S4-S5 linker. 2010. *Biochem Biophys Res Comm*. 403(1):126-32.

4. Gustina AS, Trudeau MC. Herg potassium channel gating is mediated by N- and C-terminal region interactions. *J Gen Physiol*. 2011;137(3):315-325.

5. Muskett FW, Thouta S, Thomson SJ, Bowen A, Stanseld PJ, Mitcheson JS. Mechanistic insight into hERG channel deactivation gating from the solution structure of the eag domain. *J Biol Chem*. 2011;286(8):6184-6191.

6. Ng CA, Perry MD, Tan PS, Hill AP, Kuchel PW, Vandenberg JI. The S4-S5 linker acts as a signal integrator for HERG K+ channel activation and deactivation gating. *PLoS One*. 2012;7(2):e31640.

7. Chen J, Zou A, Splawski I, Keating MT, Sanguinetti MC. Long QT syndrome-associated mutations in the PER-Arnt-Sim (PAS) domain of HERG potassium channels accelerate channel deactivation. *J Biol Chem*. 1999;274(15):10113-8.

8. Wang J, Myers CD, Robertson GA. Dynamic control of deactivation gating by a soluble amino-terminal domain in HERG K channels. *J Gen Physiol*. 2000;115(6):749-758.

9. Martinez HB, Hu D, Gollob M, Antzelevitch C. Novel gain-of-function N terminal KCNH2 mutation associated with Short QT Syndrome. *Circulation*. 2012; AHA abstract.

10. Rossenbacker T, Mubagwa K, Jongbloed RJ, Vereecke J, Devriendt K, Gewillig M, Carmeliet E, Collen D, Heidbuchel H, Carmeliet P. Novel mutation in the Per-Arnt-Sim domain of KCNH2 causes a malignant form of long-QT syndrome. *Circulation*. 2005;111:961-968.

11. Paulussen A, Raes A, Matthijs G, Snyders DJ, Cohen N, Aerssens J. A novel mutation (T65P) in the PAS domain of the human potassium channel HERG results in the long QT syndrome by trafficking deficiency. *J Biol Chem*. 2002;277(50):48610.

12. Anderson CL, Delisle BP, Anson BD, Kilby JA, Will ML, Tester DJ, Gong Q, Zhou Z, Ackerman MJ, January CT. Most LQT2 mutations reduce Kv11.1 (hERG) current by a class 2 (trafficking-deficient) mechanism. *Circulation*. 2006;113(3):365-73.

13. Gustina AS and Trudeau MC. A recombinant N-terminal domain fully restores deactivation gating in N-truncated and long QT syndrome mutant hERG potassium channels. *Proc Natl Acad Sci*. 2009. 106(31): 13082-13087.

14. Gianulis EC and Trudeau MC. Rescue of aberrant gating by a genetically encoded PAS(Per-Arnt-Sim) domain in several long QT syndrome mutant human ether-a-go-go related gene potassium channels. *J Biol Chem*. 2011;286(25):22160-22169.

15. Lu X, Yang X, Huang X, Huang C, Sun HH, Jin L, Xu W, Mao H, Guo J, Zhou J, Lian J. RNA interference targeting E637K mutation rescues hERG channel currents and restores its kinetic properties. *Heart Rhythm*. 2012 (Epub ahead of print)

16. Harley CA, Jesus CS, Carvalho R, Brito RM, Morais-Cabral JH. Changes in channel trafficking and protein stability caused by LQT2 mutations in the PAS domain of the HERG channel. *PLoS One*. 2012;7(3):e32654.

17. Vitkup D, Sander C, Church GM. The amino-acid mutational spectrum of human genetic disease. *Genome Biol*. 2003;4(11)R72.

18. Rakoczy EP, Kiel C, McKeone R, Stricher F, Serrano L. Analysis of disease-linked rhodopsin mutations based on structure, function, and protein stability calculations. *J Mol Biol.* 2010;405(2):584-606.

19. Thibodeau PH, Brautigam CA, Machius M, Thomas P. Side chain and backbone contributions of Phe508 to CFTR folding. *Nat Struct Mol Biol*. 2005;12(1)10-16.

20. Inherited Arrhythmias Databse (www.fsm.it/cardmoc)

21. Kapplinger JD, Tester DJ, Salisbury BA, Carr JL, Harris-Kerr C, Pollevick GD, Wilde AA, Ackerman MJ. Spectrum and prevalence of mutations from the first 2,500 consecutive unrelated patients referred fro the FAMILION long QT syndrome genetic test. *Heart Rhythm*. 2009;9:1297-1303.

22. Hayashi K, Shimizu M, Ino H, Yamaguchi M, Terai H, Hoshi N, Higashida H, Terashima N, Uno Y, Kanaya H, Mabuchi H. Probucol aggravates long QT syndrome associated with a novel missense mutation M124T in the N-terminus of HERG. *Clinical Science*. 2004;107:175-182.

23. Balijepalli Sy, Lim E, Concannon SP, Chew CL, Holzem KE, Tester DJ, Ackerman MJ, Delisle BP, Balijepalli RC, January CT. Mechanism of loss of Kv11.1 K+ current in mutant T421M-Kv11.1 expressing rat ventricular myocytes: interaction of trafficking and gating. *Circulation*. 2012 (epub ahead of print)

24. Thu-Thuy LT, Hayano M, Yano K. Long-term follow-up of notched T waves in female patients with LQT2 (HERG) mutations. *Jpn Heart J*. 2004;45(2):243-250.

25. Kinoshita K, Yamaguchi Y, Nishide K, Kimoto K, Nonobe Y, Fujita A, Asano K, Tabata T, Mori H, Inoue H, Hata Y, Fukurotani K, Nishida N. A novel missense mutation causing a G487R substitution in the S2-S3 loop of human ether-a-go-go-related gene channel. J *Cardiovasc Electrophysiol*. 2012 (Epub ahead of print)

26. Chen J, Zou A, Splawski I, Keating MT, Sanguinetti MC. Long QT syndrome-associated mutations in the Per-Arnt-Si (PaS) domain of HERG potassium channels accelerate channel deactivation. *J Biol Chem*. 1999;274(15):10113-10118.

27. Gong Q, Jones MA, Zhou Z. Mechanisms of pharmacological rescue of trafficking deficient hERG mutant channels in human long QT syndrome. *J Bio Chem*. 2006;281(7):4069-4074.

28. Van Goor F, Hadida S, Grootenhuis PD, Burton B, Stack JH, Straley KS, Decker CJ, Miller M, McCartney J, Olson ER Wine JJ, Frizzell RA, Ashlock M, Negulescu PA. Correction of the F508del-CFTR protein processing defect in vitro by the investigational drug VX-809. *Proc Natl Acad Sci*. 2011;108(46):18843-18848.

29. Sampson HM, Robert R, Liao J, Matthes E, Carlile GW, Hanrahan JW, Thomas DY. Identification of a NBD1-binding pharmacological chaperone that corrects the trafficking defect of F508del-CFTR. *Chem and Bio*. 2011:18:231-242.

30. Foster BA, Coffey HA, Morin MJ, Rastinejad F. Pharmacological rescue of mutant p53 conformation and function. *Science*. 1999;286:2507-2510.

Chapter III

C-terminal LQT2 mutations

Introduction

The C-terminus of Kv11.1 contains a CNBD (amino acids 750-870) coupled to the pore through a C-linker (amino acids 666-749). The crystal structure of several CNBDs are available, which all have a similar fold with a β-roll motif that binds cyclic nucleotides. **Figure 3-1** shows a homology model of the Kv11.1 CNBD (blue) aligned with that of the recently solved zELK C-linker/CNBD structure.[1] Unlike hyperpolarization-activated cyclic-nucleotide modulated (HCN) channels and cyclic-nucleotide gated (CNG) channels, Kv11.1 is not modulated by cyclic nucleotides.[2] Instead, the binding pocket likely contains a short β-strand with F860 and L862 forming an 'intrinsic ligand' based on homology to zELK.[1] Supporting this, mutations in the zELK β-strand shift activation positively, which is similar to the effect of cAMP on HCN channels. Interestingly, many LQT2 mutations lie near or in this β-strand such as N861I and N861H.

While Kv11.1 isn't directly modulated by nucleotides, it is necessary for trafficking and proper functioning of Kv11.1. Deletion of the CNBD and all characterized LQT2 mutations located within the CNBD prevent cell surface expression (**Figure 3-1**).[3,4] As described in Chapter 2, gating is modulated through interactions with the EAG/PASD (for a review, see Gustina and Trudeau)[5]. Similar to PASD mutations, many engineered CNBD mutations also speed deactivation.[6,7] Based on the homology model, there is a hydrophobic

surface patch located in the β-roll as well as an acidic patch further away, which have been suggested to interact with the hydrophobic surface of the PASD and positively charged residues of the N-terminal amphipathic helix, respectively (see **Figure 3-4B**).[6]

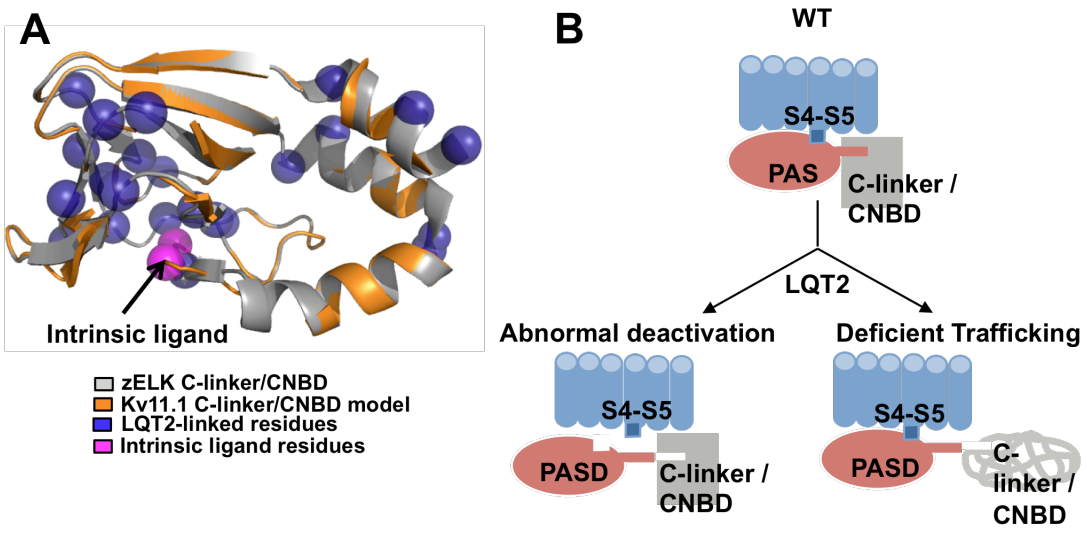

Figure 3-1. The Kv11.1 C-linker/CNBD. A. Model of the Kv11.1 C-linker/CNBD (orange) aligned with that of zELK (gray) with LQT2-linked residues as blue balls and the intrinsic ligand residues in magenta. B. Mechanistic model of how C-linker/CNBD mutations cause LQT2. Conformational changes can disrupt interactions between the PASD and CNBD resulting in abnormal deactivation or can misfold resulting in deficient trafficking.

Most of the engineered mutations reported to quicken deactivation are located in or near these regions.[6,7] Also, two LQT2-linked mutations, R784W and E788K, also shift the voltage-dependence of inactivation more positively, which has also been reported for a few PASD mutations.[8] Since the CNBD acts part and parcel with the PAS domain to regulate deactivation, it is surprising that all LQT2

mutations reported impair trafficking with none solely affecting gating like N33T or R56Q in the PASD. For similar reasons, it is surprising that no CNBD mutations have been found to be E4031 correctable. However, many of these mutations have been studied in *Xenopus oocytes* and might be temperature sensitive in mammalian cells. Moreover, the majority of Clinker/CNBD mutations are uncharacterized with at least 41 LQT2 mutations at 32 unique sites leaving these two possibilities open. A comprehensive analysis will reveal whether the molecular mechanisms for CNBD mutations are more similar to the PASD (i.e. gating or defective trafficking, see **Figure 3-1B**).

Beyond the CNBD, are the CCD and an ER retention signal (RXR), both containing LQT2-linked mutations (**Figure 1-1**).[9,10] The RXR motif is masked by a region at the distal C-terminus. Deletion of the C-terminal 147 amino acids impairs trafficking by exposing the RXR, which can be restored by mutating the RXR signal.[9] Deletion of the CCD and a LQT2-linked insertion mutation that disrupts the CCD have been reported to disrupt trafficking in *Xenopus oocytes*.[10] While two polymorphisms with very subtle gating differences in HEK cells have been reported for the CCD, it is unclear what the loss-of-function mechanism(s) are for LQT2-linked mutations in these regions.[11]

Results

Trafficking phenotype of homomeric Clinker/CNBD mutations

Over 40 C-linker/CNBD missense mutations have been linked to LQT2, yet most have not been studied. To determine the trafficking phenotype of these LQT2 mutations, immunoblot was performed on HEK cells expressing homomeric Kv11.1 cultured at physiological temperature (37^0C), reduced temperature, (27^0C) or in the presence of 10μM E4031 (see methods). **Figure 3-2A** shows representative immunoblots (n≥2) for 29 mutations and color coded as follows: trafficking deficient and uncorrectable in red, trafficking deficient but correctable at 27^0C in yellow, trafficking deficient but correctable at 27^0C and with E4031 in blue, and those that traffic similar to WT in green (Summary in **Table 3-1**). Most mutations were trafficking deficient with 24/29 (82%) having a diminished 155kD band on immunoblot when cultured at 37^0C. 15 of those 24 (62%) could be corrected by culturing cells at reduced temperature and 5 (17%) could be corrected by culturing cells in E4031. While 10 mutations were only temperature correctable, no mutations were only E4031 correctable. Since this is the first report of an E4031 correctable C-terminal mutation, the E4031 binding site was abolished to see if correction still occurs. F656C, known to disrupt E4031 binding, was introduced to make the double mutant F656C/R752Q. Immunoblot analysis showed that F656C did indeed abolish E4041 correction (**Figure 3-2B**). F656C was run as a control to show that it does not affect trafficking.

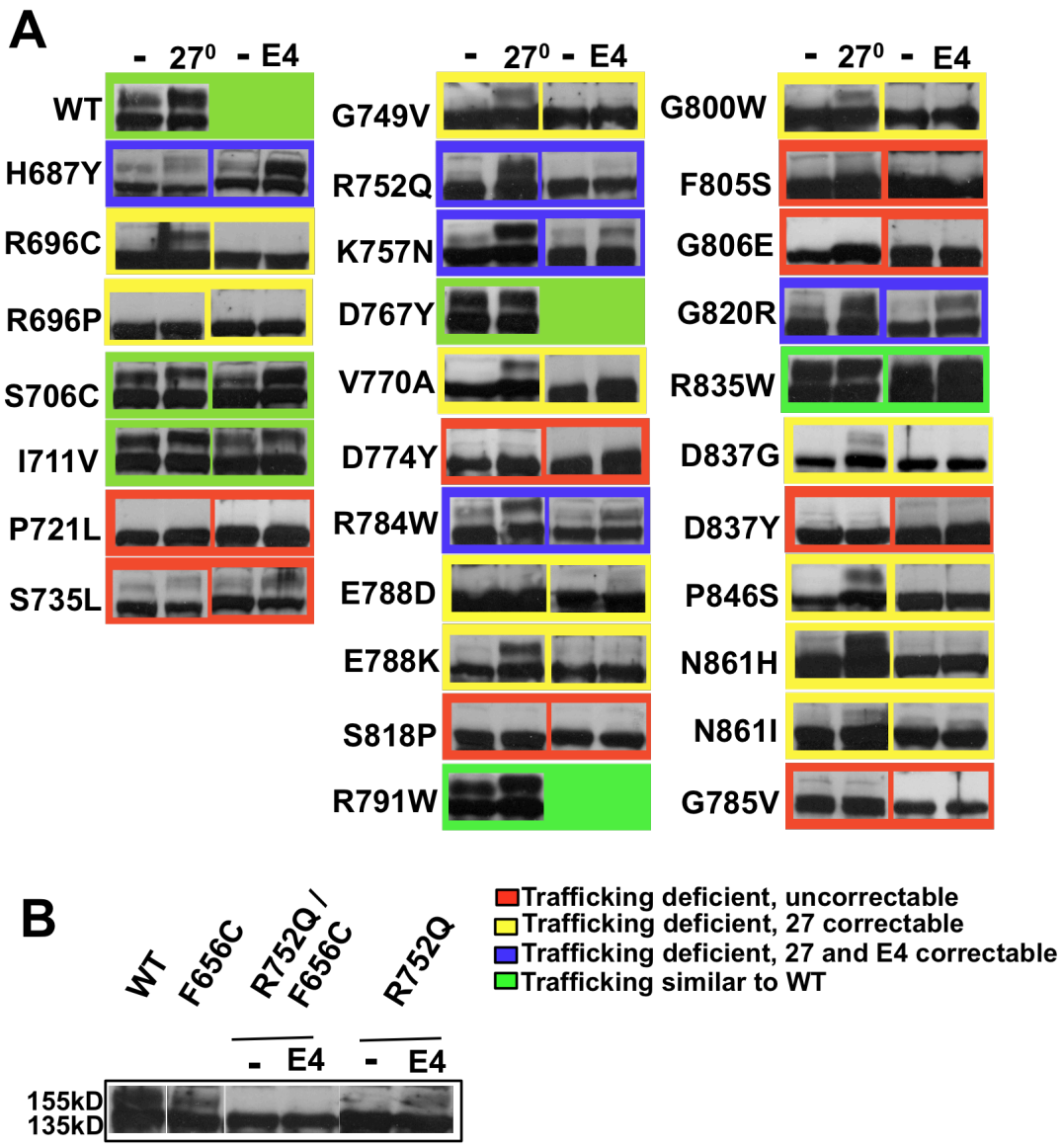

Figure 3-2. Trafficking phenotype of C-linker/CNBD mutations. A. Immunoblots of transiently transfected cells comparing control conditions (-) with reduced temperature (27^0C) or E4031 (E4). Mutations are color-coded as follows: trafficking deficient and uncorrectable in red, trafficking deficient but correctable at 27^0C in yellow, trafficking deficient but correctable at 27^0C and with E4031 in blue and those that traffic similar to WT in green. B. Immunoblot analysis of E4 correction of R752Q, a SIDS-linked mutation.[12]

Trafficking phenotype Clinker/CNBD mutations co-expressed with WT

Since LQT2 is autosomal dominant where only one abnormal allele is present, immunoblots were also performed on HEK cells co-transfected with equal amounts of WT and mutant DNA. Similar to the PASD, nearly all mutants exhibited a diminished 155kD band compared to WT alone (**Figure 3-3A**),

To determine if co-expression changes the trafficking phenotype of E4031 treated cells, ten mutations were tested and no differences were found (**Figure 3-3B**).

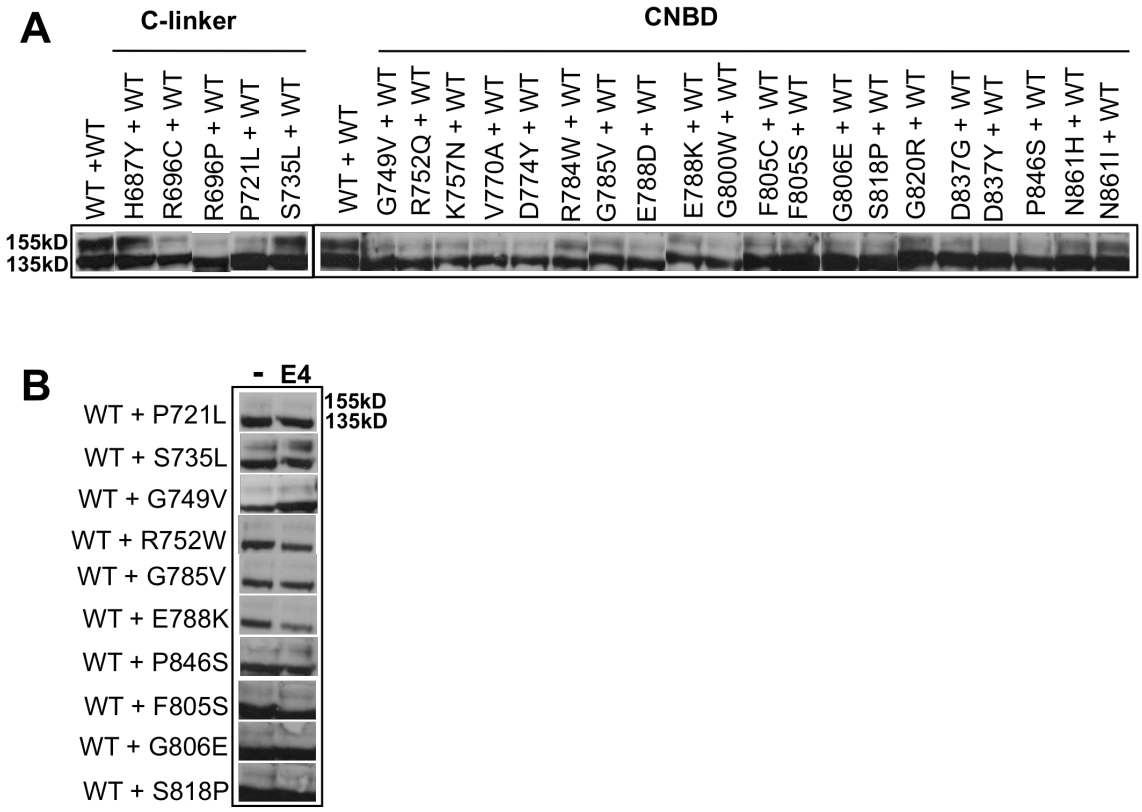

Figure 3-3. Trafficking phenotype of CNBD mutations co-expressed with WT. A. Immunoblot analysis of co-expressed channels under control conditions. B. Immunoblot analysis of heteromeric channels under control conditions (-) compared to E4031 (E4) treated cells.

Structural context of LQT2 C-linker/CNBD mutations

LQT2 mutations are located throughout the C-linker/CNBD structure (**Figure 3-1A**). To determine if any relationships exist between trafficking phenotype and location, mutations were mapped onto the structural model (**Figure 3-3)**. While no phenotype/location relationship exists for E4031 or 27^0C correction, two of the mutations that traffic normally, R791W and D767Y lie in the β-roll near the hydrophobic patch found to be important for deactivation (**Figure 2-3B**). S706C, I711V, and R835W lie outside the β-roll and are buried near each other closer to the dimer interface. To determine if these trafficking-competent mutations express currents, current densities were measured using stably transfected cells for each mutation as well as trafficking-deficient E788K for comparison. Mutations that traffic similar to WT (except for R835W) all had a 155kD band and expressed large currents compared to E788K. Since there is variability between different stable cell lines of the same mutation, statistical comparisons to WT were not done.

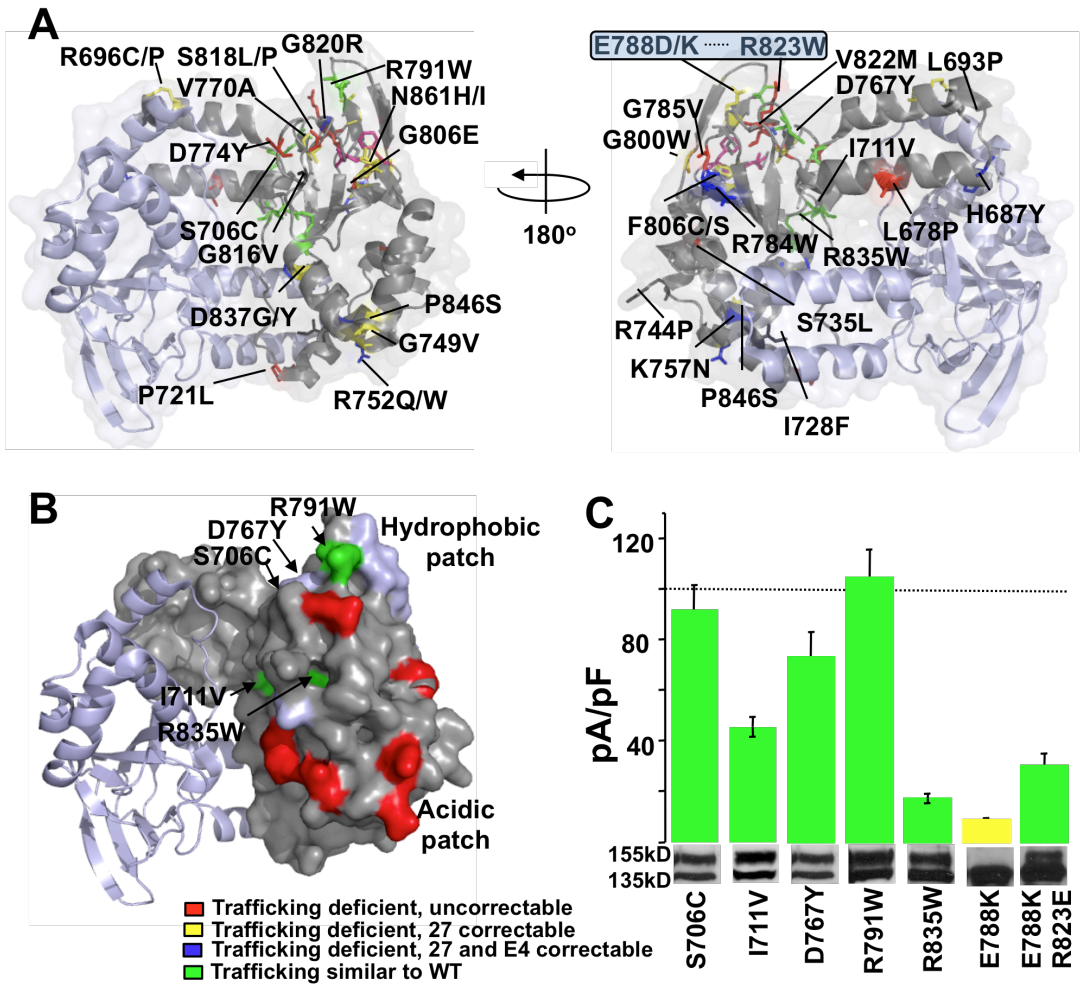

Figure 3-4. Structural context of C-linker/CNBD mutations. A. Location of all LQT2 mutations. Mutations are color-coded as follows: trafficking deficient and uncorrectable in red, trafficking deficient but correctable at 27^{0}C in yellow, trafficking deficient but correctable at 27^{0}C and with E4031 in blue and those that traffic similar to WT in green. Uncharacterized mutations shown in gray. B. Surface representation of mutations that traffic normally shown in green. Hydrophobic patch shown in light blue and acidic surface residues in red. C. Current densities and immunblots of stably transfected cells. The WT level reported in Chapter 2 is shown with a dashed line. Green indicates normal trafficking and yellow indicates trafficking deficient but correctable when cultured at 27^{0}C.

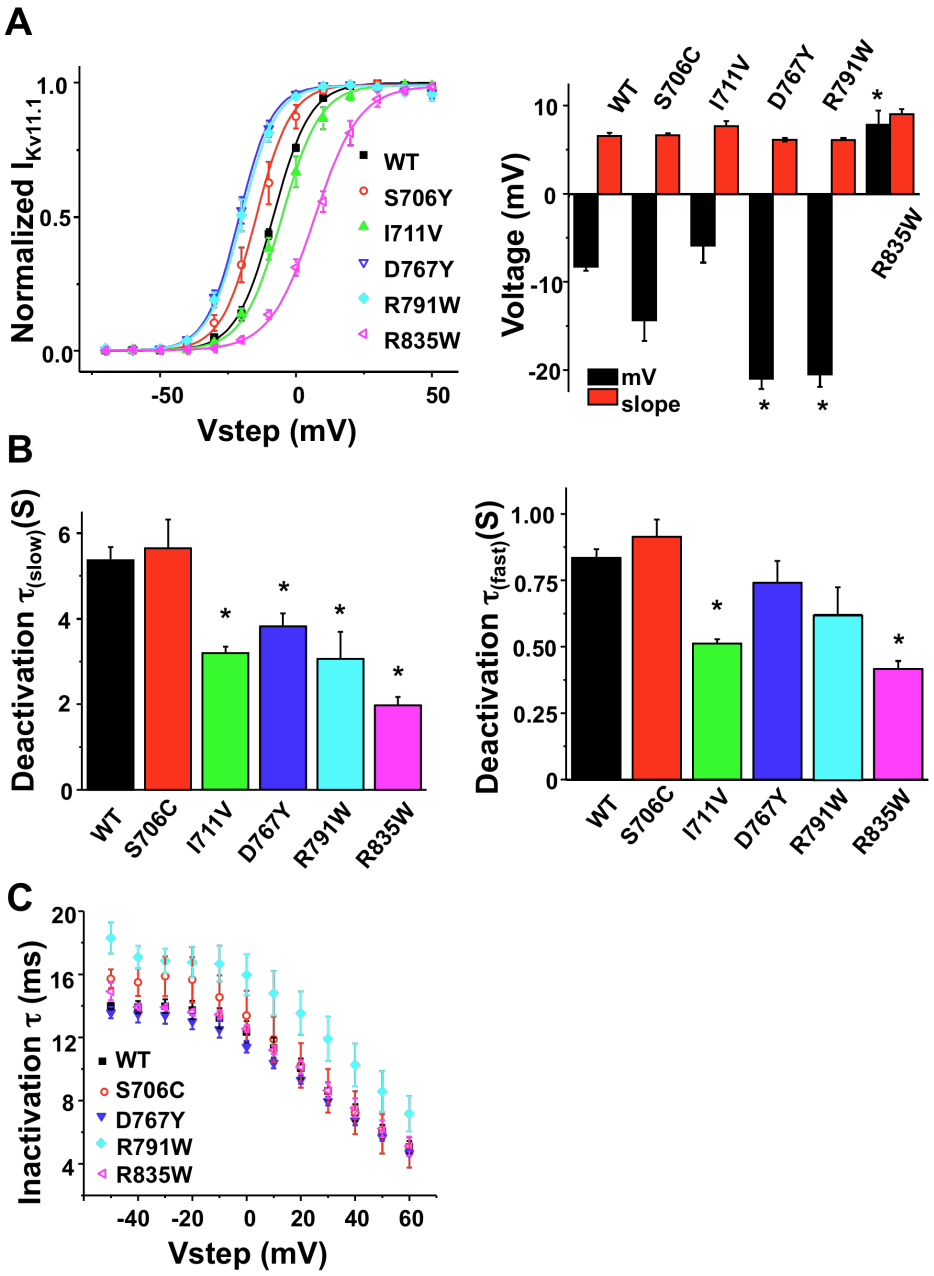

Figure 3-5. Biophysical properties of C-linker/CNBD mutations. A. I-V relationships and slope factors. B. Deactivation time constants determined at Vstep to -50mV. C. Inactivation time constants. Asterisk indicates statistical significance ($p<0.05$).

To determine if these mutations exhibit abnormal gating, activation, deactivation, and inactivation properties were studied using stably transfected cells. Values are reported in **Table 2-1**. Statistically significant differences from WT were found for all but S706C. The $V_{1/2}$ of D767Y and R791W were bothe shifted about - 12mV and R835W was shifted positively by 16mV (**Figure 2-5A**). The slow component of deactivation measured at -50mV for D767Y and R791W was faster compared to WT and both the fast and slow components of deactivation for I711V and R835W were faster than WT (**Figure 3-5B**). No statistically significant differences were found for inactivation.

Bioinformatics analysis of C-linker/CNBD LQT2-mutations.

To test destabilization as a possible cause for the 24 mutations identified as trafficking deficient, a similar bioinformatics analysis was done as for the PASD (**Figure 2-2**). Using ASAView and ConSurf, the average solvent accessibility of LQT2 residues was 26 % compared to 32% for all residues and the average conservation score for LQT2 residues was 6.8 (9 being the highest) compared to 4.7 for all residues. Values for LQT2 residues are listed in **Table 3-1**. Next, FoldX was used to calculate the change in stability for all LQT2 mutations, which is plotted and color-coded based on trafficking phenotype (**Figure 3-6**). Overall, there is a broad range of stabilities with some correlation. Eight uncorrectable mutations shown in red group to the far left (most destabilizing) but there is less

correlation between stability and trafficking than seen for the PASD (**Figure 2-6 and 2-7**).

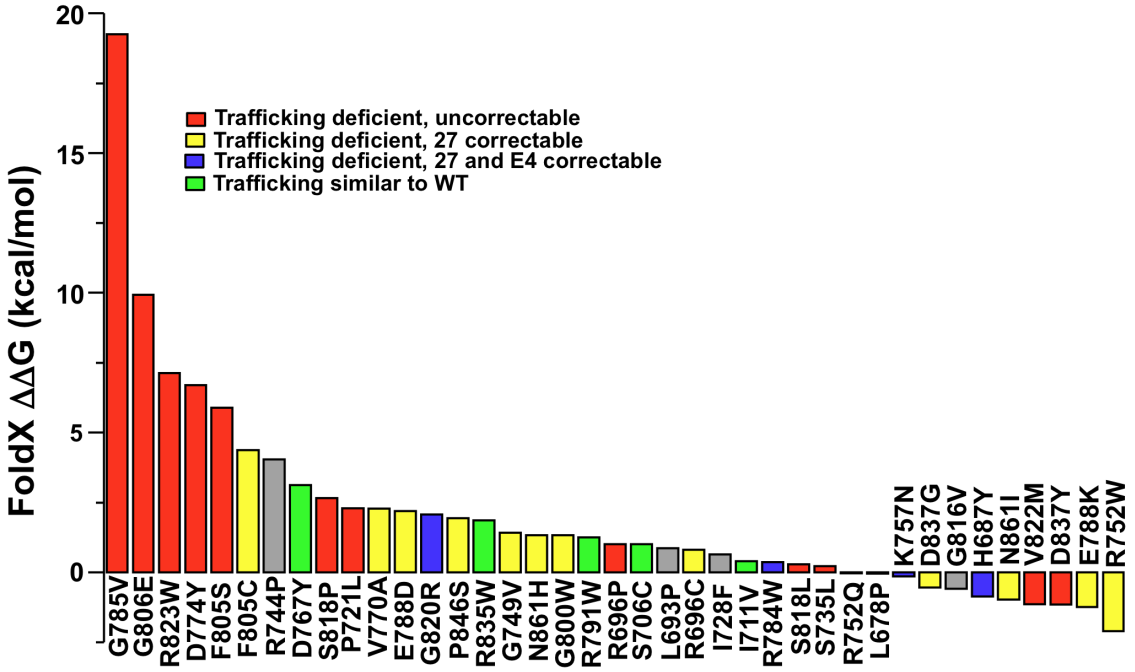

Figure 3-6. FoldX analysis of C-linker/CNBD mutations. Mutations are color-coded as follows: trafficking deficient and uncorrectable in red, trafficking deficient but correctable at 27^{0}C in yellow, trafficking deficient but correctable at 27^{0}C and with E4031 in blue and those that traffic similar to WT in green. Uncharacterized mutations are shown in gray.

Correcting a CNBD mutation with a second-site suppressor mutation

The solvent accessibility, conservation and FoldX analysis point to loss of stability as a possible cause for some CNBD mutations, the structural basis for any mutations is unknown. As mentioned in Chapter 2, several factors can lead to loss of stability including loss of ionic interactions. Using the web server ESBRI, E788 and R823 were predicted to form an energetically favorable

interaction. No cation-pi interactions were predicted with CaPTURE. Three LQT2 mutations locate to these residues (E788D, K and R823W). Surprisingly, R823W have a more severe trafficking phenotype (not correctable) than the E788D or the charge reversal E788K (temperature correctable) (**Figure 3-2A**). FoldX analysis correlates to a degree with these findings where R823W and to a lesser extent E788D are predicted to be destabilizing where E788K has no effect (**Figure 3-6**). To test loss of the salt-bridge as a cause for destabilization, R823D and R823E were introduced to make the double mutations E788K/R823D. Immunoblot analysis of stably transfected cells showed that the second-site mutation R823E but not R823D was able to correct E788K (**Figure 3-4C**). R823K was also not able to correct E788D (data not shown). FoldX $\Delta\Delta G$ calculations showed that none of the double mutations improved stability (results not shown).

Trafficking analysis of CCD and RXR LQT2-mutations

LQT2-linked mutations in the distal C-terminus including the CCD and RXR signal are mostly uncharacterized. Immunoblot analysis of transiently transfected cells showed that 7 LQT2 mutations, 2 polymorphisms and 1 SIDS mutation all lying in or near the CCD and RXR signal (except A913C) traffic normally (**Figure 3-7B**).

To test whether any of these mutations disrupt the CCD, the Paircoil2 web server identified L1049P, which lies in the hydrophobic region between helices similar to L1066V (**Figure 3-7A**). To determine if these trafficking-competent mutations express currents, current densities were measured using stably

transfected cells for L1049P, L1066V, and R1005Q. All express currents and have a 155kD band on immunoblot (**Figure 3-7C**). Activation, deactivation and inactivation were also measured and statistically significant differences from WT were found for all mutations. The $V_{1/2}$ of R1005Q shifted -5mV and inactivation was slightly slower. The $V_{1/2}$ of L1049P shifted -9mV and had slower fast and slow components of deactivation. By contrast, the $V_{1/2}$ of L1066V shifted positively 8mV and had slower inactivation.

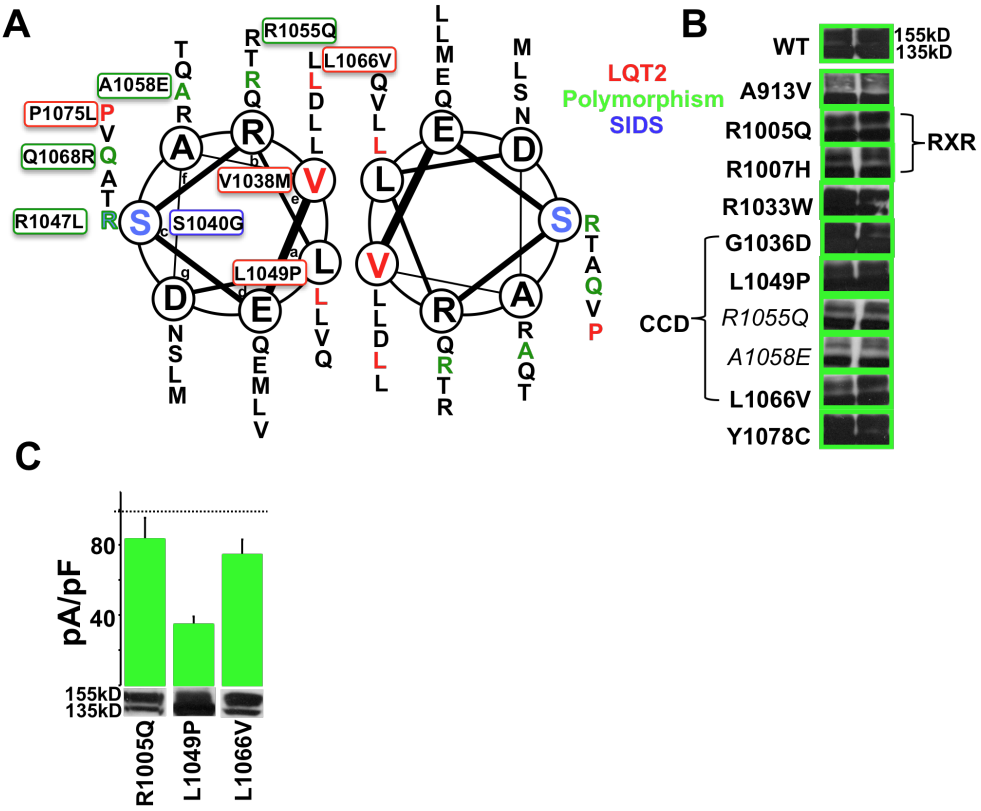

Figure 3-7. Structural context of distal C-terminus mutations. A. Helical wheel diagram showing location of LQT2 mutations outlined in red, polymorphisms outlined in green, and one SIDS mutation outlined in blue. B. Immunoblot analysis of transiently transfected cells and colored green indicating normal trafficking. C. Immunoblot analysis and current densities of stably transfected cells. The WT level measured in Chapter 1 is shown with a dashed line. Green indicates normal trafficking.

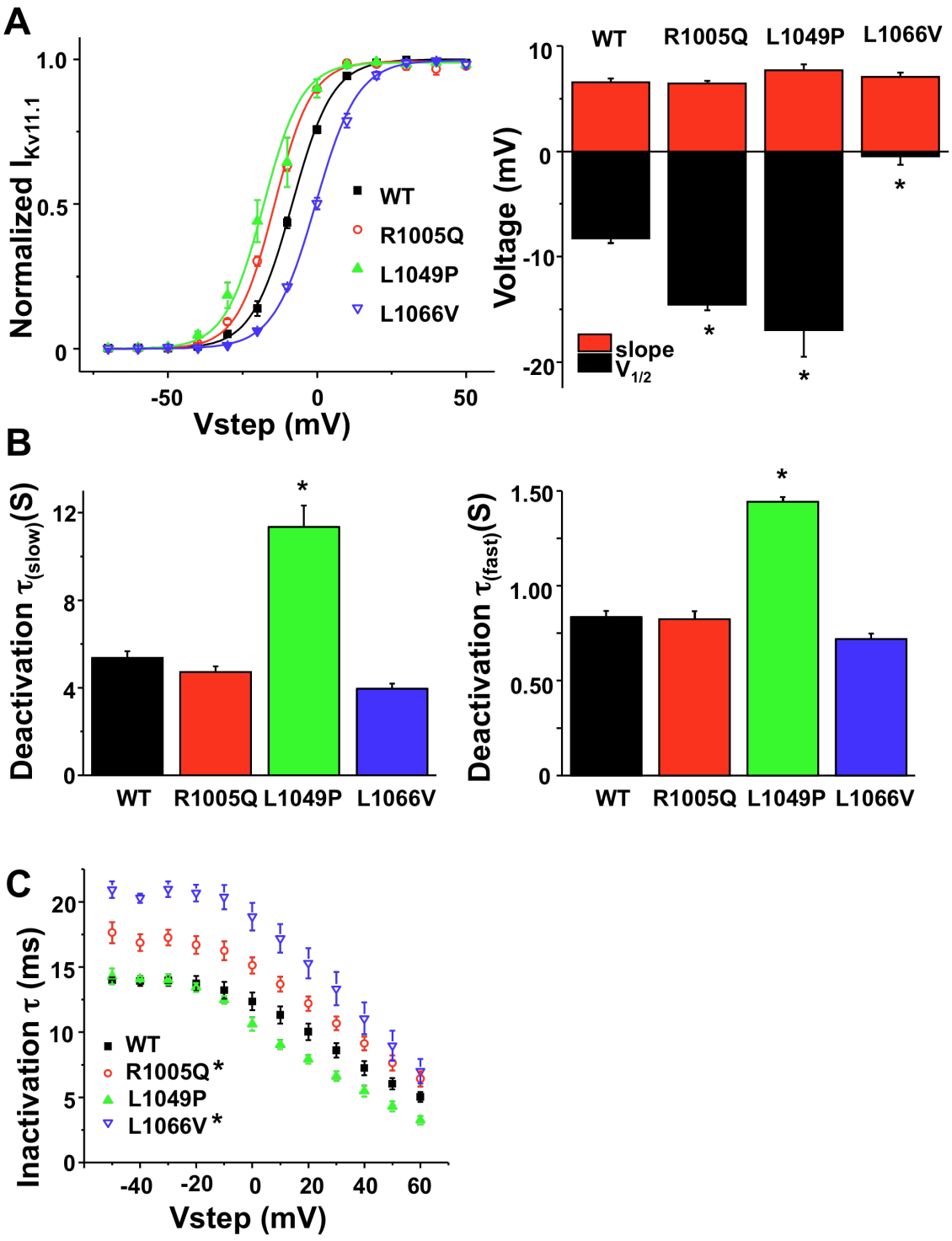

Figure 3-8. Biophysical properties of distal C-terminus mutations. A. I-V relationships and slope factors. B. Deactivation time constants determined at Vstep to -50mV. C. Inactivation time constants measured at 0mV. Asterisks indicate statistical significance ($p<0.05$).

Table 3-1. Properties of C-linker/CNBD mutations

LQT2 PAS	Class 2	27	E4	WT	Gen Ref	Phen Ref	Con Surf	ASA View	FoldX
L678P	n/a	n/a	n/a	n/a	2	n/a	4	60.6	-0.04
H687Y	Y	+	+	+	2	a	8	61.5	-0.87
L693P	n/a	n/a	n/a	n/a	2	n/a	7	36.0	0.86
R696C	Y	+	-	+	1	a	9	86.0	0.81
R696P	Y	-	-	+	1	a	9	86.0	1.02
S706C	N				1	a	5	0	1.01
I711V	N				2	a	6	6.5	0.4
P721L	Y	-	-	+	1	a	8	50.0	2.3
I728F	n/a	n/a	n/a	n/a	2	n/a	8	25.4	0.65
S735L	Y	-	-	+	1	a	1	21.3	0.22
R744P	n/a				3		1	100	4.04
G749V	Y	+	-	+	2	a	4	40.7	1.42
R752Q	Y	+	+	+	1	a	6	32.3	-0.03
R752W	Y	+	-	+	1	b	6	32.3	-2.11
K757N	Y	+	+	+	2	a	3	5.3	-0.14
D767Y	N				2	a	9	13.9	3.13
V770A	Y	+	-	+	2	a	5	0	2.28
D774Y	Y	-	-	+	1	a	8	23.5	6.7
R784W	Y	+	+	+	1	a	6	63.3	0.36
G785V	Y	-	-	+	2	a	9	31.7	19.25
E788D	Y	+	-	+	1	a	7	14.3	2.19
E788K	Y	+	-	+	2	a	7	14.3	-1.24
R791W	Y				2	a	1	79.9	1.26
G800W	Y	+	-	+	2	a	2	28	1.33
F805C	Y	+	-	+	1	b	8	0	4.38
F805S	Y	-	-	+	2	a	8	0	5.88
G806E	Y	-	-	+	2	a	9	0	9.92
G816V	n/a	n/a	n/a	n/a	2	n/a	6	1.2	-0.58
S818L	Y	-	-	+	1	b	7	0.9	0.29
S818P	Y	-	-	+	1	a	7	0.9	2.67
G820R	Y	+	+	+	1	a	7	1.2	2.08
V822M	Y	-	-	+	1	b	9	0	-1.13
R823W	Y	-	-	+	1	b	7	48.4	7.13
R835W	Y				1	a	6	11	1.86
D837G	Y	+	-	+	1	a	3	9	-0.55
D837Y	Y	-	-	+	2	a	3	9	-1.14
P846S	Y	+	-	+	2	a	7	63.4	1.93
N861H	Y	+	-	+	1	a	6	32.1	1.34
N861I	Y	+	-	+	1	a	6	32.1	-0.97

Columns same as Figure 2-2

Discussion

In contrast to previous reports in the literature showing that all CNBD mutations fail to traffic or correct with E4031, several mutations in this study did traffic and some were E4031 correctable. This underscores the importance of this comprehensive analysis in understanding the molecular properties of CNBD mutations. Consistent with reports of engineered mutations in the CNBD, several of the trafficking-competent mutations had quicker deactivation, which supports the model proposed in **Figure 3-1B**. Interestingly, there are also differences in activation between mutations. R835W channels open at more negative potentials relative to WT channels whereas D767Y and R791W channels open at more positive potentials relative to WT channels. This may reflect differences in location as R835W lies buried in the CNBD dimer while R791W and D767Y lie near the hydrophobic patch on the β-roll. S706C is the only mutation that behaves similar to WT. Similar to the discussion in Chapter 2 for a few of the PASD mutations, this mutation may be a benign variant or trafficking deficient as some immunoblots showed a slightly diminished 155kD band. Also similar to the PASD, immunoblot analysis shows that E4031 only corrects mutations that are also temperature correctable and that sometimes show a significant 155kD band under control conditions. This suggests that E4031 corrects C-linker/CNBD (and PASD) mutations that have a less severe affect on channel trafficking.

In contrast to the PASD, pore (see Chapter 4) and C-linker/CNBD, mutations in the distal C-terminus affect gating, not trafficking. In fact, they affect activation, deactivation and inactivation, which is in agreement with previous

reports showing that the C-terminus plays a role in most aspects of Kv11.1 gating. Interestingly, L1049P and L1066V properties are different but both lie at the CCD interface. One possible explanation is disruption of the CCD predicted for L1049P but not L1066V. These results are in agreement with previous reports showing that the C-terminus plays a role in most aspects of Kv11.1 gating.[13]

Given that at about 82% of the C-linker/CNBD mutations are trafficking deficient with some likely destabilizing, one correction strategy might be to identify drugs that target CNBD stability and thereby improve trafficking without block similar to that discussed in Chapter 2 for the PASD. In fact, one study identified regulators of EAG1 channels that bind to the C-terminal region.[14] Identifying such compounds might reveal stabilizers but also gain-of-function modulators, which could be another therapeutic strategy. For example, several different Ginsenoside compounds isolated from ginseng slow deactivation of Kv11.1 by directly binding the channel.[15] Drugs with similar pharmacology might have therapeutic potential for PASD and CNBD mutations that quicken deactivation.

References

1 Brelidze TI, Carlson AE, Sankaran B, Zagotta WN. Structure of the carboxy-terminal region of a KCNH channel. *Nature*. 2012:481(7382):530-533.

2 Brelidze TI, Carlson AE, Zagotta WN. Absence of direct cyclic nucleotide modulation of mEAG1 and hERG1 channels revealed with fluorescence and electrophysiological methods. *J Biol Chem*. 2009;284:27989-27997.

3 Akhavan A, Atanasiu R, Shrier A. Identification of a COOH-terminal segment involved in maturation and stability of human ether-a-go-go-related gene potassium channels. *J Biol Chem*. 2003;278(41):40105-40112.

4 Akhavan A, Atanasiu R, Noguchi T, Han W, Holder N, Shrier A. Identification of the cylci-nucleotide-binding domain as a conserved determinant of ion-channel cell-surface localization. *J Cell Science*. 2005;118:2803-2812.

5. Gustina AS, Trudeau MC. HERG potassium channel regulation by the N-terminal eag domain. Cellular Signalling. 2012:24(8):1592-1598.

6 Muskett FW, Thouta S, Thomson SJ, Bowen A, Stansfeld PJ, Mitcheson JS. Mechanistic insight into human ether-a-go-go-related gene (hERG) K+ channel deactivation gating from the solution stucture of the EAG domain. *J Biol Chem*. 2011;286(8):6184-6191.

7 Al-Owais M, Bracey K, Wray D. Role of intracellular domains in the function of the herg potassium channel. *Eur Biophys J*. 2009;38:569-576.

8 Chen J, Zhou A, Splawski I, Keating MT, Sanguinetti MC. Long QT syndrome- associated mutations in the PER-ARNT-SIM (PAS) domain of HERG potassium channels accelerate channel deactivation. *J Biol Chem*. 1999;274(15):10113-10118.

9 Kupershmidt S, Yang T, Chanthaphaychith S, Wang Z, Towbin JA, Roden DM. Defective human ether-a-go-go-related gene trafficking linked to an endoplasmic reticulum retention signal in the C terminus. *J Biol Chem*. 2002;277(30):27442-27448.

10 Jenke M, Sanchez A, Monje F, Stuhmer W, Weseloh RM, Pardo LA. C-terminal domains implicated in the functional surface expression of potassium channels. *EMBO J*. 2003;22(3):395-403.

11 Anson BD, Ackerman MJ, Tester DJ, Will ML, Delisle BP, Anderson CL, January CT. Molecular and functional characterization of common polymorphisms in HERG (KCNH2) potassium channels. *Am J Physiol Heart Circ Physiol*. 2004;286:2434-3441.

12 Johnson Jr WH, Yang P, Yang T, Lau YR, Mostella BA, Wolff DJ, Roden DM, Benson DW. Clinical, genetic, and biophysical characterization of a homozygous HERG mutation causing severe neonatal long QT syndrome. *Pediatr Res*. 2003;53(5):744-748.

13 Aydar E, Palmer C. Functional characterization of the C-terminus of the human ether-a-go-go-related gene K(+) channel (HERG). *J Physiol*. 2001;534(Pt1):1-14

14 Brelidze TI, Carlson AE, Davies DR, Stewart LJ, Zagotta WN. Identifying regulators for EAG1 channels with a novel electrophysiology and tryptophan fluorescence based screen. *PLoS One*. 2010;5(9)e12523.

15 Choi SH, Shin TJ, Hwang SH, Lee BH, Kang J, Kim HJ, Jo SH, Choe H, Nah Sy. Ginsenoside Rg(3) decelerates hERG K(+) channel deactivation through Ser631 residue interaction. *Eur J Pharmacol*. 2011;663(1-3):59-67.

Chapter IV

Pore domain LQT2 mutations

Introduction

Kv11.1 contains 6 transmembrane spanning helices with the first four (S1-S4) making up the voltage sensor domain (VSD). Positive charges in S4 move in response to depolarization, which is coupled to opening of the pore allowing K+ ions to flow through a selectivity filter conserved among K^+ channels.[1] Kv11.1 and the EAG family of channels do contain some differences from most other K^+ channels. First, they have a much longer S5-pore linker (turret) that contains an α-helix important for its fast inactivation property, which is absent in other major classes of K^+ channels (see **Figure 4-5A,B**).[2] The selectivity filter SVGFG (starting at the serine at residue 624), differs slightly by two amino acids from other K^+ channels (TVGYG). The S5 domain does not contain highly conserved residues unlike the pore helix and S6 domain.[3] Finally, the pore is extremely promiscuous to drug block, which can lead to drug-induced LQT2.[4] As a result, numerous drugs have been pulled from the market that block Kv11.1 including Terfenadine shown in **Figure 4-1**. All drug candidates now have to be screened before FDA approval. In fact, the WT stable cell line used in this study is licensed by the Wisconsin Alumni Research Foundation (WARF) to dozens of pharmaceutical companies worldwide for screening drug block. Most drugs that block Kv11.1 are largely hydrophobic and often contain a positive charge. These

features are thought to form cation-pi and pi-pi stacking interactions with several aromatic amino acids in S6 of the pore (**Figure 4-1**).[5]

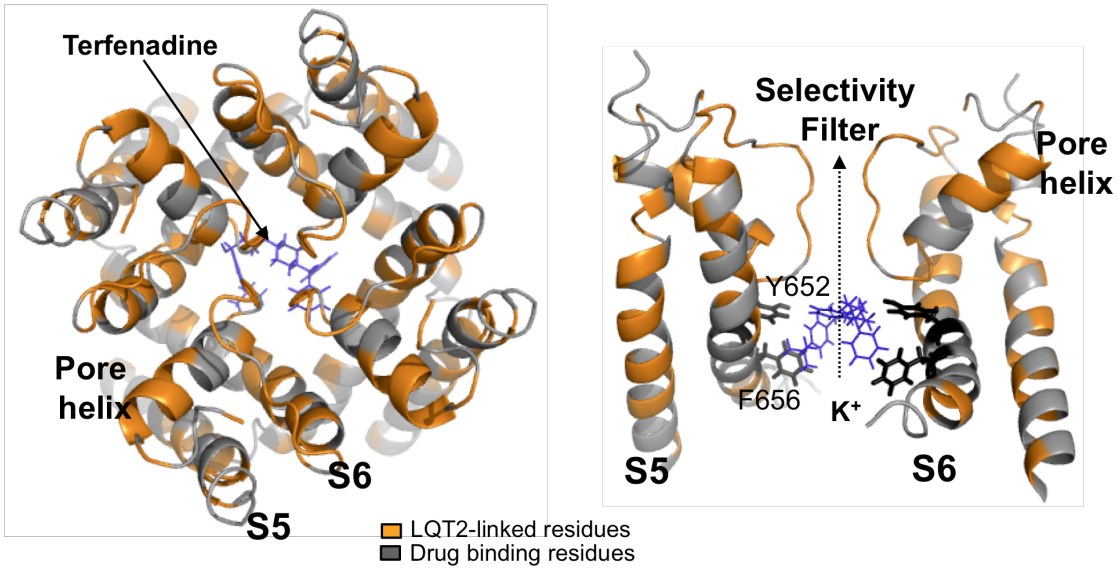

Figure 4-1. The Kv11.1 pore domain. Model of terfenadine docked to the open state of the Kv11.1 pore. View is from the outside looking in. LQT2 residues in orange.

Mutating Y652 and F656 for example disrupt drug block and abolish E4031 correction (see **Figure 3-4D**).[6] Interestingly, the mutation Y652C can also correct several trafficking deficient mutations.[7] As shown in Chapters 2 and 3, pore blockers like E4031 can also correct the trafficking defect of many mutations in the PASD, CNBD as well as the VSD and pore.[8]

LQT2 mutations in the pore are associated with an increased risk in patients of arrhythmia-related cardiac events compared to the other domains.[9,10] Over 30 mutations in the pore have been characterized in the literature and most are trafficking deficient. This is similar to the results shown in Chapters 2 and 3

for the PASD and CNBD making it unclear why pore mutations are more clinically severe. However, the pore is a mutational "hotspot" containing 1/3 of all LQT2-linked mutations with at least 98 at 58 unique sites peppered through out the domain (**Figure 4-1, Figure 4-4,** and **Table 4-1**). Given the large number of mutations that remain uncharacterized and different gating processes regulated by the pore, a comprehensive mutational analysis should 1) help address why pore mutations are more clinically severe, 2) identify interesting gating abnormalities since many of these mutations are likely dysfunctional and 3) show how robust E4031 correction is to demonstrate the feasibility of using pharmacological chaperones as a therapeutic strategy.

Results

Trafficking phenotype of homomeric LQT2-pore mutations

Nearly 100 pore missense mutations have been linked to LQT2, yet the majority of them have not been functionally expressed and studied. To determine the trafficking phenotype of these LQT2 mutations, immunoblot was performed on HEK cells expressing homomeric Kv11.1 cultured at physiological temperature (37^0C), reduced temperature, (27^0C) or in the presence of 10μM E4031.

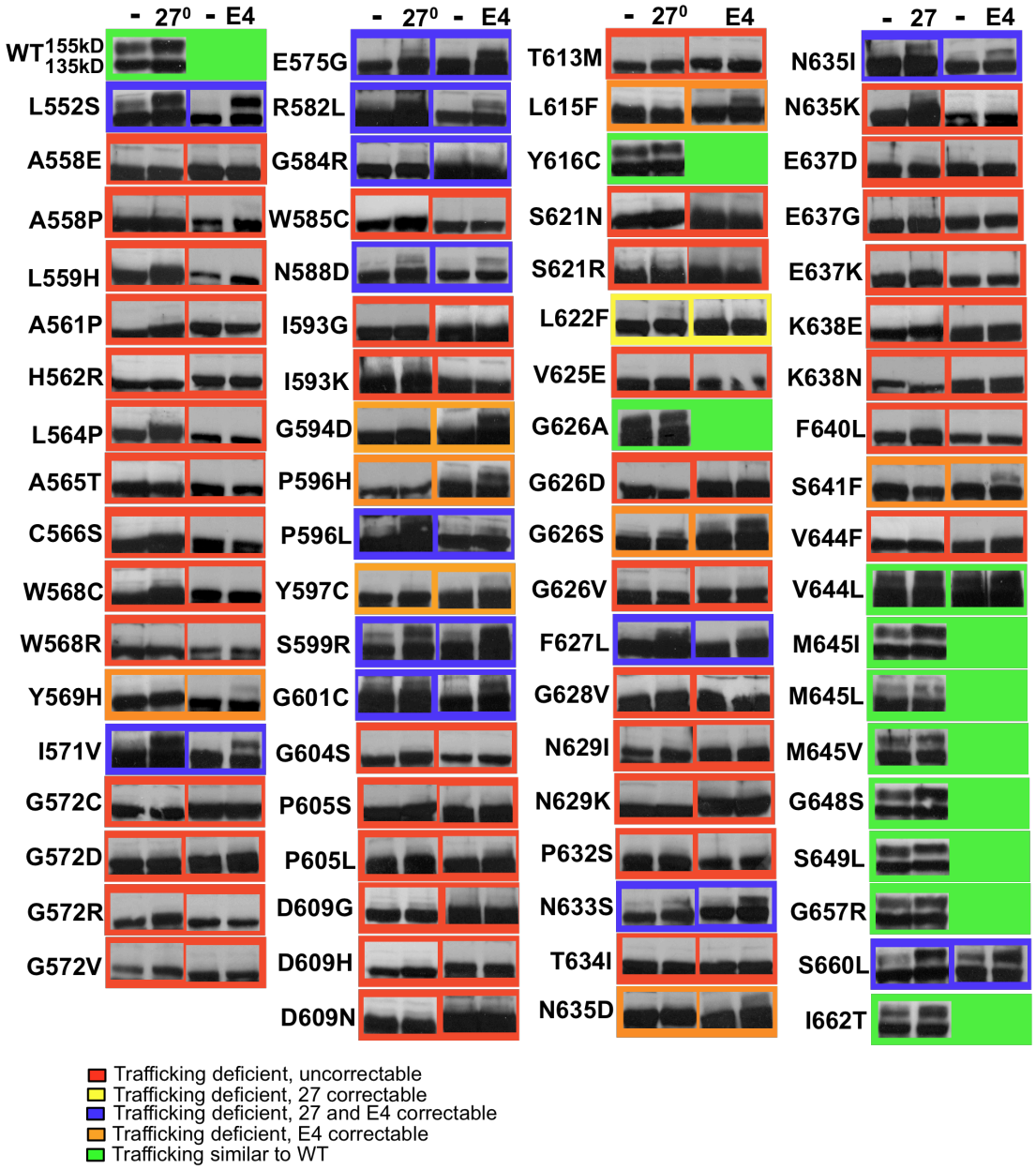

Figure 4-2. **Trafficking phenotype of pore mutations**. Immunoblots of transiently transfected cells comparing trafficking under control conditions (-) with reduced temperature (27^0C) or E4031 (E4). Mutations are color-coded as follows: trafficking deficient and uncorrectable in red, trafficking deficient but correctable at 27^0C in yellow, trafficking deficient but correctable with E4031 in orange, trafficking deficient but correctable at 27^0C and with E4031 in blue, and those that traffic similar to WT in green.

Figure 4-2 shows representative immunoblots (n≥2) for 74 mutations studied and color coded as follows: trafficking deficient and uncorrectable in red, trafficking deficient but correctable with E4031 in orange, trafficking deficient but correctable at 27^0C in yellow, trafficking deficient but correctable at 27^0C and with E4031 in blue, and those that traffic similar to WT in green. (Summary in **Table 4-2**) Most mutations were trafficking deficient with 64/74 (86%) having a diminished or no 155kD band on immunoblot compared to WT under control conditions. 14 of those 64 (20%) could be corrected by culturing cells at 27^0C and 21 (33%) could be corrected by culturing cells in E4031. In contrast to the PASD and CNBD, only one mutation, L622F, was correctable by temperature only showing a very faint 155kD band.

Trafficking phenotype of pore mutations co-expressed with WT

Since LQT2 is autosomal dominant where only one abnormal gene is needed, immunoblots were also performed on HEK cells co-transfected with equal amounts of WT and mutant DNA. As shown in **Figure 4-3**, 43/64 (67%) of mutations tested show complete loss of the 155kD band compared to WT alone. This is in stark contrast to the PASD and C-linker/CNBD where no mutations show complete loss of the 155kD band. Thus, in the pore domain the presence of mutant α-subunit(s) is strictly dominant negative.

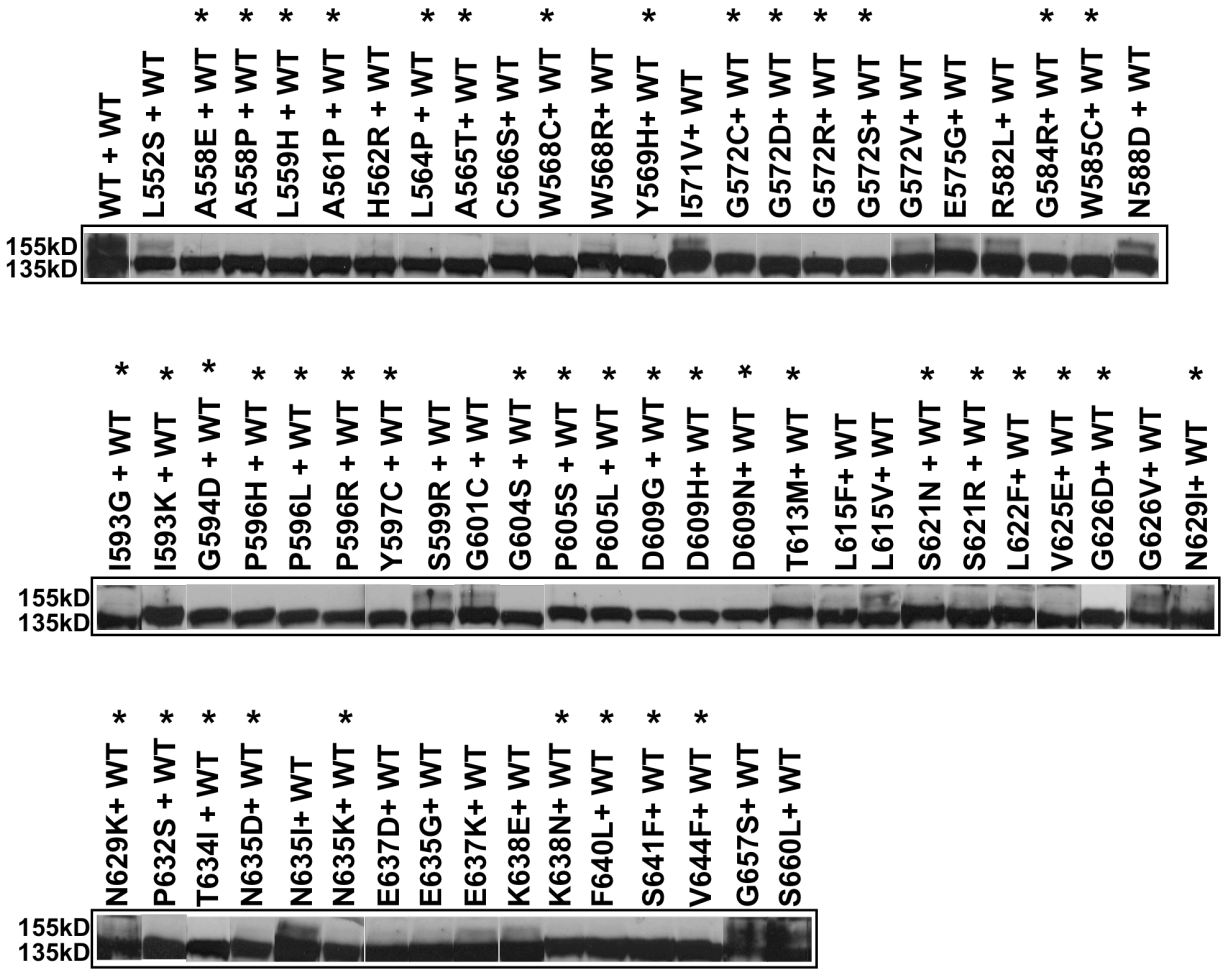

Figure 4-3. Trafficking phenotype of pore mutations co-expressed with WT. Immunoblot analysis of co-expressed channels under control conditions. Asterisks indicate complete loss of the 155kD band.

To determine if co-expression changes the trafficking phenotype of cells cultured at 27^0C or in E4031, immunoblot analysis was performed on all 43 mutations identified in **Figure 4-3** that completely impair Kv11.1 trafficking and as controls five other mutations previously reported (A561P, A561T, H562P, Y611H, and A614V).[8] In contrast to the PASD and C-linker/CNBD where 0 of 20 mutations showed no difference in trafficking phenotype, 38/48 (79%) did show a

difference between correction of homomeric and heteromeric channels (**Figure 4-4**). Of the 38, 22 mutations could be corrected with 27^0 and E4 that were not correctable as homomeric channels (blue asterisks). 7 mutations could be corrected with E4 that were not E4 correctable as homomeric channels (orange asterisks). Finally, 9 mutations could be corrected by culturing cells at 27^0C, which were not temperature correctable as homomeric channels (yellow asterisks). Thus, correction of trafficking deficient mutations depends on subunit composition for pore mutations but not for PASD or CNBD mutations.

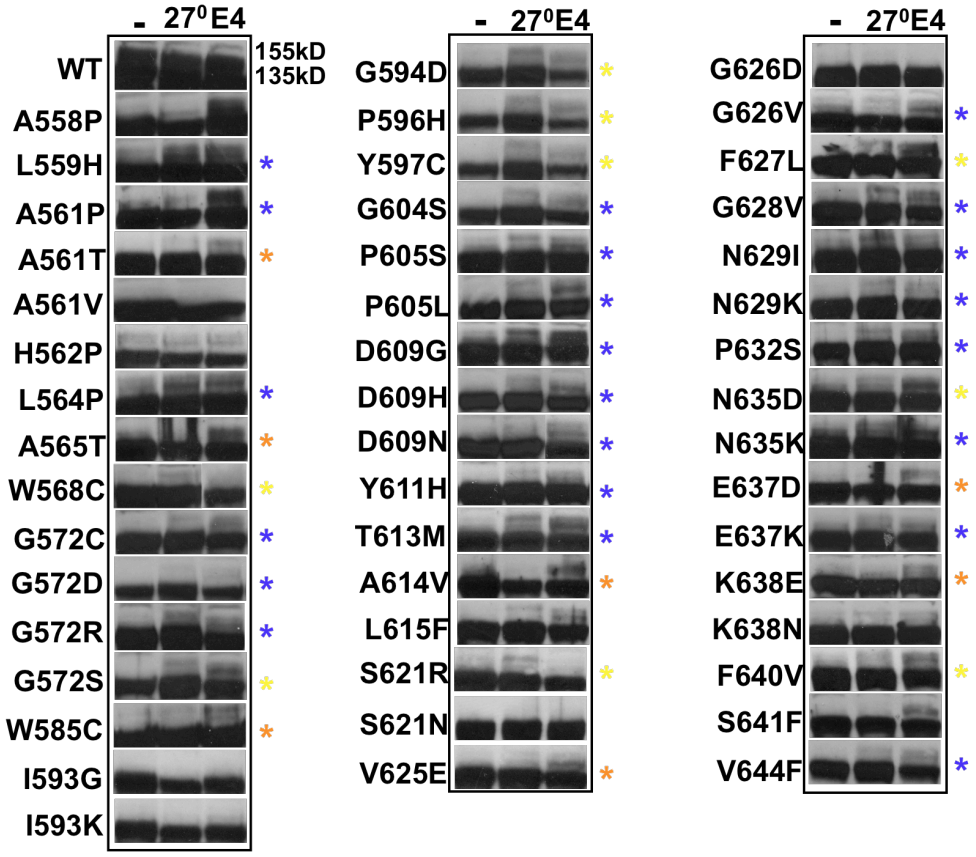

Figure 4-4. Correction of heteromeric channels. Immunoblot analysis of heteromeric channels under control conditions at 37^0C (-) compared to cells cultured at 27^0C or with E4031 (E4). Yellow, orange, and blue asterisks indicate correction at 27^0C, correction with E4031, or correction with E4031 and at 27^0C, respectively, in contrast to the lack of correction under those conditions for homomeric channels.

Structural context of pore mutations

As shown in **Figure 4-1**, pore domain mutations are located throughout the S5, S6, and pore linker regions. To determine if any relationships exist between trafficking phenotype and location, mutations were mapped onto a published model of the open state.[11] (**Figure 4-5A,B**). Included are a few mutations previously reported in the literature (see **Table 4-1**). A few patterns emerge. First, most trafficking-competent mutations are located in S6 (**Figure 4-5A**). Second, all 14 S5 mutations are trafficking deficient and only two are correctable. Third, most trafficking deficient but correctable mutations lie in the pore between S5 and S6 (**Figure 4-5B**). Finally, many of the LQT2 residues have different trafficking phenotypes for different mutations shown in Figure 4-5B with colored dots indicating trafficking phenotypes.

Of the 13 trafficking-competent mutations, eight lie in S6 and 5 lie in the S5-S6 pore linker region. To determine if these trafficking-competent mutations express currents, we generated stably transfected cells for several uncharacterized mutations including S649L, V644L, G657R (a conserved glycine), and I662T all located in S6 as well as Y616C located in the pore helix (see mutations in green **Figure 4-5A,B**). **Figure 4-5C** shows that while all stable cell lines show a 155kD band, only V644L, G657R and I662T show large currents. By contrast, two different stable cell lines for Y616C (6.0±1.0 pA/pF, n=8) and S649L (2.5±0.6 pA/pF, n=8) showed little to no current. Notably, the inward tail current elicited by Vstep to -120mV for G657R is markedly different

than WT. (**Figure 4-5D**). To determine if the trafficking-competent mutations that express current exhibit abnormal gating, we studied activation, deactivation, and inactivation properties using the stably transfected cells (see methods). Notably, when the activation protocol was run for G657R, no currents were recorded at any test pulse from -70 to 50mV (**Figure 4-5E**). V644L and I662T behaved similar to WT with the exception of slightly faster inactivation for V644L (**Figure 4-6**).

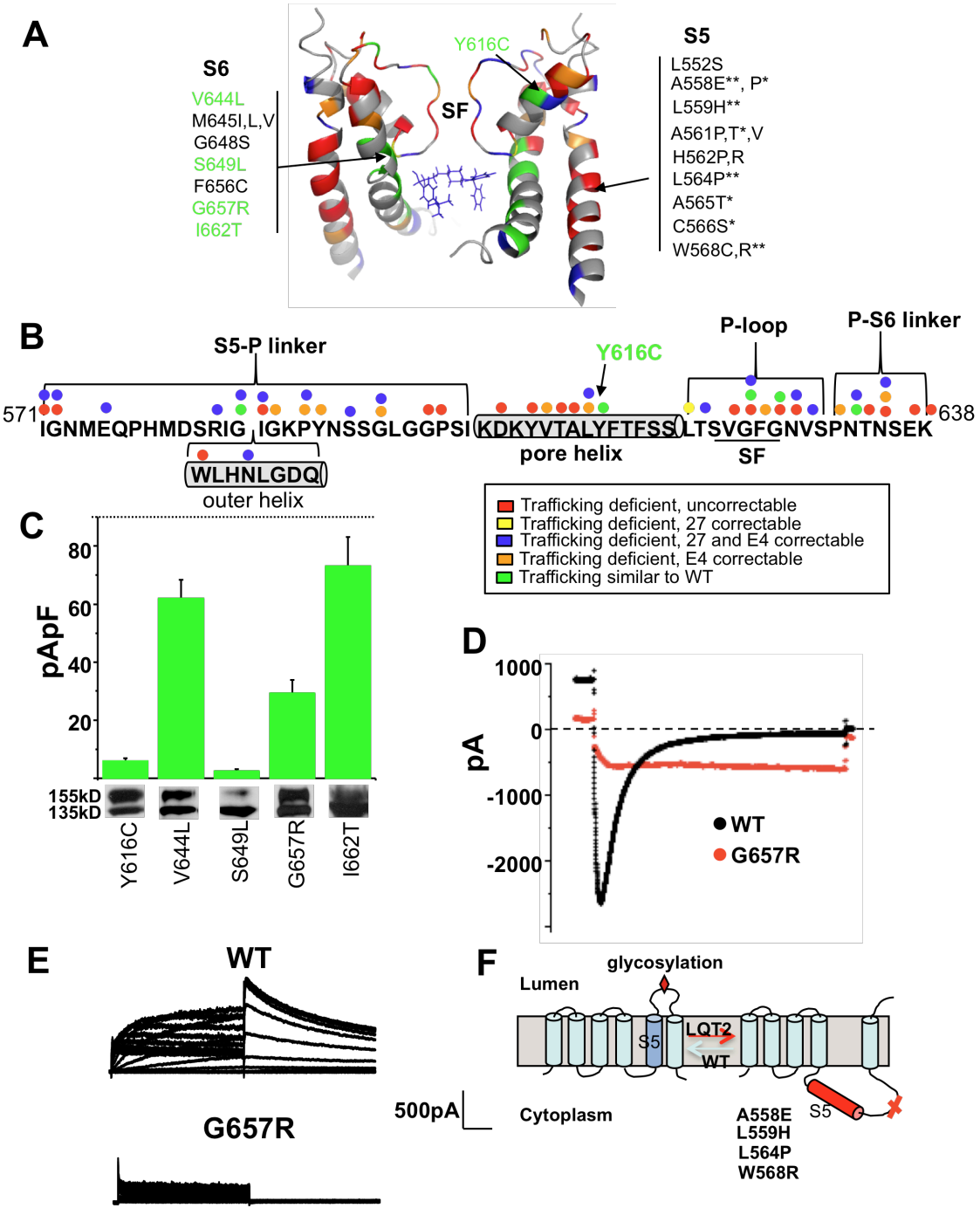

Figure 4-5. Structural context of pore mutations. A. Location of all LQT2 mutations. Mutations are color-coded as follows: trafficking deficient and uncorrectable in red, trafficking deficient but correctable at 27^{0}C in yellow, trafficking deficient but correctable with E4031 in orange, trafficking deficient but correctable at 27^{0}C and with E4031 in blue, and those that traffic similar to WT in green. B. Residues of the pore linker region between S5 and S6. Dot colors

indicate trafficking phenotypes found for homomeric channels. C. Current densities and immunoblots of stably transfected cells. WT levels determined in Chapter 2 shown with a dashed line. Green indicates normal trafficking. D. Representative current traces of inward tail currents used to measure WT and G657R current densities. E. Representative current traces from the activation protocol. F. Cartoon illustrating membrane insertion efficiency.

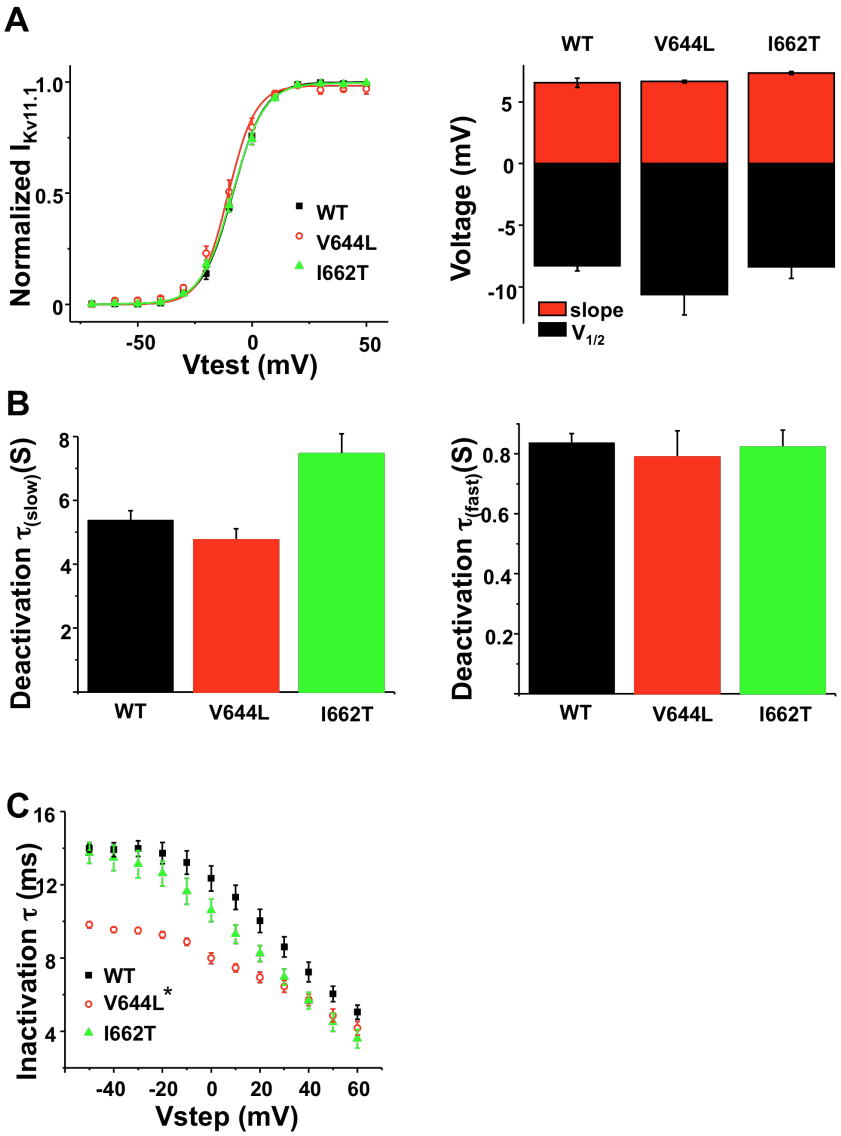

Figure 4-6. Biophysical properties of pore mutations. A. I-V relationships and slope factors. B. Deactivation time constants determined at Vstep to -50mV. C. Inactivation time constants determined at 0mV. Asterisks indicate statistical significance ($p<0.05$)

Membrane insertion efficiency of pore mutations

Since nonpolar to polar mutations reduce hydrophobicity, membrane insertion efficiency, ΔG_{app}, was calculated for all mutations in S5 and S6 using the ΔG predictor (see methods). **Table 4-1** shows the values for each mutation and $\Delta\Delta G_{app}$ values showing differences from WT. **Figure 4-5E** illustrates the predicted shift in equilibrium for several mutations towards less insertion. Nine of the S5 mutations have a positive $\Delta\Delta G_{app}$ with four > 1kcal/mol. Only G657R in S6 has a $\Delta\Delta G_{app}$>1 (**Table 4-2**).

Table 4-1. S5 and S6 membrane insertion

S5 LQT2	ΔG_{app}	$\Delta\Delta G_{app}$	S6 LQT2	ΔG_{app}	$\Delta\Delta G_{app}$
WT	3.150		WT	1.103	
A558E	4.227	1.077	F640L	1.002	-0.101
A558P	3.913	0.763	F640V	1.354	0.251
L559H	4.488	1.338	S641F	0.562	-0.541
A561T	3.364	0.214	V644F	0.906	-0.197
A561V	3.026	-0.124	M645L	0.767	-0.336
H562P	2.991	-0.159	M645V	1.090	-0.013
H562R	2.862	-0.288	G648S	1.242	0.139
L564P	4.402	1.252	S649L	0.081	-1.022
A565T	3.628	0.478	F656C	1.317	0.214
C566S	4.030	0.880	G657R	2.199	1.096
W568C	2.901	-0.249	G657S	1.368	0.265
W568R	4.375	1.225	S660L	0.033	-1.07
Y569H	3.983	0.883	I662T	1.546	0.443

Larger ΔG values indicate less efficient membrane insertion.

Table 4-2. Properties of pore muations

LQT2	Class	27	E4	WT	Ref	LQT2	Class	27	E4	WT	Ref
L552S	Y	+	+	+	1,a	A614V	Y	-	-	-	1,b
A558E	Y	-	-	-	2,a	L615F	Y	-	+	+	1,a
A558P	Y	-	+	-	1,a	L615V	Y	+	+	+	1,c
L559H	Y	-	-	-	1,a	Y616C	N				2,a
A561P	Y	-	-	-	1,a	S621N	Y	-	-	-	1,a
A561T	Y	-	-	-	1,b	S621R	Y	-	-	-	1,a
A561V	Y	-	-	-	1,b	L622F	Y	-	-	-	1,a
H562R	Y	-	-	+	2,a	T623I	Y	+	+	+	1,b
H562P	Y	-	-	+	1,b	V625E	Y	-	-	-	1,a
L564P	Y	-	-	-	1,a	G626A	N				1,a
A565T	Y	-	-	-	2,a	G626D	Y	-	-	-	2,a
C566S	Y	-	-	+	1,a	G626S	Y	-	+	n/a	1,a
W568C	Y	-	-	-	1,a	G626V	Y	-	-	+	3,a
W568R	Y	-	-	+	1,a	F627L	Y	+	+	n/a	1,a
Y569H	Y	-	+	-	1,a	G628S	N				1,c
I571L	Y	+	+	+	1,b	G628V	Y	-	-	n/a	1,a
I571V	Y	+	+	+	1,a	N629D	Y	+	+	-	1,b
G572C	Y	-	-	-	1,a	N629I	Y	-	-	-	2,a
G572D	Y	-	-	-	1,a	N629K	Y	-	-	+	1,c
G572R	Y	-	-	-	1,a	N629S	Y	+	+	-	1,b
G572S	Y	-	+	-	1,b	V630A	Y	+	+	-	1,b
G572V	Y	-	-	+	2,a	V630L	Y	+	+	+	1,b
E575G	Y	+	+	-	1,a	P632S	Y	-	-	-	1,a
R582C	Y	+	+	n/a	1,c	N633D	N				1,c
R582L	Y	+	+	+	1,a	N633S	Y	+	+	n/a	1,a
G584R	Y	+	+	-	2,a	T634I	Y	-	-	-	2,a
G584S	N				1,c	N635D	Y	-	+	-	1,a
W585C	Y	-	-	-	1,a	N635I	Y	+	+	+	1,a
N588D	Y	+	+	+	1,a	N635K	Y	-	-	-	2,a
I593G	Y	-	-	-	1,a	E637D	Y	-	-	+	1,a
I593K	Y	-	-	-	2,a	E637G	Y	-	-	+	3,a
I593R	Y	+	+	-	1,b	E637K	Y	-	-	+	1,a
G594D	Y	-	+	-	2,a	K638E	Y	-	-	+	1,a
P596H	Y	-	+	-	2,a	K638N	Y	-	-	-	1,a
P596L	Y	+	+	-	1,a	F640V	Y	-	+	+	1,b
P596R	Y	+	+	-	1,a	F640L	Y	-	-	-	1,a
Y597C	Y	-	+	-	3,a	S641F	Y	-	+	-	1,a
S599R	Y	+	+	+	2,a	V644L	N				2,a
G601C	Y	+	+	+	1,a	V644F	Y	-	-	-	1,a
G601S	Y	+	+	+	1,b	M645I	N				2,a
G604S	Y	-	-	-	1,a	M645L	N				1,a
P605S	Y	-	-	-	2,a	M645V	N				1,a
P605L	Y	-	-	-	2,a	G648S	N				2,a
D609G	Y	-	-	-	1,a	S649L	N				1,a
D609H	Y	-	-	-	1,a	F656C	N				1,a

D609N	Y	-	-	-	1,a	G657R	N				2,a
Y611H	Y	-	-	-	1,b	G657S	Y	-	+	+	2,a
V612L	Y	-	+	+	1,b	S660L	Y	+	+	+	1,a
T613M	Y	-	-	+	1,a	I662T	N				2,a

Columns same as Table 2-2

Discussion

Consistent with previous studies, most pore mutations are trafficking deficient. However, this comprehensive analysis has revealed several new findings showing major differences with the intracellular domains. First, a higher percentage of PASD mutations (45%) compared to pore mutations (33%) are E4031 correctable. This result is surprising since E4031 binds to the pore domain; a result suggesting that for most pore mutations, misfolding is too severe for E4031 to bind or improve folding. However, PASD misfolding can be compensated for through apparent cooperative folding with the pore or some other domain. One possibility is that E4031, which acts post-translationaly, helps stabilize tetramerization to allow favorable PASD interactions with other domains such as the CNBD.[12] This cooperative folding helps stabilize the PASD sufficiently to pass quality control. These results also suggest that PASD misfolding has little effect on pore formation since most mutant PASD channels still bind E4031. It is also interesting that unlike the PASD and CNBD, where all E4031 correctable mutations are also temperature correctable, several pore mutations can be corrected with E4031 alone. This suggests that there are structural differences between PASD / CNBD misfolding and pore misfolding that is recognized by quality control. Also of note, unlike the PASD / CNBD, L622F is

the only mutation that is only temperature correctable. Presumably this mutation has a slight misfolding effect that also disrupts E4031 binding.

Secondly, the reason why pore mutations are more clinically severe is because they have a more severe dominant-negative effect than other domains. The majority of pore mutations completely knocked down WT whereas none of the PASD or C-linker/CNBD mutations did.

Third and contrary to the PASD and C-linker/CNBD domain, E4031 rescue is dramatically improved if mutant subunits are co-expressed with WT. Without WT subunits present, only 33% of pore mutations are E4031 correctable, whereas with WT subunits, 75% (48/64) are correctable. This suggests that homotetrameric channels are more severely misfolded than heteromeric channels, and homotetramers may not be a great model for understanding pore mutations in the context of LQT2. This result makes identifying pharmacological chaperones that can correct without block much more promising.[13] Combined, these results underscore the importance of this large-scale analysis in understanding the molecular properties of LQT2 mutations.

References

1. Doyle DA, Cabral JM, Pfuetzner RA, Kuo A, Gulbis JM, Cohen SL, Chait BT, MacKinnon R. The structure of the potassium chanel: molecular basis of K+ conduction and selectivity. *Science*. 1998:280:69-77.

2. Liu J, Zhang M, Jian M, Tseng GN. Structural and functional role of the extracellular S5-P linker in the HERG potassium channel. *J Gen Physiol*. 2002;11:723-737.

3. Ju P, Pages G, Riek RP, Chen P, Torres AM, Bansal PS, Kuyucak S, Kuchel PW, Vandenberg JI. The pore domain outer helix contributes to both

activation and inactivation of the hERG K+ channel. *J Biol Chem*. 2009;284(2):1000-1008.

4. Spector PS, Curran ME, Keating MT, Sanguinetti MC. Class III antiarrhythmic drugs block HERG, a human cardiac delayed rectifier K+ channel. *Circ Res*. 1996;78:499-503.

5. Mitcheson JS, Chen J, Lin M, Culberson C, Sanguinetti MC. A structural basis for drug-induced long QT syndrome. *Proc Natl Acad Sci*. 2000;97(22):12329-12333.

6. Ficker E, Obejero-Paz CA, Zhao S, Brown AM. The binding site for channel blockers that rescue misprocessed human Long QT Syndrome Type 2 ether-a-go-go-related gene (HERG) mutations. *J Biol Chem*. 2002;277:4989-4998.

7. Delisle BP, Slind J, Kilby JA, Anderson CL, Anson BD, Balijepalli RC, Tester DJ, Ackerman MJ, Kamp TJ, January CT. Intragenic suppression of trafficking-defective KCNH2 channels associated with Long QT Syndrome. *Mol Pharmacol*. 2005;68:233-240.

8. Anderson CL, Delisle BP, Anson BD, et al. Most LQT2 mutations reduce Kv11.1 (hERG) current by a class 2 (trafficking-deficient) mechanism. *Circulation*.2006;113:365-373.

9. Moss AJ, Zareba W, Kaufman ES et al. Increased risk of arrhythmic events in longQT syndrome with mutations in the pore region of the human ether-a-go-go-related Gene potassium channel. *Circulation*. 2002;105:794-799.

10. Shimizu W, Moss AJ, Wilde AAM, Towbin JA, Ackerman MJ, January CT, Tester DJ, Zareba W, Robinson JL, Qi M, Vincent GM, Kaufman ES, Hofman N, Noda T, Kamakura S, Miyamoto Y, Shah S, Amin V, Goldenberg I, Andrews ML, McNitt S. Genotype- phenotype aspects of type 2 Long QT Syndrome. *J Am Col Cardiol*. 2009;54(22):2052-2062.

11. Farid R, Day T, Friesner RA, Pearlstein RA. New insights about HERG blockade obtainedfrom protein modeling, potential energy mapping, and docking studies. *Bioorg Med Chem*. 2006;14:3160-3173.

12. Zhou Z, Gong Q, January CT. Correction of defective protein trafficking of a mutant HERG potassium channel in human long QT syndrome. Pharmacological and temperature effects. *J Biol Chem*. 1999;274(44):31123-31136.

13. Rajamani S, Anderson CL, Anson BD, January CT. Pharmacological rescue of human K(+) channel long-QT2 mutations: human ether-a-go-go-related gene rescue without block. *Circulation*. 2002:105(24):2830-2835.

Chapter V

Future Directions

Future Directions

This large-scale analysis of 170 Kv11.1 mutations revealed several molecular insights into LQT2. The main findings were 1) defective trafficking is the dominant loss-of-function mechanism for all structural domains except for the distal C-terminus, 2) destabilization of the PASD is one major determinant of LQT2, which can be corrected with second-site suppressor mutations, 3) E4031 correction also occurs in the C-terminus, 4) dominant-negative interactions are more severe for pore mutations explaining their increased clinical severity, and 5) pharmacological correction of pore mutations is dramatically better for heteromeric channels than it is for homomeric channels. Based on these results and reports in the literature, a model of Kv11.1 biogenesis and correction is proposed to illustrate differences between domains and trafficking phenotypes. Future experiments should help validate and increase the resolution of this model.

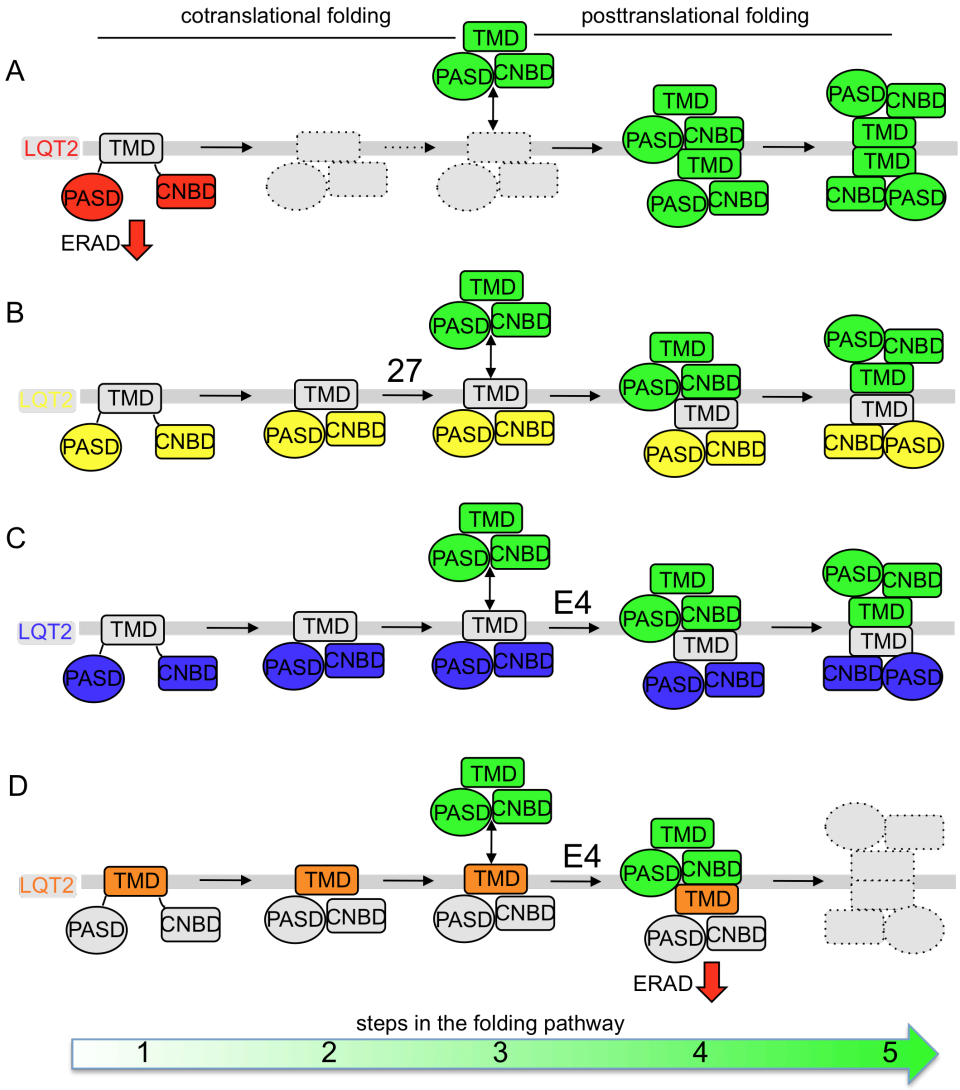

Figure 5-1. Model of Kv11.1 biogenesis and correction. A. The most destabilizing PASD and CNBD mutations (red) fail to make it to step 2 (dashed outlines) and instead undergo ERAD. These are uncorrectable at 27^0 or with E4. As a result, only WT channels (green) are present at the membrane. B. PASD and CNBD mutations that are less destabilizing (yellow) make it further along the folding pathway (step 2) allowing 27^0 correction but not E4 correction. These channels co-assemble with WT resulting in heteromeric channels at the membrane. C. PASD and CNBD mutations only slightly destabilizing (blue) make it to step 3 and form interactions with WT. E4031, which acts posttranslationally[1], is able to correct these through favorable interactions between subunits resulting in heteromeric channels at membrane. D. Most pore mutations (orange) are stable enough to make it to step 4 but result in dominant-negative behavior causing both WT and mutant to undergo ERAD. These channels fail to make it to step 5 (dashed outlines) required for ER exit and trafficking to the membrane.

Structural basis of PASD misfolding

As illustrated in **Figure 5-1**, trafficking correlates with stability. This is supported partly by the FoldX analysis but more convincingly by the solubility screen. However, quantitative measures of mutant PASD stability are needed to validate this conclusion.[2] Not shown in **Figure 5-1** is the result that introducing mutations at a second-site can also improve solubility and trafficking. This strategy could be applied to other mutations to gain insight into the structural basis of misfolding. For example, E58K-K101 was predicted to form a salt-bridge by ESBRI but other engineered "salt-bridges" between those residues did not traffic.[3] Perhaps E58 and K101, which are conserved across PASDs, are important during PASD folding and less so for the final folded structure. This could be tested using double-mutant cycle analysis for example.[4] The most straightforward approach to understand the structural basis for misfolding of these domains would be X-ray crystallography or NMR.[5,6].

Kv11.1 co-assembly dynamics

Figure 5-2A shows that trafficking deficient channels, which are ununcorrectable cause loss of function through haploinsufficiency. Although no direct evidence was provided, reports in the literature have demonstrated this for the PASD.[7] Co-assembly with WT has been shown for a CNBD mutation but the

immunoblot results shown in Chapter 3 do not support their conclusion, which showed no difference in current densities between WT channels and WT/CNBD mutant channels.[8] Directly assessing co-assembly using co-immunoprecipitation, imaging, or electrophysiology is needed to help validate this model. Moreover, if channels do co-assemble, then gating might play a role in loss-of-function as well. However, trafficking defects likely contribute more to the prolonged action potential duration for PASD and CNBD mutations. A study using the Luo-Rudy dynamic model showed a 2-fold reduction in current density prolonged the action potential more than even a 5-fold decrease in the time constants of deactivation.[9,10]

Correcting Kv11.1 trafficking defects without block

One of the more interesting results is that in contrast to homomeric channels, most heteromeric channels with pore mutations were E4031 correctable (**Figure 5-1D**). Finding pharmacological chaperones that correct misfolding is a major goal for several diseases.[11]. However, E4031 blocks the pore and so while it is a promising result showing that most of the mutations might be amenable to correction, drugs that do not block the channel are needed. Based on these results, one approach might be to identify drugs that stabilize the PASD or CNBD. This could be done using a high throughput small-molecule screen coupled with ThermoFluor analysis.[12] An alternative strategy might be to screen Kv11.1 channel trafficking with the drug binding domain

knocked out. (e.g. LQT2 mutant / F656C). Immunoblot would be relatively low throughput but perhaps a more high throughput approach could be developed using imaging or a functional assay.

Studying Kv11.1 in native cells

One major limitation to all the work done in understanding LQT2 is the use of heterologous sytems. It is largely unknown whether the mechanisms identified in these various models occur in native cells. Recent advances in iPS technology combined with new genome editing techniques should make this possible.

References

1. Zhou Z, Gong Q, January CT. Correction of defective protein trafficking of a mutant HERG potassium channel in human long QT syndrome. Pharmacological and temperature effects. *J Biol Chem*. 1999;274(44):31123-31136.

2. Harley CA, Jesus CS, Carvalho R, Brito RM, Morais-Cabral JH. Changes in channel trafficking and protein stability caused by LQT2 mutations in the PAS domain of the HERG channel. *PLoS One*. 2012;7(3):e32654.

3. Costantini S, Colonna G, Facchiano AM. ESBRI: a web server for evaluating salt bridges in proteins. *Bioinformation*. 2008;3(3):137-138.

4. Serrano L, Horovitz A, Avron B, Bycroft M, Fersht AR. Estimating the contributions of engineered surface electrostatic interactions to protein stability by using double-mutant cycles. *Biochemistry*. 1990;29(40):9343-9352.

5. Gayen S, Li Q, Chen AS, Nguyen TH, Huang Q, Hill J, Kang C. An NMR study of the N-terminal domain of wilde-type hERG and a T65P trafficking deficient hERG mutant. *Proteins*. 2011;79(8):2557-2565.

6. Morais-Cabral JH, Lee A, Cohen SL, Chait BT, Li M, Mackinnon R. Crystal structure and functional analysis of the HERG potassium channel N terminus: a eukaryotic PAS domain. *Cell.* 1998;95(5):649-55.

7. Paulussen A, Raes A, Matthijs G, Snyders DJ, Cohen N, Aerssens J. A novel mutation (T65P) in the PAS domain of the human potassium channel HERG results in the long QT syndrome by trafficking deficiency. *J Biol Chem*. 2002;277(50):48610

8. Cui J, Kagan A, Qin D, Mathew J, Melman YF, McDonald TV. Analysis of the cyclic nucleotide-binding domain of the HERG potassium channel and interactions with KCNE2. *J Biol Chem*. 2001;276(20):17244-51.

9. Rossenbacker T, Mubagwa K, Jongbloed RJ, Vereecke J, Devriendt K, Gewillig M, Carmeliet E, Collen D, Heidbuchel H, Carmeliet P. Novel mutation in the Per-Arnt-Sim domain of KCNH2 causes a malignant form of long-QT syndrome. *Circulation*. 2005;111:961-968.

10. Clancy CE, Rudy Y. Linking a genetic defect to its cellular phenotype in a cardiac arrhythmia. *Nature*. 1999;400:566-569.

11. Sampson HM, Robert R, Liao J, Matthes E, Carlile GW, Hanrahan JW, Thomas DY. Identification of a NBD1-binding pharmacological chaperone that corrects the trafficking defect of F508del-CFTR. *Chem and Bio*. 2011:18:231-242.

12. Cummings MD, Farnum MA, Nelen MI. Universal screening methods and applications of ThermoFluor. *J Biomol Screen*. 2006;11(7):854-863.

13. Zhang J, Wilson GF, Soerens AG, Koonce CH, Yu J, Palacek SP, Thomson JA, Kamp TJ. Functional cardiomyocytes derived from human induced pluripotent stem cells. *Circ Res*. 2009;104(4)e30-41.

14. Soldner F, Laganiere Josee, Cheng AW, Hockemeyer D, Gao Q, Alagappan R, Khurana V, Golbe LI, Myers RH, Lidquist S, Zhang L, Guschin D, Fong LK, Vu BJ, Meng X, Urnov FD, Rebar EJ, Gregory PD, Zhang HS, Jaenisch R. Generation of isogenic pluripotent stem cells differing exclusively at two early onset Parkinson point mutations. *Cell*. 2011;146;318-331.